Deanship of Graduate Studies

Al-Quds University

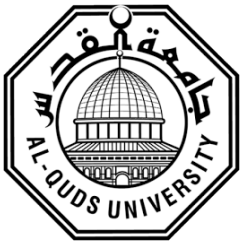

Monitoring The Quality of Liver Tissue For Transplantation Surgery Using Bioimpedance Measurements

Reem Yousef Ahmad Naser

M.Sc Thesis

Jerusalem-Palestine

1438-2017

Monitoring The Quality of Liver Tissue For Transplantation Surgery Using Bioimpedance Measurements

Prepared By:

Reem Yousef Ahmad Naser

B.Sc.: Biomedical Engineering,Hashemite University,Jordan

Supervisor: Dr.Omar I. Al- Surkhi

A thesis submitted in partial fulfillment of the requirements for the degree of Master of Electronic and Computer Engineering/Department of Electronic and Computer Engineering/ Faculty of Engineering- Al-Quds University

1438-2017

Al-Quds University

Deanship of Graduate Studies

Master of Electronics and Computer Engineering

Thesis Approval

Monitoring The Quality of Liver Tissue For Transplantation Surgery Using Bioimpedance Measurements

Prepared By: Reem Yousef Ahmad Naser

Registration No: 21220090

Supervisor: Dr.Omar I. Al- Surkhi

Master thesis submitted and accepted, Date: 15/1/2017

The name and signatures of examining committee members are as follows:

1- Head of committee	Dr.Omar Al-Surkhi	Signature:.....
2- Internal Examiner	Dr.Imad Alzeer	Signature:.....
3- External Examiner	Dr.Zaidoun Salah	Signature:.....

Jerusalem-Palestine

1438-2017

Declaration

I certify that this thesis submitted for the degree of Master, is the result of my own research, except where otherwise acknowledged, and that this study (or any part of the same) has not been submitted for a higher degree to any other university or institution.

Signed: .....

Reem Yousef Ahmad Naser

Date: 15/1/2017

Acknowledgments

I would like to sincerely thank all of those who helped me during the period of this work. Firstly, I would like to thank Dr.Omar Surkhi for his guidance, continuing support, encouragement, advices and insightful comments. My special thanks go to Al-Quds University for its support in providing us with the required equipment and labs.

I want to thank my brothers : Abdallah, Abdalrahman, and Abdalraheem, who encouraged me to take the decision to leave everything behind and engage my-self in the adventure of studying this master programme in Palestine with the aim of shifting my career towards research.

At last but not least, my deep gratitude goes to my beloved parents for the endless love and support they have provided me with during my whole life.

Abstract

Bioimpedance Spectroscopy (BIS) is a powerful tool used to characterize the electrical properties of biological materials. It is a promising method for tissue ischemia monitoring and measurements. From the fact that Liver transplantation surgery takes long time, removing the donated liver, transportation, removing the diseased liver, and then implanting the healthy one, there is a real need to monitor the quality of liver tissues during the whole liver transplantation procedure to improve the success of the transplantation procedure. There are some clinical tests performed discretely to check the quality of liver tissue during transplantation procedure (enzymes, biopsy, and histology) but there is no technique for continuous monitoring of the liver quality during the whole transplantation process. In this thesis, we have proposed an online ischemia monitoring system using BIS approach for continuous monitoring of ischemia level in liver. In addition, we have detected structural cell alterations during the event of cell ischemia and cell necrosis and confirmed the theoretical relation between cell morphological changes and the corresponding observed changes in electrical bioimpedance. The general behavior for tissue has been analyzed. Cole parameters were extrapolated from BIS measurements and their behavior was studied with respect to time. Then, cell parameters were estimated from Cole parameters. A detailed analysis for changes of cell parameters was done in parallel with explanations for these changes depending on the physiological mechanism of ischemia and necrosis bioprocess. These explanations give a confirmation of the established relation between cell morphological changes and the corresponding BIS measurements. And as a step forward, the intra/extra cellular volumes (ECV and ICV) were estimated from BIS measurements with respect to time. The proposed system might have significant repercussions in the design of future online instrument for ischemia continuous monitoring. Results show that BIS measurements could be used as a method for estimating the reversibility domain which helps in comparing organ preservative solutions efficiency. The results will contribute to improve the success rate of human liver transplantation surgery.

keywords: Bioimpedance spectroscopy, Cole model, four-terminal configuration electrodes, tissue ischemia monitoring, cell fluid estimation.

Contents

List of Tables

List of Figures

Acronyms and Abbreviations

BIS Bioimpedance Spectroscopy

ICW Intracellular Water

ICV Intracellular Volume

ECW Extracellular Water

ECV Extracellular Volume

AC Alternating Current

LF Low Frequency

HF High Frequency

CSF Cerebrospinal Fluid

BCM Body Cell Mass

TBK Total Body Potassium

TBW Total Body Water

HIV Human Immunodeficiency Virus

HCT Haematocrit

MRI Magnetic Resonance Imaging

ANN Artificial Neural Network

CPE Constant Phase Element

TUM Tissue Under Measurement

IEC International Electrotechnical Commission

TTV Total Tissue Volume

TTW Total Tissue Water

Notations

Re Extracellular Resistance

Ri Intracellular Resistance

Cm Membrane Capacitance

α Characteristic Parameter (Shape factor)

fc Characteristic Frequency

ω_{max} Radian characteristic frequency

Z Measured Impedance

R_0 Resistance at zero frequency

Z_0 Impedance at zero frequency

R_∞ Resistance at infinite frequency

Z_∞ Impedance at infinite frequency

G_0 Conductance at zero frequency

G_∞ Conductance at infinite frequency

τ Characteristic time constant

I Injected current

V Measured Voltage

ρ_a Apparent resistivity

ρ Actual resistivity of a conductive material

L Hight of the modeled cylinder

C Volumetric concentration of the nonconductive material

V_{TTV} Total tissue volume.

k_ρ ICW to ECW resistivity ratio

Chapter 1

Introduction

1.1 Research Problem

Bioimpedance Spectroscopy (BIS) is a powerful tool used to characterize the electrical properties of biological materials. It is a promising method for tissue ischemia monitoring and measurements. As tissue undergoes ischemia, its biochemical and physiological properties changes, which influence its electrical properties. These changes can be measured by impedance spectroscopic techniques. Furthermore, BIS can be used to detect cell structure and morphology. This can be done by performing bioimpedance measurements and fitting these measurements to Cole-Cole model to extract Cole parameters, then evaluating electrical cell parameters.

From the fact that Liver transplantation surgery takes long time; removing the donated liver, transportation, removing the diseased liver, and then implanting the healthy one, there is a real need to monitor the quality of liver tissues during the whole liver transplantation procedure to improve the success of the transplantation procedure. There are some clinical tests performed discretely to check the quality of liver tissue during transplantation procedure (enzymes, biopsy, and histology) but there is no technique for continuous monitoring of the liver quality during the whole transplantation process. The purpose of this work is to develop an online technique for continuous monitoring of the quality of liver tissue during transplantation procedure.

Moreover, investigation of the characterization of biological tissues and monitoring ischemia in different organs is very important for the development of different methods for protecting and preserving human tissues during clinical procedures, such as surgical operations and transplants . Besides that, monitoring of tissue alterations during ischemia allows better time management during organ surgical transplantation and improves the success rate of the transplantation procedure.

This research work presents evolution of Cole-Cole parameters and cell parameters with time, and establishes a relation between cellular morphological changes during cell ischemia and necrosis with bioimpedance measurements at different frequencies. So the cellular structural changes were detected during the events of cell ischemia and cell necrosis depending on measurements at low frequency alternating current (AC) and at high frequency AC. And as a step forward, the intra/extra cellular volumes were estimated from BIS measurements with respect to time.

The research goals of this thesis are: (1) Developing online technique for continuous monitoring of ischemia level in organ. (2) Verification of the relation between electrical properties changes and morphological changes in ischemic tissue. (3) Monitoring of tissue alterations during ischemia and estimation of the reversibility domain which helps in comparing organ preservative solutions efficiency.

1.2 Research Objectives

The main objectives of this research work are:

1. Perform electrical bioimpedance spectroscopy measurements using wide frequency range on animal liver tissue.
2. Fitting bioimpedance measurements to Cole-Cole model and extract Cole-Cole parameters.
3. Study Cole-Cole parameters in relation with tissue impedance changes with respect to time.
4. Evaluate electrical cell parameters:
    - Extracellular space resistance (R_e)
    - Intracellular space resistance (R_i)
    - Membrane capacitance (Cm)
5. Estimate extracellular space volume and intracellular space volume based on these resistances and Hanai's mixture theory.

1.3 Research Contributions

1. Establish the relation between cellular morphological changes during cell ischemia and necrosis with bioimpedance measurements at different frequencies.

2. Predict the cellular structural changes during the events of cell ischemia and cell necrosis.

3. Develop an online technique for continuous monitoring of the quality of liver tissue during transplantation procedure based on bioimpedance measurements.

4. The results will contribute to improve the success rate of human liver transplantation surgery.

The whole thesis report is organized in 6 chapters and final sections for the references and appendix A including Matlab Codes and appendix B including Cole parameters plots for all samples. Chapter 1 contains the introduction part of this thesis report. Chapter 2 provides a literature review for using BIS in different applications. Chapter 3 describes principle of BIS and a brief theoretical background ,while Chapter 4 describes the experimental methods and instruments used in this research work. Finally Chapter 5 presents and discuss the obtained results and Chapter 6 ends the report with the conclusions and proposes future work to be done in this line.

Chapter 2

Literature Review

Bioimpedance research has attracted the interest of many researchers from different fields of specialization with biological, industrial and medical background. Bioimpedance approaches has the potential advantages of being applicable, enables on-line monitoring, and requires low-cost instrumentation and low hazard.

Hobner was one of the first researchers in bioimpedance filed, in 1910 he measured the electrical impedance of suspensions of erythrocytes up to frequencies of 10 MHz, he found that their impedance decreased with increasing frequency, he concluded that the cells were composed of a poorly conducting membrane surrounding a cytoplasm of relatively low resistivity [1]. The theoretical aspects and the main findings in this filed have been widely reviewed by Schwan, Foster and Pethig. Foster and Schwan reviewed the basic concepts of dielectric phenomena in biological materials and their interpretation in terms of interactions at the cellular level [2]. In 1987, Ronald Pethig *et al.* studied the passive electrical properties of mammalian tissues for the frequency range 1 Hz to 10 GHz. The properties considered are the frequency variations of the relative permittivity and electrical conductivity. He first outlined the dielectric properties of aqueous solutions of amino-acids, polypeptides, proteins, and then cells. The electrical characteristics of various tissues and blood are presented in tabular and graphical form, and he discussed the differences between normal and cancerous tissue [1].

Several large-scale studies have been published on the electric impedance properties of healthy tissue; perhaps the largest one is that published by Gabriel in 1996 [2][3][4]. In 1996, C Gabriel *et al.* reported a survey about the dielectric properties of biological tissues. The dielectric properties of tissues was extracted from the literature and presented in a graphical format. And in 2009, he adopted measurement to characterize the conductivity of tissues at frequencies below 1MHz. The measurements were carried out on pig tissue, *in vivo*, and pig body fluids *in vitro*. Conductivity data have been obtained for skeletal and myocardial muscle, liver, skull, fat, lung and body fluids (blood, bile,cerebrospinal fluid (CSF) and urine) [5].

The main research areas that used bioimpedance spectroscopy approach in different applications are: body composition assessment, cellular measurements, tissue classification, and tissue monitoring.

Bioimpedance spectroscopy is a unique bioimpedance approach in estimation of body cell mass (BCM), it has the potential advantage of not only measuring total body water (TBW), but also offering the unique capacity to differentiate between extracellular water ECW and intracellular water (ICW) and to provide an estimate of BCM. The procedure of using bioimpedance spectroscopy in estimation of body cell mass involves fitting the spectral data to the Cole-Cole model and generating Cole model terms, including extracellular resistance (R_e), and intracellular resistance (R_i), characteristic parameter of the distribution of the relaxation frequencies (α), and characteristic frequency (f_c). Cole model terms are then applied to equations derived from Hanai mixture theory, which is essentially based on the notion that the body is a conducting medium of water, electrolytes, and lean tissue in addition to non-conducting material within it (bone and fat). ECW and ICW are thus calculated individually; TBW is calculated as the sum of ECW and ICW.

A. De Lorenzo *et al.* in 1997, proposed a theoretical method for predicting body cell mass; he reported the relationship between BIS predicted intracellular water (ICW) and total body potassium (TBK) predicted ICW, and the relationship between a BIS predicted volume of extracellular water (ECW), intracellular water(ICW), and measuring total body water (TBW) [6].

In 2000, C. Earthman *et al.* used bioimpedance spectroscopy to detect body cell mass change in HIV infection. He stated that the ability to accurately monitor changes in BCM is essential to the successful treatment of individuals with HIV infection and acquired immunodeficiency syndrome. He concluded Bioimpedance measurements can be used to estimate BCM noninvasively by measuring ICW and ECW [7]. And in 2007 he presented a review of validation studies in various populations - including HIV patients, dialysis patients, normal-weight individuals, and others - presented in order to elucidate the clinical applicability of the BIS method for the quantification of body water compartments. From these studies he concluded that BIS may provide accurate measurements for fluid measurements and BCM [8].

From the need for a method to continuously monitor the hydration state during haemodialysis, in 2008, O Al-Surkhi *et al.* proposed a new indicator for well-balanced dehydration of patients undergoing hemodialysis. It is based on an estimator for the extra-cellular volume and the ultrafiltration rate (a measure for the whole water drainage from all over the body). The extra-cellular fluid was computed from continuous tetrapolar bio-impedance measurements taken on the lower leg in a frequency range of several kilohertz up to 500 kHz. The measured impedance spectrum was fitted to a Cole model at every time step. Two parameters in the Cole model were assumed to be known beforehand. These were the characteristic frequency (f_c = 37 kHz) and the exponential factor (α= 0.73). The values were taken from Rigaud(1996) and were also used for the finite element simulations. From the fitted values; resistance at zero frequency (R_0) and resistance at infinite frequency (R_∞), it is straightforward to compute the conductance at zero frequency (G_0) and conductance at infinite frequency (G_∞) which are the basis of their fluid volume estimator [9].

Based on the hypothesis that it is possible to detect edema from the impedance data, In 2014, Soren Weyer *et al.* used BIS as a fluid management system in heart failure. The change of the body impedance, measured by BIS, is an indicator of the water content. She concluded that BIS can detect and follow the changes in lung impedance in patients and is sensitive to extracellular volume [10].

In 2015 R Buendia *et al.* proposed a new method for predicting all three compartment volumes, he also reported a state of the art methods and reviewed the validity of the models

as well as errors and inaccuracies in every stage in each approach [11].

Bioimpedance spectroscopy is used at the cellular level also; it is used in different applications; the cell counter, and measurement of haematocrit (HCT). Cell growth characterization during culturing is an important issue in a variety of biomedical applications. In 2013, Yi-Yu Lu *et al.* used impedance spectroscopy as an index for cell growth characterization. He stated that impedance of cultured cells is determined by cell size, cell gaps and cell populations. He made a correlation between impedance and cell growth and he verified his results using images from an optical microscope for cell counting. In his study, he developed an electrical bioimpedance spectroscopy-based multi-electrode culture monitoring system to characterize cell growth. This electrode-based cell culture could be applied to the study of cell functions for the development of new drugs. Compared to optical microscopes and fluorescence staining, electrical impedance technology is less expensive, non-invasive, portable, and provides immediate results [12].

Maasrani, Jaffrin, and Boudailliez in 1997 studied haematocrit and plasma volume variations during dialysis based on continuous impedance measurements. Their study was relied on two assumptions; the first was that the plasma resistivity does not change during dialysis and the second was that the blood resistivity obeys Hanai's model. *In vivo* Haematocrit measurements are found to be in good agreement with direct measurements from blood samples. The haematocrit variation is then used to monitor changes in plasma volume, assuming conservation of erythrocyte volume [13].

In 2012 under the supervision of O.Al-Surkhi, Enas Qabaja in her thesis entitled "Characterization of Human Blood Tissue Using Bioimpedance Measurements" studied blood Haematocrit, blood intracellular water content ICW, and extracellular water content ECW, for each blood sample, the multi-frequency impedance measurements were taken at six frequencies,resistance at zero frequency (R_0), and at infinite frequency (R_∞) were then extrapolated from the Cole-Cole model and used in the estimators to determine ECW ,ICW and HCT. Different estimators were used : Xitron first generation Estimator, Xitron second generation Estimator, and Surkhi Estimator which was the most accurate estimator [14].

BIS can be applied in the field of tissue classification, since different tissue types exhibit different electrical properties. In 2004, Peter Aberg *et al.* used electrical bio-impedance to assess skin cancers and other cutaneous lesions. The aim of his study was to distinguish skin cancer from benign nevi using multi frequency impedance spectra [15].

In 2006, Christina Skourou *et al.* used BIS to detect the presence of malignant tumors based on their electrical properties. The amount of edema associated with the tumors was calculated from magnetic resonance imaging (MRI) images. Electrical parameters (resistivity, permittivity, and fluid index ratio and peak frequency) were extracted from the BIS spectra. The resulting electrical parameters strongly indicate that edema is the dominating pathological feature in BIS characterization and can at times conceal the presence of the tumor [16].

As an application of using bioimpedance in the field of tissue classification; Antoni Ivorra *et al.* In 2007 reported a direct impedance measurements on liver tissue as an accurate predictor of hepatic steatosis and as a promising method alternative to the conventional diagnostic methods in surgery and transplantation which rely mainly on biopsy and blood tests, and are thus time consuming and expensive. Measurements of electrical impedance of liver tissues with variable degrees of steatosis were simulated using The BioZsim bioimpedance simulator which generates SPICE netlists, that represent a slice of living tissue, described as a two-dimensional mesh of passive electric components that depend on numerical parameters, such as the plasm (extracellular medium) and cytoplasm resistivities. Each square pixel of the map is thus transformed into a set of passive circuit components (resistances and capacitances). The electrode, plasmic and cytoplasmic elements are modeled as pure resistive media, while plasmic–cytoplasmic interfaces are assumed to correspond to cell membranes are modeled as parallel capacitance–resistance elements. Steatosis was simulated by the intrusion of fat vacuoles inside cells. Results show that swelling reduces the available extracellular space and therefore results in the observed increase in impedance modulus at low frequencies, which is even more acute when the extracellular volume is assumed to shrink due to swelling. This is supported by a comparison of experimental and simulated data. The study also shows that some parameters (f_c and R_0) obtained through a multi-frequency analysis of impedance correlate well with the histological assessment of steatosis [17] .

Another application in tissue classification field was reported by Shlomi Lufer and Antoni Ivorra, in 2010 they reported experimental data on the complex electric properties of normal and malignant human liver tissue. It was a great contribution to report human tissue data not for normal or healthy tissue, but also for malignant tissue. Measurements were done in the frequency range 1–400 kHz. The four-electrode method was used to measure the ex vivo complex electrical impedance of tissues from 14 hepatic tumors and the surrounding normal liver from six patients. It was found that the conductivity at the lower frequency range is much higher in cancerous tissue. This could be due to higher extra-cellular water content in the tumor and lower cell membrane density due to necrosis. At the high frequency range the conductivity is still higher, although less significant than in the lower range [18].

Investigation of the characterization of biological tissues and the study of ischemia in different organs is very important for the development of different methods for protecting and preserving human tissues during clinical procedures, such as surgical operations and transplants.

Heroux and Bourdages (1994) reported changes in extracellular resistance (Re), intracellular resistance (Ri) and cell membrane capacitance (*Cm*) for rat liver, rat cortex and rat gluteus while a toxic drug was administered and up to 10 h after animal death [19].

As an important contribution in the field of ischemia monitoring, in 1999 O. Casas *et al.* studied changes of the main parameters for representing the behavior of ischemia in time. Casas measurements enabled relationships to be established between changes in Cole parameters and the evolution of the ischemia in time. He concluded that the parameters that best characterize Cole parameters changes are R_0 and f_c [20]. D.Heammerich *et al.* worked on the same idea to investigate changes in cell parameters; in 2002, they studied changes in electrical resistivity of swine liver after occlusion and postmortem. Measurements were taken for 12 hours after excision. Heammerich results were as follows: Re increased during the first 2 hours by 95% and then decreased, suggesting an increase in extracellular volume. *Cm* increased during the first 4 hours by 40%, possibly owing to closure of membrane channels, and then decreased, suggesting membrane breakdown. R_i stayed constant during the initial 6 hours and then increased. He concluded that there is a significant change in tissue resistivity after removing the organ [21].

Establishing a relationship between impedance measurements and tissue ischemia depending on pH was done by Stevan Kun *et al.* in 2003, they developed an algorithm for real time estimation of skeletal muscle ischemia. Twenty-nine in vivo animal studies on rabbit anterior tibias muscle were performed to gather data on the behavior of tissue impedance during ischemia. An artificial neural network (ANN) was used to quantitatively describe the relationship between the parameters of complex tissue impedance spectra and tissue ischemia via pH. The ANN was trained on 1249, and tested on 946 ischemic tissue impedance data sets. A correlation of 94.5% and a standard deviation of 0.15 pH units was achieved between the ANN estimated pH and measured tissue pH values [22].

In 2005, Lin Xin *et al.* studied changes of characteristic parameters of different tissue organs within 5 to 360 minutes after excision at the frequency range from 1Hz to 1MHz. He analyzed changes of characteristic parameters (R_o, R_∞, f_c and α) of different tissues in the time course. The results of measurements showed that the measurement time plays a remarkable effect on the BIS measurement of tissue [23]. And in the same year, H. S. Ahn *et al.* proposed a real time monitoring system for monitoring ischemia reperfusion injury in liver based on BIS. In his research, he took Liver tissue and blood samples at 30, 60, 90, and 120 min after reperfusion for morphologic examination, biochemical tests and ATP of the liver. He pointed to the importance of BIS role in predicting the extent of ischemia-reperfusion injury in liver [24].

Previous studies showed that there is a relationship between impedance measurements and ischemia level in tissue. Moreover, BIS is a useful technique to monitor the intra/extracellular volume and detect tissue structural alterations. In this thesis, we have proposed an online ischemia monitoring system using BIS approach for continuous monitoring of ischemia level in liver. In addition, we have detected structural cell alterations during the event of cell ischemia and cell necrosis and confirmed the theoretical relation between cell morphological changes and the corresponding observed changes in electrical bioimpedance. The general behavior for tissue has been analyzed. Cole parameters were extrapolated from BIS measurements and their behavior was studied with respect to time. Then, cell parameters were estimated from Cole parameters. A detailed analysis for changes of cell parameters was done in parallel with explanations for these changes depending on the physiological mechanism of ischemia and necrosis bioprocess. These explanations give a confirmation of the

established relation between cell morphological changes and the corresponding BIS measurements. And as a step forward, the intra/extra cellular volumes (ECV and ICV) were estimated from BIS measurements with respect to time.

Chapter 3

Theoretical Background

3.1 Liver anatomy and cell structure

Liver is a vital organ located in the upper right quadrant of the abdomen, below the diaphragm. Figure (3.1) shows the location of this organ in human body.

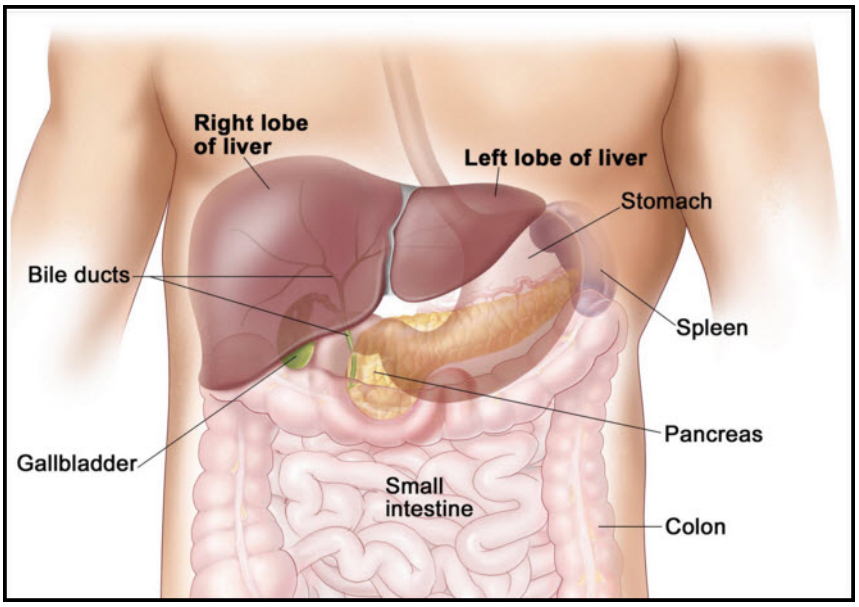

Figure 3.1: Liver anatomy (Source: Terese Winslow 2009, adapted from [25])

Liver serves many critical functions including metabolism of drugs and toxins, removing degradation products of normal body metabolism (for example clearance of ammonia and bilirubin from the blood), and synthesis of many important proteins and enzymes (such as factors necessary for blood to clot).

As any other organ in our bodies, liver consists of cells as the basic unit and the main building blocks of any biological tissue. As shown in figure (3.2-a); biological cell microstructure consists of three main components which are: Extracellular water (ECW), Intracellular water (ICW) and the cell membrane (*Cm*) that separates between those components.

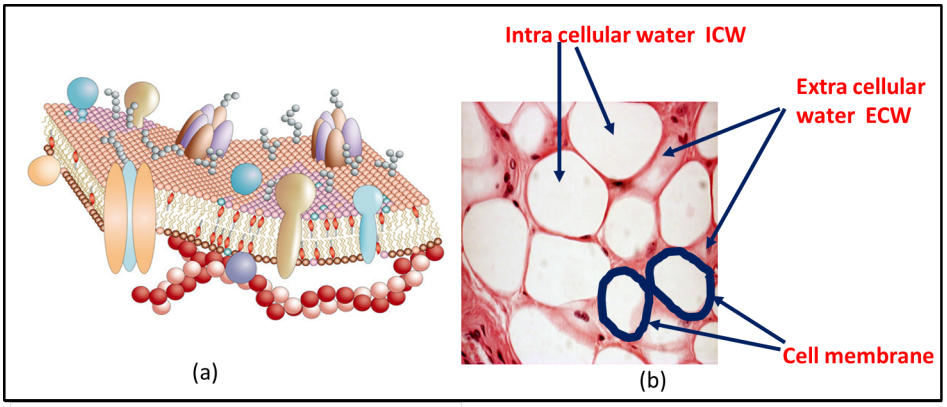

Figure 3.2: (a): Membrane structure (Source: Nature Publishing Group 2004, adapted from [26]) (b): Microstructure of biological tissues and cells

As shown in figure (3.2-b), the fundamental structure of the membrane is the phospholipid bilayer, which forms a stable barrier between two aqueous compartments; the medium surrounding cells (ECW), and liquid contained within the phospolipid bilayer (ICW). Proteins embedded within the phospholipid bilayer carry out the specific functions of the plasma membrane, including selective transport of molecules and cell-cell recognition.

3.2 Electrical model of biological tissue

Based on the structure of the biological cell, the equivalent electrical model for biological tissue is shown in figure (3.3); it consists of a resistance for the extra-cellular electrolytic medium (R_e) in parallel with the series combination of a resistance for the intra-cellular electrolytic medium (R_i) and a capacitance for the cell membrane (Cm).

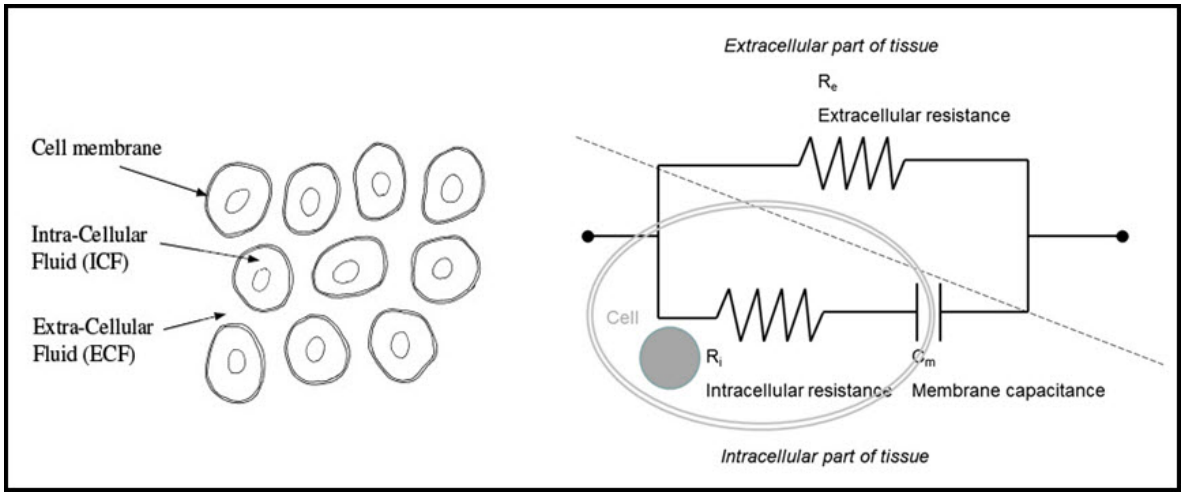

Figure 3.3: Electrical model of biological tissue(Source: Modified from [6])

It is necessary to substitute the capacitance in the previous model by a part called Constant Phase Element (CPE) in order to fit accurately the modeled impedance values to the actual bioimpedance measurements. The CPE is not physically realizable with ordinary lumped electric components but it is usually described as a capacitance that is frequency dependent. The impedance of the CPE is:

$$Z = \frac{1}{(j2.\pi.f.C)^{\alpha}} \tag{3.1}$$

The α parameter usually is between 0.5 and 1, when it is 1 the behavior of the CPE is exactly the same of an ideal capacitance. The Physical meaning of the CPE is not clearly understood; some authors suggest that α can be regarded as a measure of a distribution of resistance-capacitance combinations. That is, the tissue is not homogeneous and the size of the cells are randomly distributed, thus, the combination of the equivalent circuits can differ from the simple RC model.

One of the first successful electrical models for the electrical properties of living tissue was introduced by Frick and Morse in 1925. As it shown in figure (3.3), it consists of a resistance for the extra-cellular electrolytic medium (R_e) in parallel with the series combination of a resistance for the intra-cellular electrolytic medium (R_i) and a capacitance for the cell membrane (Cm). The FrickeMorse model has been extensively used and, even today, some authors make use of it (Haemmerich, Konishi) because of its simplicity and because it is able to describe qualitatively the observed main dispersion in the β dispersion region as defined by Schwan. However, since the first studies, it was observed that this capacitive model was not accurate enough to fit the experimental results in cell suspensions or living tissues studies. When the impedance values measured at multiple frequencies are represented in a Bode plot, it is observed that the behavior of the capacitive model is stepper that the results from the actual bioimpedance characterization. Moreover, in the Nyquist plot (imaginary part versus real part) both, the capacitive model and the experimental results, produce a semicircle but, in the case of the actual data the center is not on the real axis. This phenomenon is usually described as depressed semicircles [27].

In 1940, Cole introduced the first mathematical expression able to describe the depressed semicircles found experimentally. It is known as Cole equation to describe impedance of biological tissue:

$$Z = R_\infty + \frac{R_0 - R_\infty}{1 + (j\omega\tau)^\alpha} \tag{3.2}$$

where ω_{max} is the radian characteristic frequency; ω =1/τ, and ω_c = 2π f$_c$.

R_∞ is the impedance at infinite frequency , R_0 is the impedance at zero frequency, τ is the characteristic time constant and α is a dimensionless parameter accounts for different distributions of cells and different cell shapes and sizes with a value between 0 and 1. For it's simplicity, Cole model is still valid and useful [11].

The representation of Cole equation on the Wessel diagram, imaginary part versus real part appears as a circular arc as shown in figure (3.4). R_0 and R_∞ are where the arc cuts the horizontal axis, and τ is the circuit time constant corresponds to the inverse of the angular frequency at the impedance with the highest reactance.

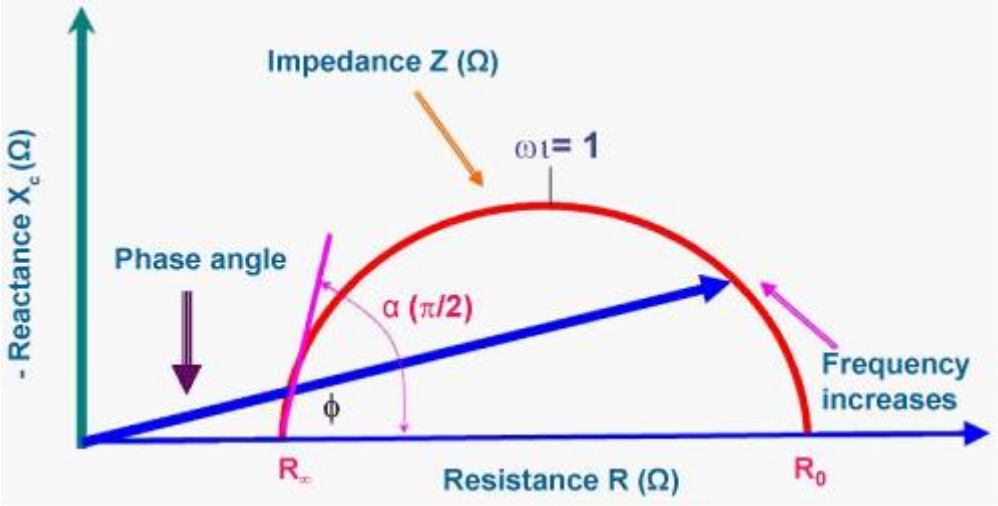

Figure 3.4: Impedance locus for a biological tissue (Source: Adapted from [28])

Schawn defined three frequency regions for the dielectric properties of biological materials from the observed main dispersions of the conductivity and the permittivity as shown in figure (3.5).

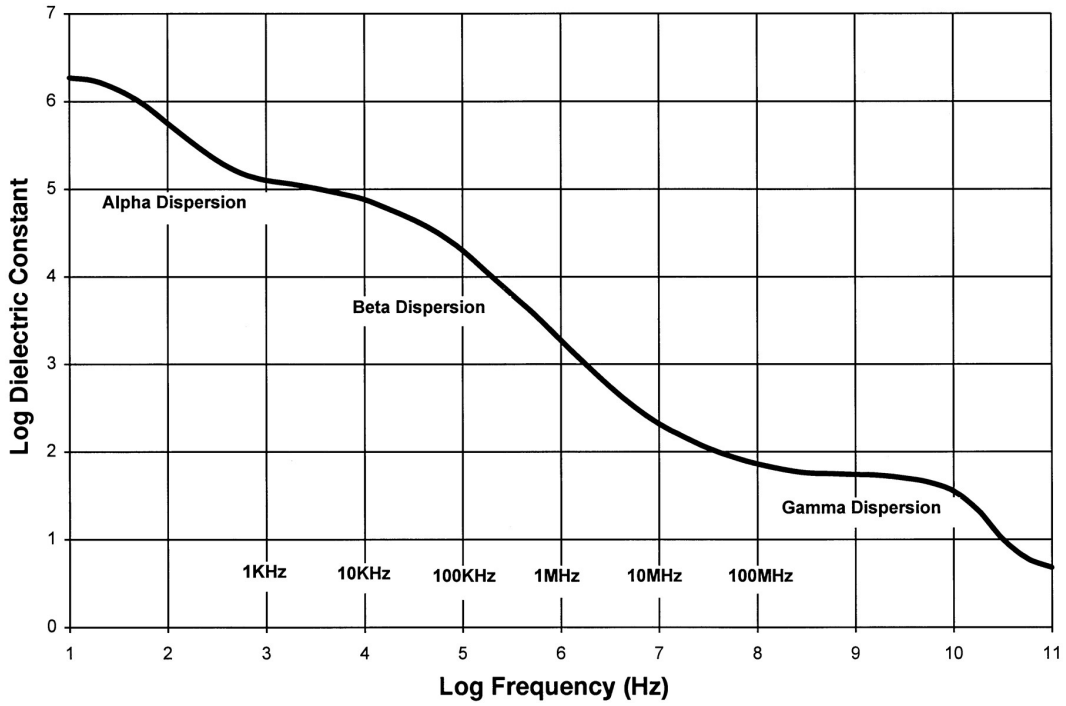

Figure 3.5: Frequency depends regions for dielectric properties of biological tissue. (Source: Adapted from [6])

The large dielectric dispersions appearing between 10 Hz and tens of MHz (α and β dispersion regions) are generally considered to be associated with the diffusion processes of the ionic species (α dispersion) and the dielectric properties of the cell membranes and their interactions with the extra and intra-cellular electrolytes (β dispersion). The dielectric properties at the γ region are mostly attributed by the aqueous content of the biological species and the presence of small molecules [29]. The purpose of this research is to describe the tissue impedance changes observed between 1 kHz and 300 KHz which means in the β dispersion region.

3.3 Principles of bioimpedance spectroscopy

Bioimpedance spectroscopy is an emerging tool for biomedical research and for medical practice. It is one of the diagnostic methods based on the study of the passive electrical properties of the biological tissues. The principle of BIS is to measure the impedance of biological tissue at series of frequencies. As shown in figure (3.6), this is done by sending a weak alternating current to tissue through injection electrodes and then measuring the voltage drop through detection electrodes, then impedance is calculated according to Ohm's law.

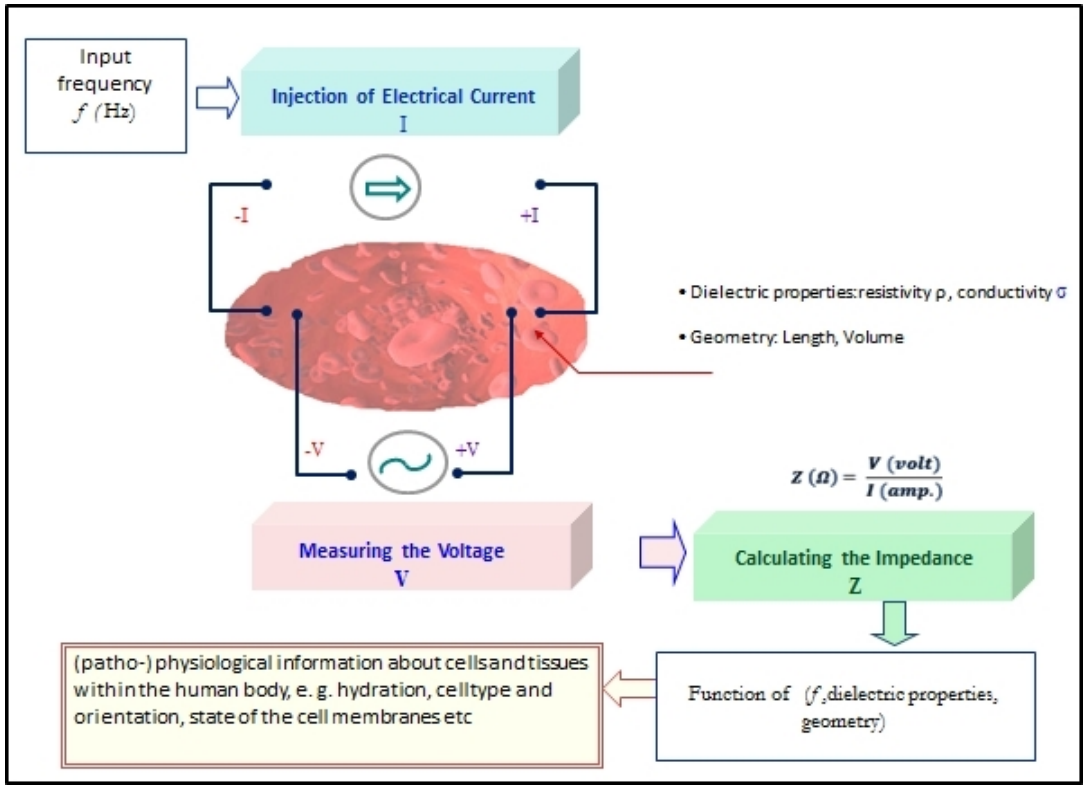

Figure 3.6: BIS principle

The current amplitude shouldn't exceed a threshold level, because there is a possibility of causing different sort of damage and undesirable effects such as severe burns and heating. According to the International Electrotechnical Commission (IEC) 60601-1 electrical safety regulations [30], the maximum allowable current for DC (0 Hz) is less than 10 μ A_{rms} and less than 10 mA_{rms} at 1 kHz. The maximum allowable current for frequencies above 1 kHz could be estimated by employing the following equation:

$$I(f) = 10^{-7} * f \tag{3.3}$$

where f is the frequency of excitation current.

Although these limitations are human safety regulations, it was taken into consideration. In this research work, Multi Frequency Impedance Analyzer Microtest is a Voltage Controlled instrument with 10 mV applied to tissue, and then the induced current response is detected. Based on the limits of the measured impedance $\simeq$ (300 Ω - 2000 Ω) and the applied voltage, the current amplitude was in the allowable range.

Current paths in biological tissue

The measured bio-impedance is a function of injected current frequency, figure (3.7-a) shows the current paths in the biological tissue at low frequency, and figure (3.7-b) at high frequency

.

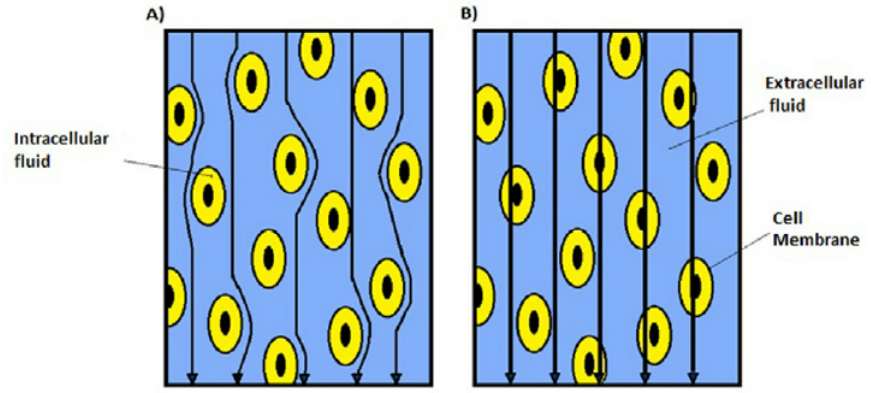

Figure 3.7: Current paths (a): at low frequency and (b): at high frequency (Source: Adapted from [11])

At low frequency (LF) (approaching to zero Hz), the cell membrane acts as an open circuit capacitor and blocking the electrical current to penetrate the ICW space and the current passes though only the ECW space, as illustrated in figure (3.8); the measured impedance is pure resistive and represents the impedance of the ECW volume (Z=R_E).

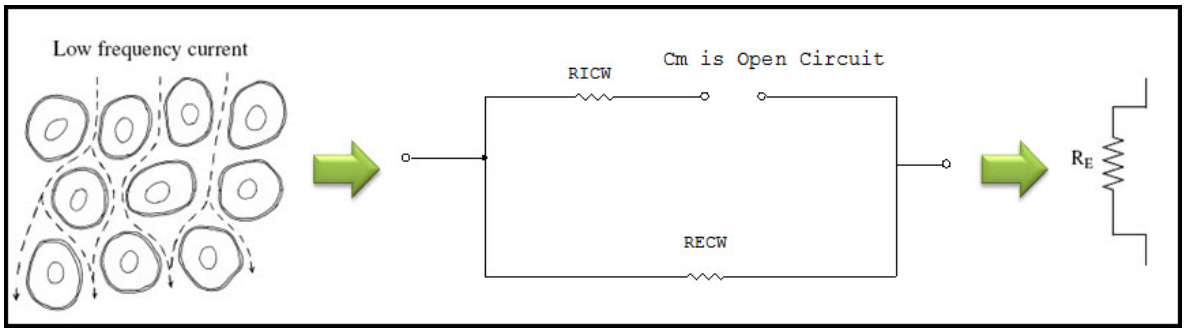

Figure 3.8: Z at low frequency R_0 (Source: Modified from [6])

At high frequency (HF) (approaching to infinite Hz) the cell membrane acts as a short circuit capacitor allowing the electrical current to penetrate both the ICW and ECW spaces, as illustrated in figure (3.9); and the measured impedance is also pure resistive and represents the impedance of the ICW and ECW volumes (Z=R$_E//R_i$).

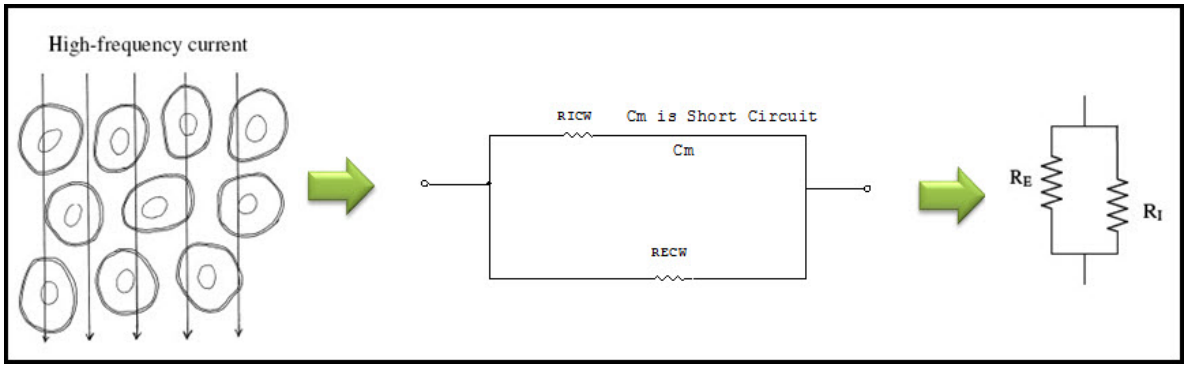

Figure 3.9: Z at high frequency R_∞ (Source: Modified from [6])

At Frequencies between low and high frequencies, cell membrane acts as a capacitor; hence bio-impedance will consist of two parts which are real and complex.

Hanai theory

Tissue is a mixture of cells and extracellular fluid. The problem of calculating the resistivity of a conducting fluid mixed with non-conducting spheres has been analyzed by the Japanese researcher Tetsuya Hanai [31]. According to the Hanais theory, the specific resistivityρ_a of a suspension of nonconductive spheres in a conductive medium is greater than the specific resistivity of the medium ρ and depends on the fractional volume of the nonconductive spheres. This apparent resistivity is related to the conducting suspending medium resistivity ρ and the volume fraction C (dimensionless) of non-conducting spheres by:

$$\rho_a = \frac{\rho}{(1-C)^{3/2}} \tag{3.4}$$

where ρ_a is the apparent resistivity of a conductive material, ρ is the actual resistivity of a conductive material, and C is the volumetric concentration of the nonconductive material contained in the mixture.

3.4 Cell death

Cell death and the subsequent post-mortem changes, called necrosis, are integral parts of normal development and maturation cycle. Cell death is said to occur by two alternatives, opposite modes: apoptosis, a programmed, managed form of cell death, and necrosis, an unordered and accidental form of cellular death.

3.4.1 Differences between necrosis and apoptosis

There are many observable morphological and biochemical differences between necrosis and apoptosis, table (3.1) shows the main differences between the two death modes.

Table 3.1: Differences between necrosis and apoptosis

Feature	Necrosis	Apoptosis
Cell size	Enlarged (swelling)	Reduced (shrinkage)
Plasma membrane	Disrupted	Intact
Adjacent inflammation	frequent	no
Physiologic/pathologic role	pathologic	physiologic or pathologic

Necrosis occurs when cells are exposed to extreme variance from physiological conditions (e.g., hypothermia, hypoxia) which may result in damage to the plasma membrane. Necrosis begins with an impairment of the cell's ability to maintain homeostasis, leading to an influx of water and extracellular ions. Intracellular organelles, most notably the mitochondria, and the entire cell swell and rupture (cell lysis). Due to the ultimate breakdown of the plasma membrane, the cytoplasmic contents including lysosomal enzymes are released into the extracellular fluid. Figure (3.10) illustrates these changes.

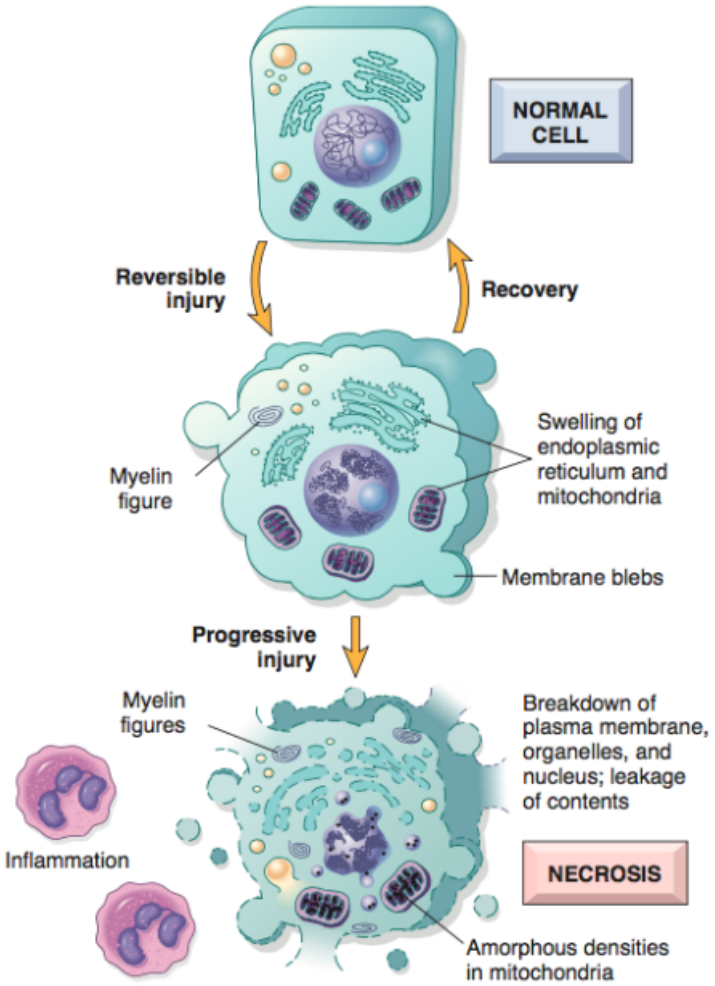

Figure 3.10: Necrosis pathway (Source: Adapted from [32])

Apoptosis, in contrast, is a mode of cell death that occurs under normal physiological conditions and the cell is an active participant in its own demise (cellular suicide). It is most often found during normal cell turnover and tissue, embryogenesis, induction and maintenance of immune tolerance, development of the nervous system and endocrine-dependent tissue atrophy. Figure (3.10) and table (3.2) shows the Morphological features for cell necrosis and apoptosis.

Table 3.2: Morphological differences between necrosis and apoptosis

Necrosis	Apoptosis
Loss of membrane integrity	Membrane blebbing, but no loss of integrity
Begins with swelling of cytoplasm	Begins with shrinking of cytoplasm
Ends with total cell lysis	Ends with fragmentation of cell into smaller bodies

In this research work, necrosis stages can be discriminated, ECV and ICV were estimated from BIS measurements with respect to time, cellular structural changes were detected during the events of cell ischemia and cell necrosis depending on measurements at low frequency and at high frequency, and membrane status can be observed.

Chapter 4

Experimental Methods and Instruments

4.1 Instruments and tools

This section presents the hardware and software were used in this work.

4.1.1 Multi Frequency Impedance Analyzer Microtest 6379(Materials Lab)

Impedance analyzer measures the complex impedance between electrical ports of a system under test in dependence of frequency. This instrument Provides all the well-known measurement parameters: Impedance, Admittance, Phase Angle and provides a continuous variable frequency from 20Hz to 10MHz, 5 digits resolution and provides a graph of the parameter against frequency or AC drive level.

Figure (4.1) shows Microtest 6379 instrument and the table below contains some of the specifications for this model.

Figure 4.1: Multi Frequency Impedance Analyzer (Source : Adapted from [33])

Table 4.1: Microtest 6379 specifications (Source : Adapted from [33])

Measurement Parameters	|Z|,|Y|, Θ, R, X, G, B, L, C, Q, D, ESR, DCR
Measurement Circuit	Series/Parallel
Test Frequency	20Hz $\sim$ 10MHz
Frequency Step Resolution	5 Digits
Frequency Accuracy	$\pm$0.005%
Output Impendence	100Ω
Measurement Range	0.1mΩ $\sim$ 100MΩ

4.1.2 Electrodes

Four-terminal configuration electrodes were built and used for measurements in this research work, the configuration consists of four electrodes; the outer electrodes are the injection electrodes, and the inner electrodes are the detection electrode. As shown in figure (4.2), this configuration is a straight line configuration with 8 mm distance between each two electrodes, 4 mm long, and 0.15 mm diameter. These dimensions are close to those were used in literature; Casas et.al (1999) used 5 mm long, 0.4 mm diameter, and distance between electrodes of 2.5 mm [20]. Haemmerich et.al (2002) used 0.38 mm diameter with electrode spacing of 1.5 mm and depth of 4 mm [21]. Shlomi Laufer and Antoni Ivorra (2010) used 2.3 mm distance between needles, 5.5 mm depth [18].

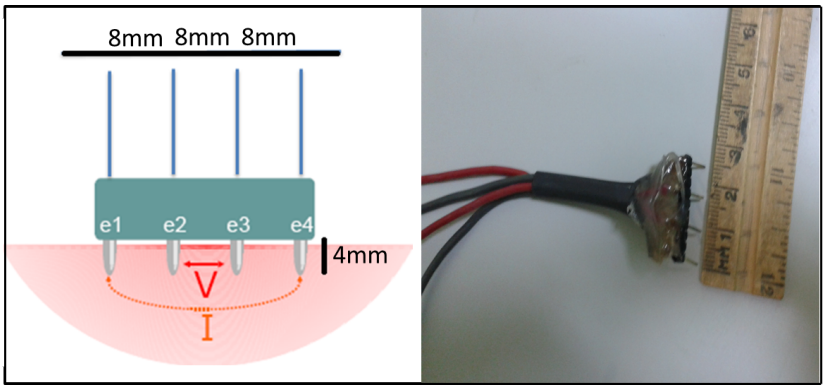

Figure 4.2: Four-terminal configuration electrodes

In principle, because no current flows through the voltage measurement circuit, the injected currents completely flows through the sample and the voltage drop at the sample is the same that the detection circuit record. According to S.Laufer, this configuration gives a better signal to noise ratio when compared to the square shape configuration [18], and the effect of electrode polarization on the results is minimized in the four-electrode measurement compared with two electrode configuration[26].

4.1.3 Dissection tools

The surgical tools that were used are: scalpel blade holder and disposable blades, surgical scissors, tissue forceps, and dissection pan.

4.1.4 Softwares and programs

Computer program for data acquiring

A LABVIEW program was designed and built to communicate and control the Microtest 6379 impedance analyzer using PC. In this research work, the number of frequencies was 20, and the range was from 1 KHz to 300 KHz. Figure (4.3) shows the front panel for this program.

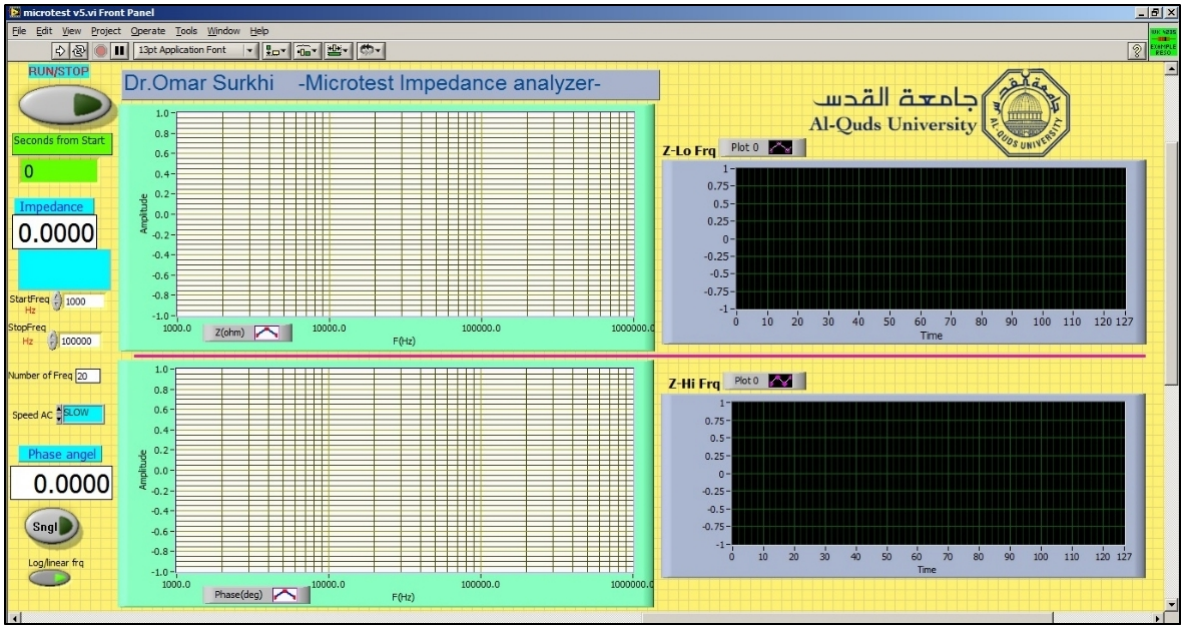

Figure 4.3: LABVIEW program for Data acquiring

The self-designed program has the following features:

- Ability to select number of frequencies.
- Ability to select ranges of frequencies.
- Ability to choose the type of plots to display(a function of frequency or a function of time).

Computer program for data analysis

A MATLAB program was designed and built for data analysis; appendix A contains the MATLAB program codes. Moving average filter was selected with 25 span window to smooth data and to remove artifacts.

The program has the following features:

- Ability to fit impedance data into Cole-Cole model.
- Ability to plot impedance module and phase angel variations with time and to plot their relative changes as shown in figure (4.4).

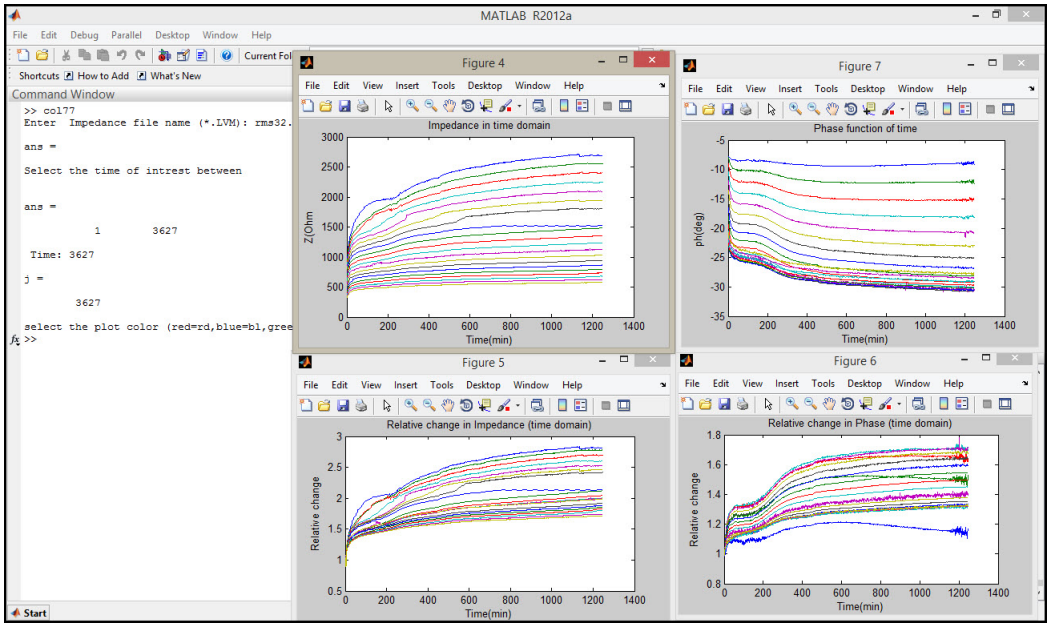

Figure 4.4: Matlab plots of impedance module and phase angel variations with time

- Ability to plot impedance modules and phase angel as function of frequency as shown in figure (4.5).

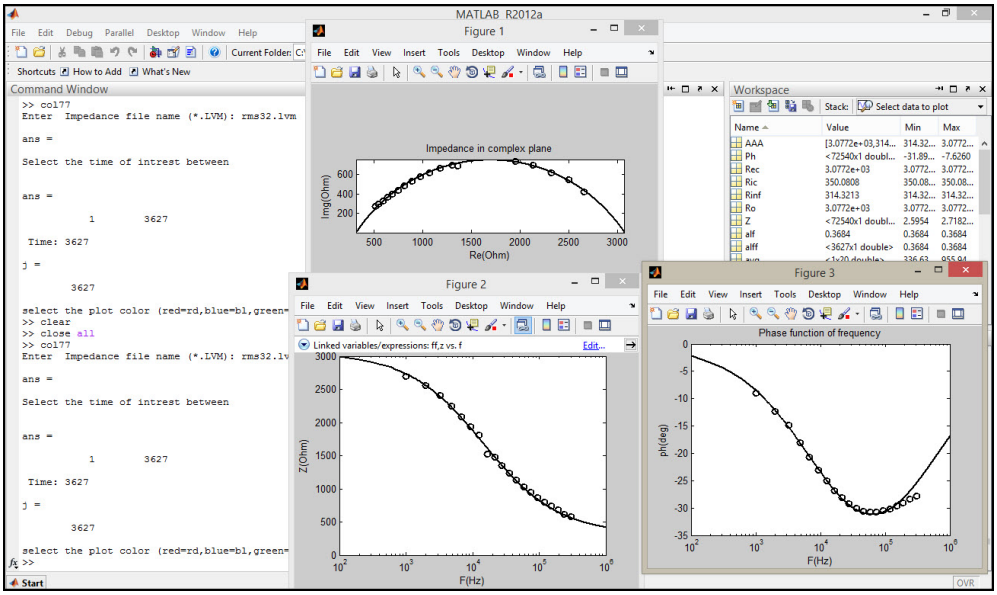

Figure 4.5: Matlab plots of impedance modules and phase angel in frequency domain

- Ability to calculate and plot cell parameters as shown in figure (4.6).

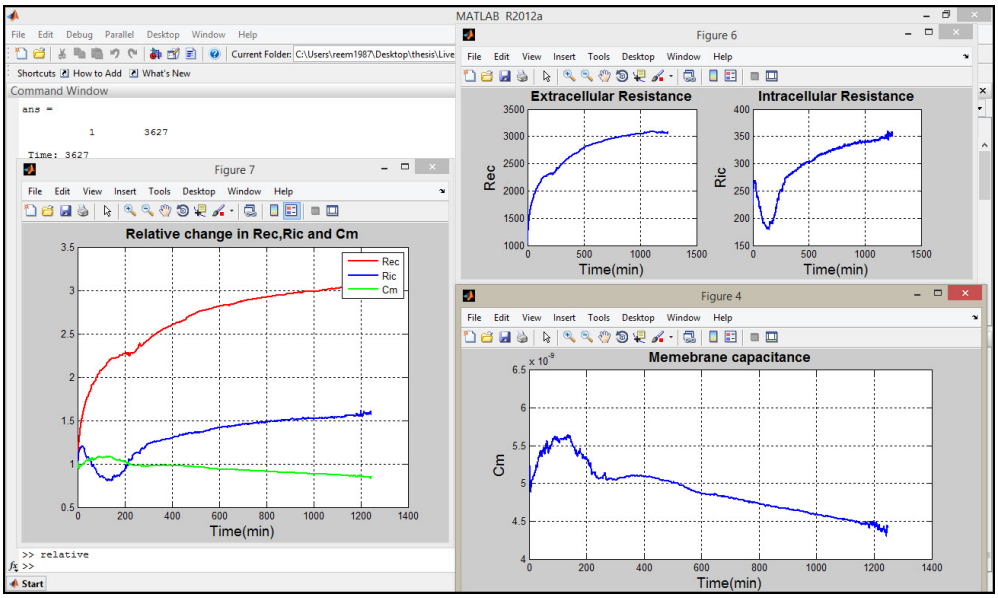

Figure 4.6: Matlab plots of cell parameters

- Ability to calculate Cole-Cole parameters as shown in figure (4.7).

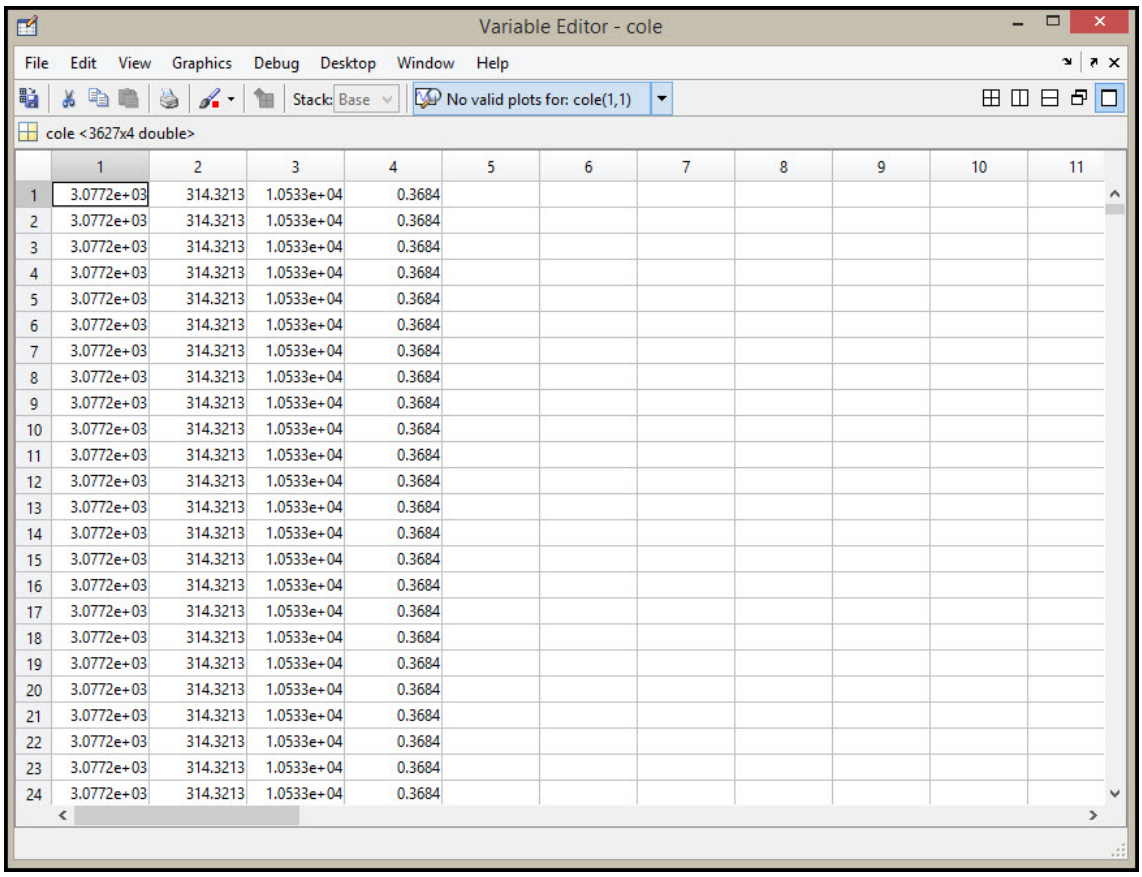

	1	2	3	4	5	6	7	8	9	10	11
1	3.0772e+03	314.3213	1.0533e+04	0.3684							
2	3.0772e+03	314.3213	1.0533e+04	0.3684							
3	3.0772e+03	314.3213	1.0533e+04	0.3684							
4	3.0772e+03	314.3213	1.0533e+04	0.3684							
5	3.0772e+03	314.3213	1.0533e+04	0.3684							
6	3.0772e+03	314.3213	1.0533e+04	0.3684							
7	3.0772e+03	314.3213	1.0533e+04	0.3684							
8	3.0772e+03	314.3213	1.0533e+04	0.3684							
9	3.0772e+03	314.3213	1.0533e+04	0.3684							
10	3.0772e+03	314.3213	1.0533e+04	0.3684							
11	3.0772e+03	314.3213	1.0533e+04	0.3684							
12	3.0772e+03	314.3213	1.0533e+04	0.3684							
13	3.0772e+03	314.3213	1.0533e+04	0.3684							
14	3.0772e+03	314.3213	1.0533e+04	0.3684							
15	3.0772e+03	314.3213	1.0533e+04	0.3684							
16	3.0772e+03	314.3213	1.0533e+04	0.3684							
17	3.0772e+03	314.3213	1.0533e+04	0.3684							
18	3.0772e+03	314.3213	1.0533e+04	0.3684							
19	3.0772e+03	314.3213	1.0533e+04	0.3684							
20	3.0772e+03	314.3213	1.0533e+04	0.3684							
21	3.0772e+03	314.3213	1.0533e+04	0.3684							
22	3.0772e+03	314.3213	1.0533e+04	0.3684							
23	3.0772e+03	314.3213	1.0533e+04	0.3684							
24	3.0772e+03	314.3213	1.0533e+04	0.3684							

Figure 4.7: Cole parameters

4.1.5 Tissue samples (liver tissue)

In this resarch work, measurements were performed at Materials Lab (Al-Quds University). Four-terminal configuration electrodes were built and used for measurements in experiments, ten rabbits (weighing 415-800 gm, 5 male rabbit, and 5 female rabbits) were used in experiments. Lab temperature was recorded in each experiment. Experiments were performed for different duration periods.

Table 4.2: Samples and lab conditions

Samples	Weight (gm)	Sex	Temperature (C^o)	Date of measurements
Sample 1	803	F	15	16/2/2015
Sample 2	697	M	13	23/2/2015
Sample 3	675	F	15	24/2/2015
Sample 4	750	M	17	28/2/2015
Sample 5	480	M	17	1/3/2015
Sample 6	455	F	16	2/3/2015
Sample 7	515	M	20	10/3/2015
Sample 8	420	M	20	14/3/2015
Sample 9	415	F	18	15/3/2015
Sample 10	420	F	19	18/3/2015

4.2 Experimental protocol

Ten rabbits (weighing 415-800 gm, 5 male rabbit, and 5 female rabbits) were used in experiments. Subject was anesthetized with Ether, once adequate anaesthesia had been achieved, subject was dissected and the abdomen was opened while it alive. Electrodes were inserted on the liver, measurements were taken for 30 minutes, then liver was excised. After liver excision, measurements were taken for longer periods (5-22) hours. Figure (4.8) shows the experimental setup.

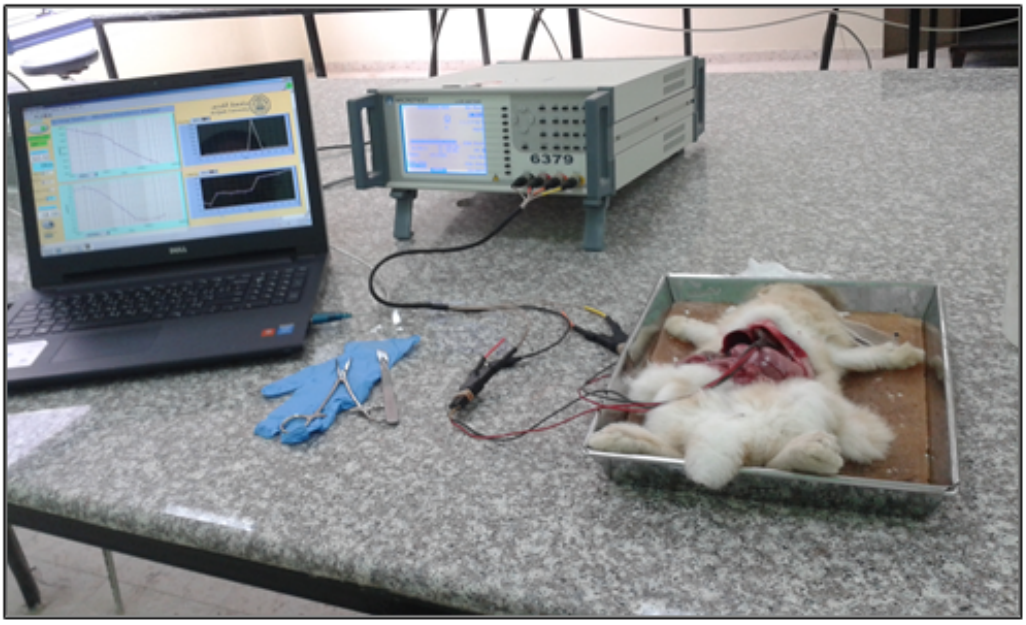

Figure 4.8: Experiment setup

The detailed protocol is described in the following steps :

1. Subject was anesthetized using Ether.
2. Subject was dissected by opening the abdomen by a midline incision.
3. Subject was killed in a merciful way by increasing the dosage of anesthesia.
4. Liver was excised.
5. Electrodes were inserted in liver .
6. Continuous bioimpedance measurements were taken at 20 frequencies, ranging from 1 KHz to 300 KHz for different periods (5-22 hours).

Chapter 5

Results and Discussion

In this chapter the results of experiments are presented as follows :

1. Measured impedance and phase.
2. Cole parameters.
3. Cell parameters.
4. Extracellular and intracellular volumes.

Some results are presented as absolute values and others are presented as relative values.

5.1 Measured impedance and phase

The results of the measured impedance are as follows:

1. Impedance and phase variations with time.
2. Impedance in the complex plane.
3. Impedance and phase in frequency domain.

5.1.1 Impedance and phase variations with time

In this research work, experiments were performed on 10 subjects. Bioimpedance measurements were taken from liver tissue in the β dispersion region at 20 frequencies range from 1 KHz to 300 KHz. Bioimpedance measurements were taken after organ extraction in order to study impedance variations with time and how tissue impedance changes with time after organ extraction. Figures (5.1) and (5.2) show sample (4) measured impedance (module, phase) variations respectively with time.

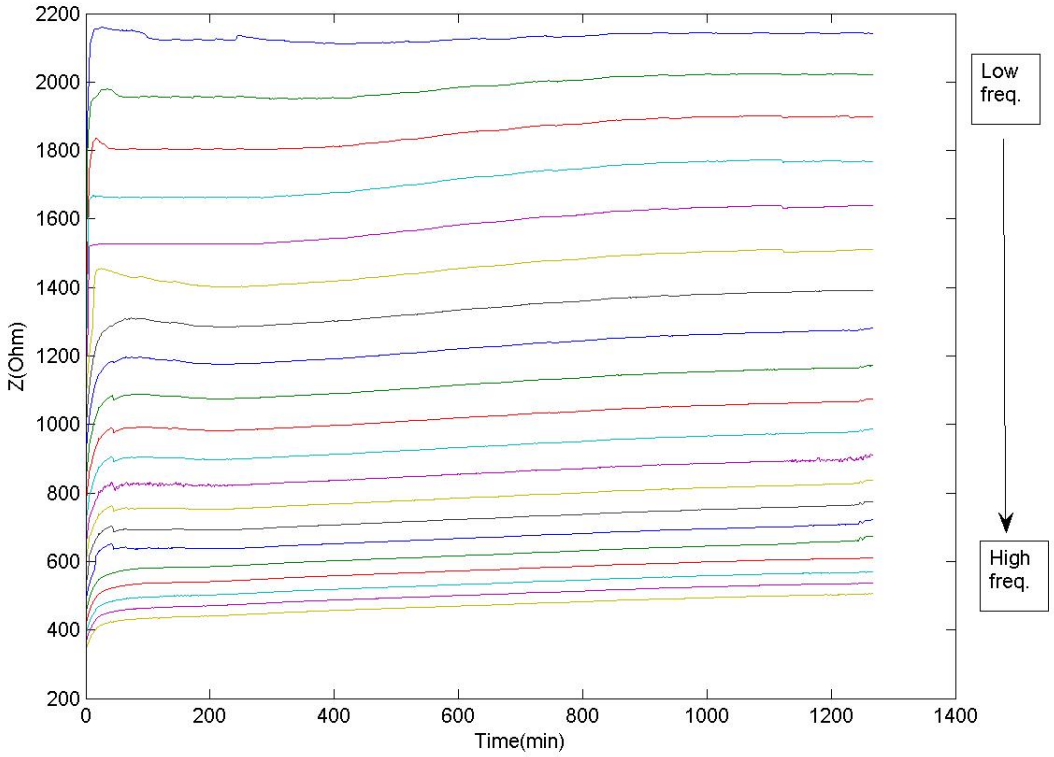

Figure 5.1: Impedance module variation with time (sample 4). Each coloured curve represents impedance variations with time at a specific frequency in ascending manner, the upper curves represent impedance variations with time at low frequencies, while the lower curves represent impedance variations at high frequencies.

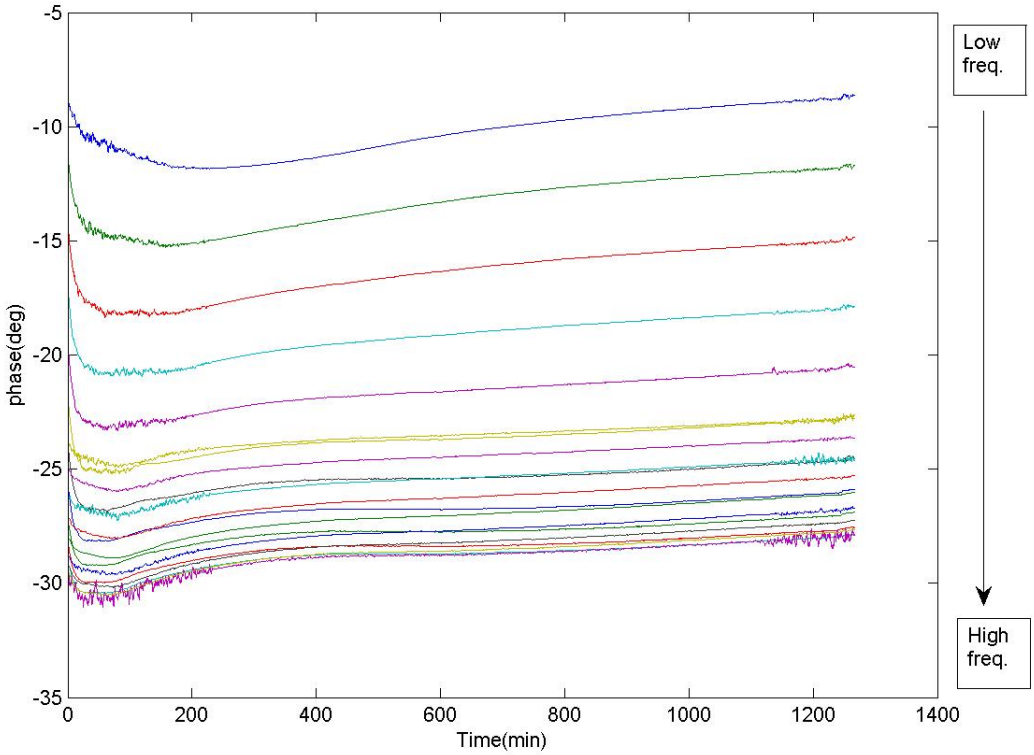

Figure 5.2: Impedance phase variation with time (sample 4). Each coloured curve represents impedance phase variations with time at a specific frequency in ascending manner, the upper curves represent impedance phase variations at low frequencies, while the lower curves represent impedance variations with time at high frequencies.

The general behavior for tissue under ischemia can be noticed; there is an increase in impedance of tissue with time. The possible explanation for this rise in impedance stems from ischemic effects; stoppage of blood flow into the liver leads to rise in resistivity. According to Gabriel et al. blood has a much lower resistivity than liver tissue has [3]. Results of the ten samples are shown in Appendix B figure (1) and figure (2). Figure (1) shows impedance module variations with time for the ten samples, and figure (2) shows impedance phase variations with time for the ten samples.

5.1.2 Impedance in the complex plane

After measurements were taken from liver tissue, bioimpedance measurements were fitted into Cole model in order to extrapolate Cole parameters. Cole parameters (R_0, R_∞, α and f_c) are the base of the BIS data analysis, and fitting the complex BIS measurements data onto the Cole equation (3.2) and then extracting the Cole parameters has become a common practice in BIS applications. The aim of this research work is to monitor structural changes of cells in a ischemic tissue by relating the evolution of Cole parameters with time to the morphology of cells in a ischemic tissue. This aim was achieved by focusing on the evolution of Cole parameters with time, particularly R_0 which represents the impedance of the ECW volume, and R_∞ which represents the equivalent impedance of the parallel combinations of ICW impedance and ECW impedance, and then relating these changes to the structural changes of cells undergo ischemia and necrosis. Figure (5.3) shows impedance in complex plane (real vs imaginary) for sample (3) at different times of the experiment.

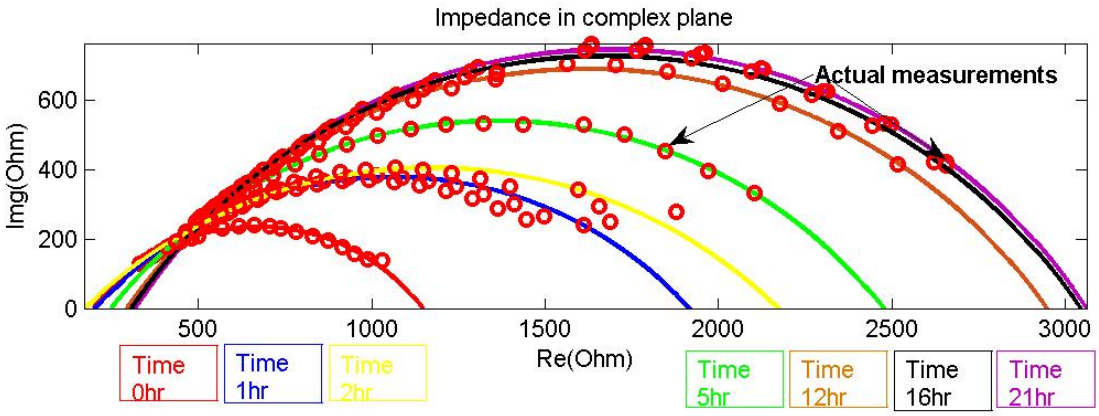

Figure 5.3: Impedance in complex plane (sample 3). Each coloured continuous semicircle denotes the corresponding Cole model at a specific time, the 20 small circles denote the measured impedance at 20 frequencies; each small circle represents the average reading of 20 readings before and after the corresponding reading. The crosses denote extrapolated impedance at zero frequency (R_0) and extrapolated impedance at infinite frequency (R_∞).

As it can be observed from figure (5.3), the actual measured impedance fits Cole model with excellent accuracy; correlation coefficient between Cole model and the actual measurements is 0.9986.

As it can be observed from figure (5.3), the general behavior for tissue under ischemia is an increase in impedance with time. As mentioned before, the possible explanation for this rise in impedance stems from ischemic effects; stoppage of blood flow into the liver leads to rise in resistivity. According to Gabriel et al. blood has a much lower resistivity than liver tissue has [3]. It can be noticed that R_0 increased largely compared to R_∞. R_0 represents the impedance of the ECW volume, while R_∞ represents the impedance of the ICW and ECW volumes which is the equivalent impedance of the parallel combinations of ICW impedance and ECW impedance and this is the explanation for the observable change in the order of variations between R_0 and R_∞. Results of the 10 samples are shown in Appendix B figure (3), which shows impedance in complex plane (real vs imaginary) for the ten samples at different times of each experiment.

5.1.3 Impedance in frequency domain

The measured bio-impedance is a function of the injected electrical current frequency. In order to discriminate cell parameters, impedance of ischemic tissue was studied as a function of frequency. At low frequency, measured impedance represents extracellular resistance (R_e) and at high frequency, the measured impedance represents equivalent resistance of intracellular and extracellular resistances. Figures (5.4) and (5.5) show measured impedance (module, phase) respectively in frequency domain for sample(3).

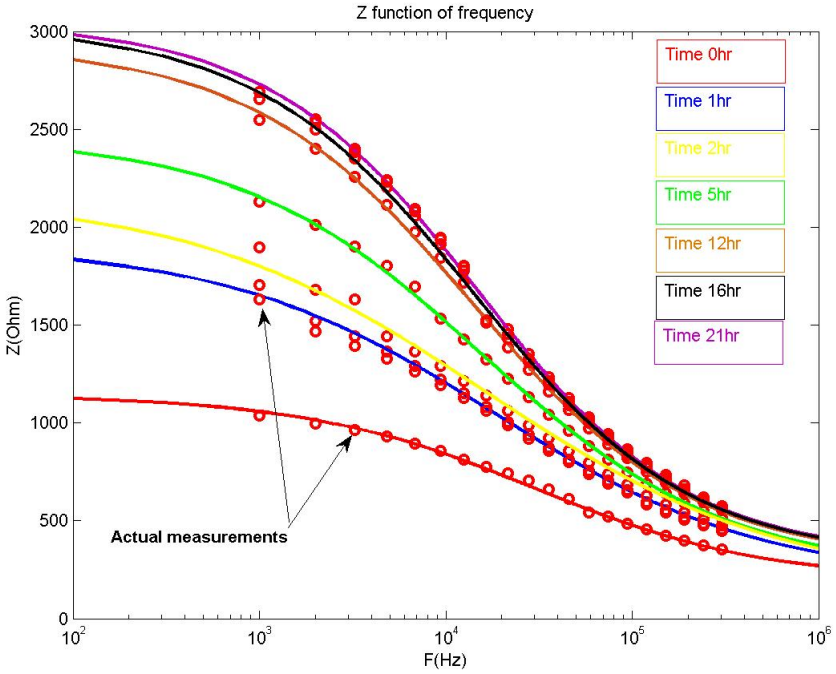

Figure 5.4: Impedance module in frequency domain (sample 3). Each coloured continuous curve denotes the corresponding impedance module of Cole model at a specific time as a function of frequency, the 20 small circles denote the actual measured impedance module at 20 frequencies. Each small circle represents the average reading of 20 readings before and after the corresponding reading.

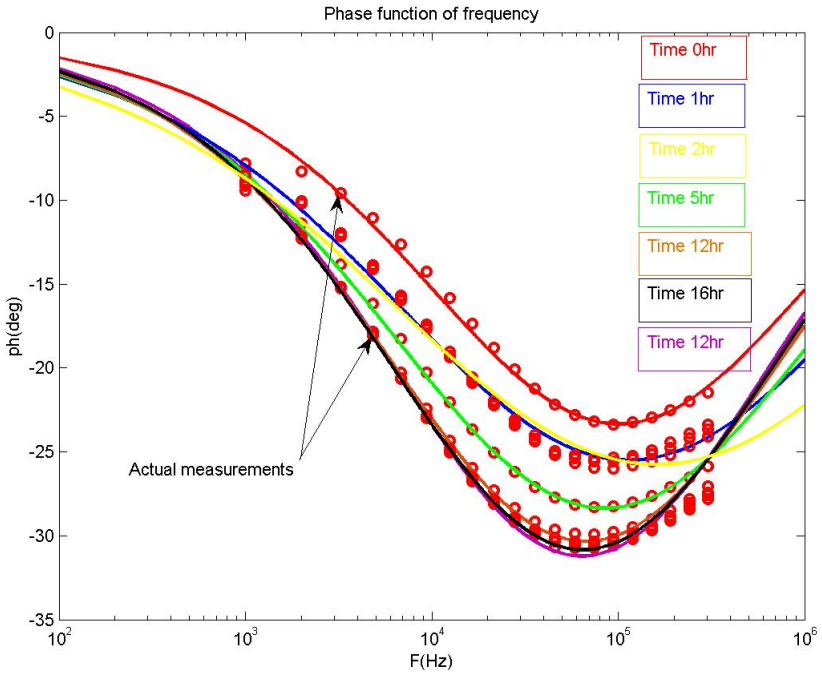

Figure 5.5: Phase in frequency domain (sample 3). Each coloured continuous curve denotes the corresponding impedance phase of Cole model at a specific time as a function of frequency, the 20 small circles denote the actual measured impedance phase at 20 frequencies. Each small circle represents the average reading of 20 readings before and after the corresponding reading.

As it can be noticed, impedance of ischemic tissue increases in with time. The second observation can be noticed is that R_0 increased largely compared to R_∞. R_0 represents the impedance of the ECW volume, while R_∞ represents the impedance of the ICW and ECW volumes which is the equivalent impedance of the parallel combinations of ICW and ECW and this is explains the difference of the order of variations between R_0 and R_∞. Results of the 10 samples are shown in Appendix B figure (4) and figure (5). Figure (4) which shows impedance module in frequency domain for the ten samples at different times of each experiment. Figure (5) shows impedance phase in frequency domain for the ten samples at different times of each experiment.

5.2 Cole parameters

Cole parameters are extrapolated after impedance measurements were fitted to Cole model. These parameters are : Impedance at zero frequency (R_0), Impedance at infinite frequency R_∞, characteristic frequency f_c, and characteristic parameter (α). This section presents results of Cole parameters and contains analysis of the general behavior of these parameters in order to relate Cole parameters changes with time to cell parameters changes of ischemic tissue. Cole analysis includes analysis of 8 samples for 5 hours, and analysis of 5 samples for longer experimental duration for 19 hours. These results are summarized in table (5.1) and table (5.2) in which relative changes of the four Cole parameters are shown in these tables as the relative mean value $\pm$ standard deviation for measurements every 30 minutes in table (5.1), and the relative mean value $\pm$ standard deviation for measurements every 1 hour in table (5.2).

Table 5.1: Cole parameters of 8 samples for 300 min (Relative Mean $\pm$ Standard Deviation)

Time	$R_0 \pm$ SD (Ω)	$R_\infty \pm$ SD (Ω)	$f_c \pm$ SD (Hz)	$\alpha \pm$ SD
30 min	1.125$\pm$ 0.086	1.059$\pm$ 0.137	0.897$\pm$ 0.077	1.00$\pm$ 0.07
60 min	1.192$\pm$ 0.067	1.081$\pm$ 0.160	0.85$\pm$ 0.070	1.01$\pm$ 0.087
90 min	1.226$\pm$ 0.076	1.079$\pm$ 0.178	0.832$\pm$ 0.075	1.021$\pm$ 0.098
120 min	1.250$\pm$ 0.084	1.076$\pm$ 0.186	0.817$\pm$ 0.071	1.026$\pm$ 0.100
150 min	1.268$\pm$ 0.092	1.078$\pm$ 0.179	0.809$\pm$ 0.067	1.027$\pm$ 0.098
180 min	1.282$\pm$ 0.097	1.077$\pm$ 0.1884	0.805$\pm$ 0.064	1.029$\pm$ 0.086
210 min	1.290$\pm$ 0.105	1.083$\pm$ 0.172	0.806$\pm$ 0.066	1.025$\pm$ 0.074
240 min	1.295$\pm$ 0.113	1.104$\pm$ 0.143	0.808$\pm$ 0.072	1.01$\pm$ 0.065
270 min	1.300$\pm$ 0.126	1.128$\pm$ 0.129	0.809$\pm$ 0.081	1.00$\pm$ 0.056
300 min	1.306$\pm$ 0.141	1.144$\pm$ 0.130	0.811$\pm$ 0.091	0.996$\pm$ 0.056

Table (5.1) contains results of 8 samples; sample 5 and sample 7 were excluded form the analysis. In sample 5 experiment was interrupted, and there was electrode repositioning in sample 7, so the two samples were excluded from analysis.

Table 5.2: Cole parameters of 5 samples for 19 hours (Relative Mean ± Standard Deviation)

Time(hour)	$R_0 \pm$ SD (Ω)	$R_\infty \pm$ SD (Ω)	$f_c \pm$ SD (Hz)	$\alpha \pm$ SD
1	1.191± 0.049	1.130 ± 0.176	0.889 ± 0.048	0.979 ± 0.082
2	1.25 ± 0.057	1.117 ± 0.216	0.848 ± 0.072	0.995 ± 0.102
3	1.30 ± 0.069	1.111 ± 0.192	0.822 ± 0.072	1.00 ± 0.080
4	1.32 ± 0.082	1.147 ± 0.143	0.819 ± 0.084	0.98 ± 0.044
5	1.355 ± 0.113	1.192 ± 0.127	0.816 ± 0.106	0.970 ± 0.034
6	1.378 ± 0.143	1.231 ± 0.129	0.817 ± 0.129	0.955 ± 0.034
7	1.395 ± 0.165	1.264 ± 0.133	0.821 ± 0.147	0.944 ± 0.035
8	1.413 ± 0.187	1.296 ± 0.173	0.826 ± 0.163	0.932 ± 0.038
9	1.427 ± 0.204	1.324 ± 0.140	0.834 ± 0.177	0.922 ± 0.040
10	1.439 ± 0.214	1.355 ± 0.147	0.842 ± 0.188	0.910 ± 0.043
11	1.447 ± 0.221	1.381 ± 0.155	0.850 ± 0.200	0.90 ± 0.045
12	1.458 ± 0.229	1.406 ± 0.159	0.856 ± 0.209	0.893 ± 0.046
13	1.465 ± 0.234	1.427 ± 0.166	0.864 ± 0.218	0.885 ± 0.047
14	1.472 ± 0.239	1.449 ± 0.169	0.87 ± 0.225	0.879 ± 0.048
15	1.478 ± 0.243	1.468 ± 0.174	0.877 ± 0.232	0.873 ± 0.048
16	1.48 ± 0.248	1.485 ± 0.175	0.883 ± 0.239	0.868 ± 0.0486
17	1.486 ± 0.250	1.50 ± 0.180	0.890 ± 0.243	0.864 ± 0.048
18	1.491 ± 0.255	1.515 ± 0.1845	0.896 ± 0.249	0.861 ± 0.048
19	1.491 ± 0.255	1.52 ± 0.184	0.902 ± 0.252	0.860 ± 0.050

These results are presented and analyzed in the following sections to infer the general behavior for each parameter. Cole parameters results of the 10 samples are shown in Appendix B figure (6-10).

5.2.1 Impedance at zero frequency:

In order to study the general behavior of the extrapolated resistance at zero frequency R_0 which represents the impedance of cell ECW volume; analysis of R_0 was done for 5 hours experimental duration and it was repeated for longer experimental duration for 19 hours. Figure (5.6) is a bar chart for the averaged values of R_0 with time up to 5 hours of 8 samples, and figure (5.7) is a bar chart for the averaged values of R_0 with time up to 19 hours of 5 samples.

Analysis of impedance at zero frequency for 5 hours

From figure (5.6), it can be noticed that the general behavior is a continuous increase.

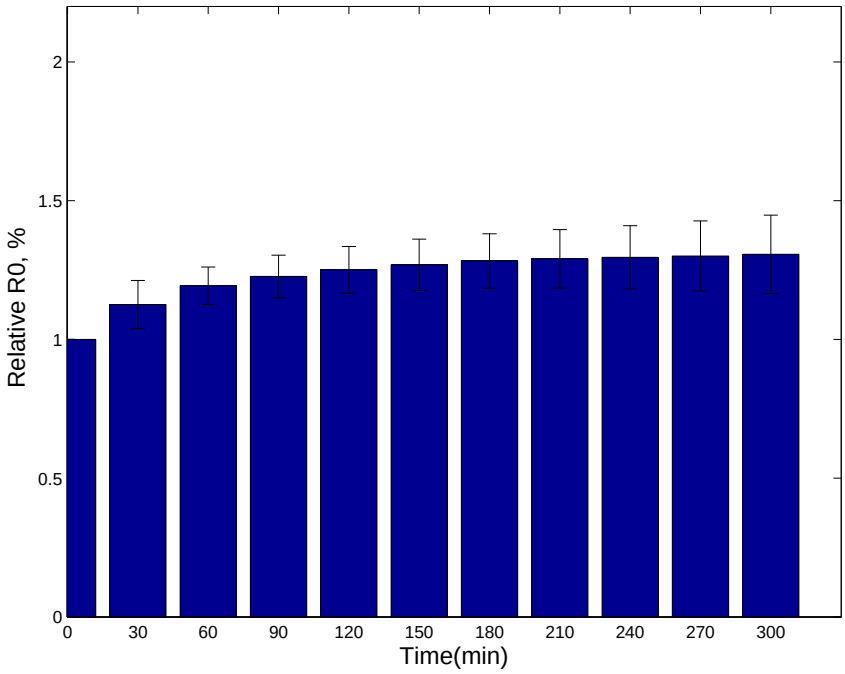

Figure 5.6: Relative change in R_0 of 8 samples for 5 hours. Each bar represents the average relative change in R_0 of 8 samples at the same period of time after organ extraction.

Analysis of impedance at zero frequency for longer experimental duration (19 hours)

In order to study the general behavior of R_0 for a longer experimental duration after organ extraction; analysis was repeated for 5 samples for longer experimental duration (19 hours). Figure (5.7) is a bar chart for the averaged values of R_0 with time up to 19 hours of 5 samples.

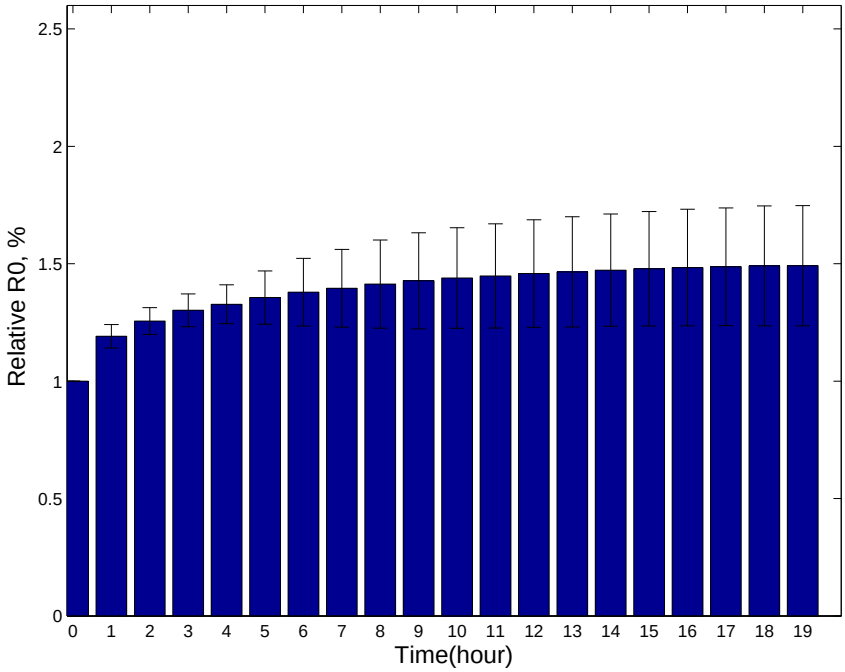

Figure 5.7: Relative change in R_0 of 5 samples for 19 hours. Each bar represents the average relative change in R_0 of 5 samples at the same period of time after organ extraction.

The possible explanations for these results are built on necrosis mechanism. As blood supply cut off, metabolism and ATP concentration decline rapidly causing reduced activity of ion pumps, which leads to changes in ions distribution between intracellular and extracellular spaces. Eventually, the result is fluid shift toward cell which causes cell swelling. The first stage of necrosis is an influx of water from outside the cell toward the cell; this explains the increase in extracellular resistance. The rise in extracellular resistance is the result of a decline in extracellular fluid volume and as a consequent of narrowed extracellular paths for low frequency current.

5.2.2 Impedance at infinite frequency

In order to study the general behavior of the extrapolated resistance at infinite frequency R_∞ which represents the equivalent impedance of the parallel combinations of ICW impedance and ECW impedance; analysis of R_∞ was done for 5 hours experimental duration and it was repeated for longer experimental duration for 19 hours. Figure (5.8) is a bar chart for the averaged values of R_∞ with time up to 5 hours of 8 samples, and figure (5.9) is a bar chart for the averaged values of R_∞ with time up to 19 hours of 5 samples.

Analysis of impedance at infinite frequency for 5 hours

Figure (5.8) shows the general behavior of 8 samples for 5 hours from liver excision. The general pattern for its behavior shows a similar behavior pattern as R_0, it can be noticed that the general behavior is a continuous increase.

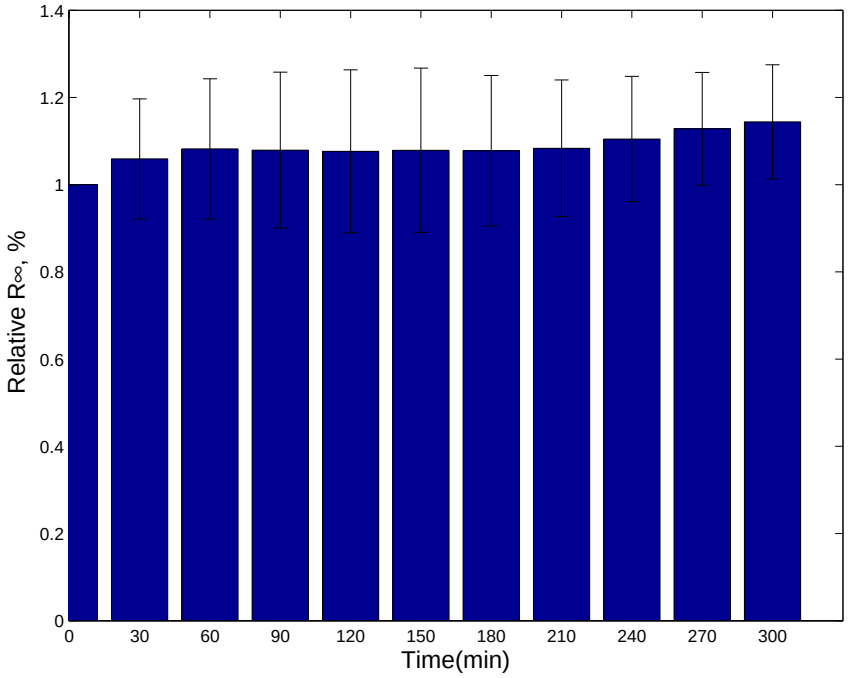

Figure 5.8: Relative change in R_∞ of 8 samples for 5 hours. Each bar represents the average relative change in R_∞ of 8 samples at the same period of time after organ extraction.

Analysis of impedance at infinite frequency for longer experimental duration (19 hours)

In order to study the general behavior of R_0 for a longer experimental duration after organ extraction; R_∞ analysis was repeated for 5 samples for longer experimental duration (19 hours). Figure (5.9) is a bar chart for the averaged values of R_∞ with time up to 19 hours of 5 samples.

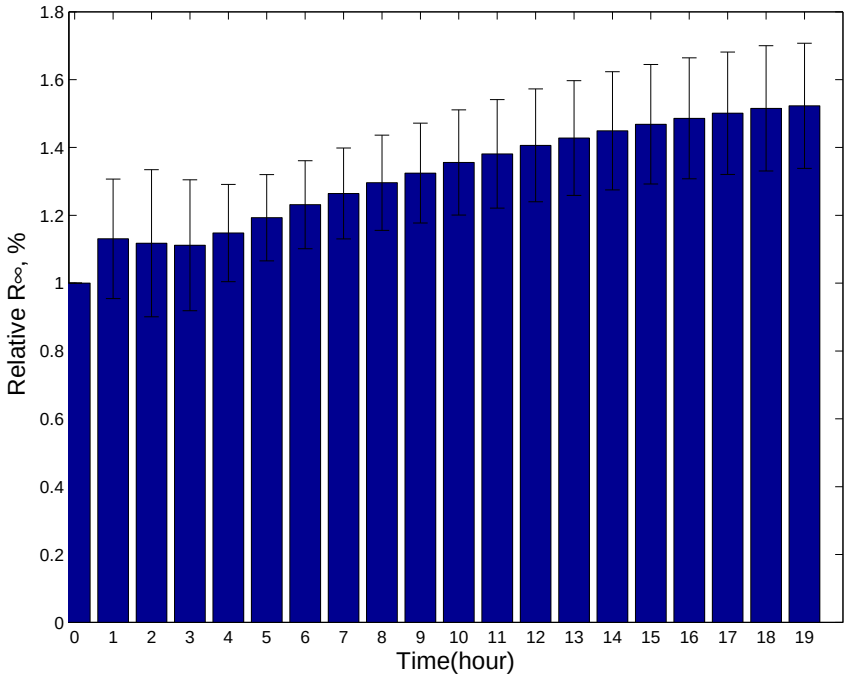

Figure 5.9: Relative change in R_∞ for 19 hours. Each bar represents the average relative change in R_∞ of 5 samples at the same period of time after organ extraction.

As can be noticed from the bar charts, the general behavior is a continuous increase. The increase in R_∞ is due to intracellular organelles swelling as can be seen from figure (3.10) which illustrates necrosis consequences stages; most notably the mitochondria and endoplasmic reticulum, which causes narrowed intracellular paths for current.

5.2.3 Characteristic frequency

The characteristic frequency f_c indicates the frequency with the highest reactance. As it can be seen from literature, characteristic frequency f_c could be used to characterize different tissues. Some researchers concluded that f_c is one of the parameters that could be used to in tissue characterization and differentiation between normal and ischemic tissue [20]. In order to study the general behavior of this parameter; analysis of f_c was done for 5 hours experimental duration and it was repeated for longer experimental duration for 19 hours. Figure (5.10) is a bar chart for the averaged values of f_c with time up to 5 hours of 8 samples, and figure (5.11) is a bar chart for the averaged values of f_c with time up to 19 hours of 5 samples.

Analysis of characteristic frequency for 5 hours

Figure (5.10) shows the general behavior of 8 samples for 5 hours from liver excision. The general pattern for its behavior is to decrease in a continuous manner.

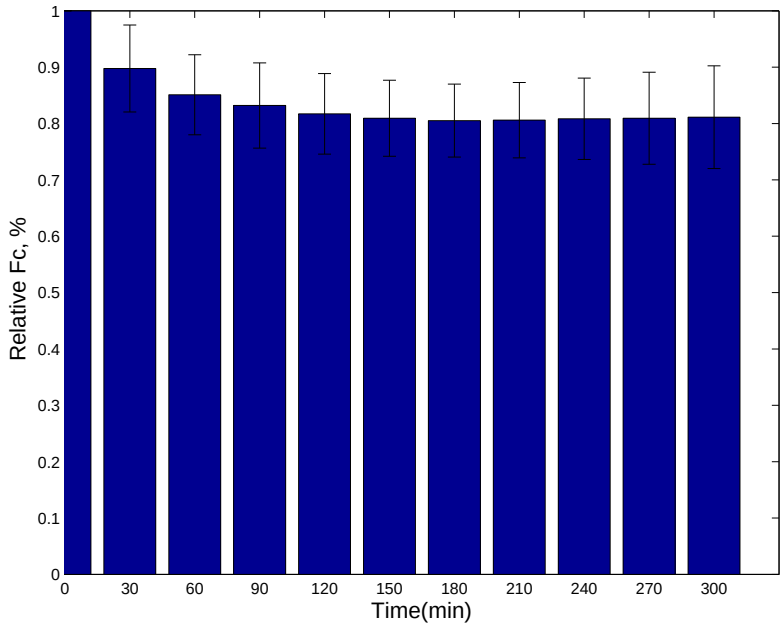

Figure 5.10: Relative change in f_c of 8 samples for 5 hours. Each bar represents the average relative change in f_c of 8 samples at the same period of time after organ extraction.

Analysis of characteristic frequency for longer experimental duration (19 hours)

In order to study the general behavior of f_c for a longer experimental duration after organ extraction; f_c analysis was repeated for 5 samples for longer experimental duration (19 hours). Figure (5.11) is a bar chart for the averaged values of f_c with time up to 19 hours of 5 samples.

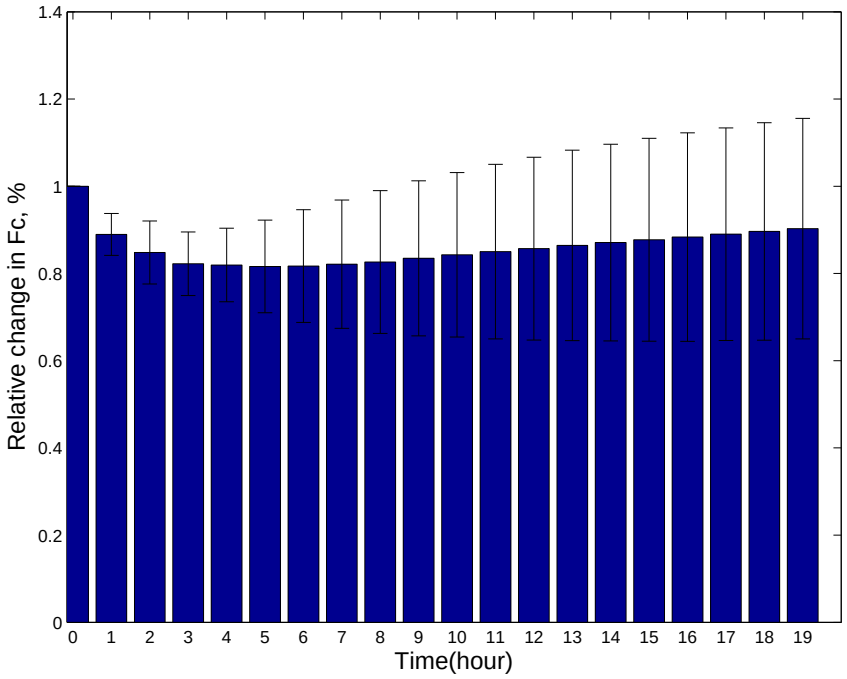

Figure 5.11: Relative change in f_c for 19 hours. Each bar represents the average relative change in f_c of 5 samples at the same period of time after organ extraction.

Characteristic frequency general behavior shows a decrease in its value with time. It has a clear predictable behavior, so it can be recommended as one of the best parameters that could be used in ischemic tissue monitoring.

5.2.4 Characteristic parameter

The characteristic parameter (α) denotes the shape factor. Analysis of α was done for 5 hours experimental duration and it was repeated for longer experimental duration for 19 hours. Figure (5.12) is a bar chart for the averaged values of α with time up to 5 hours of 8 samples, and figure (5.13) is a bar chart for the averaged values of $\alpha$with time up to 19 hours of 5 samples.

Analysis of characteristic parameter for 5 hours

Figure (5.12) shows the general behavior of 8 samples for 5 hours from liver excision. The general pattern for this parameter is not clear; it was hard to predict its general behavior.

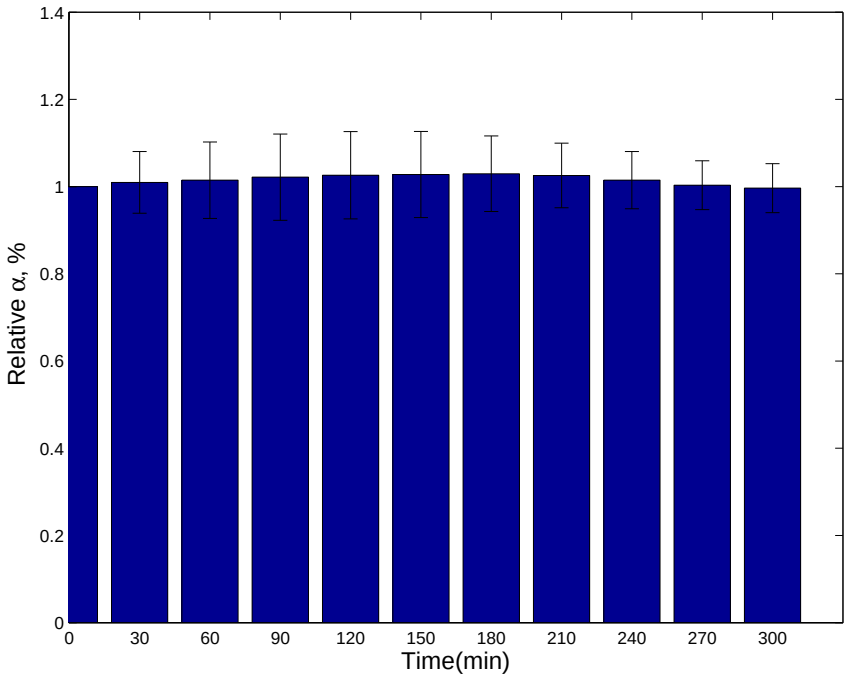

Figure 5.12: Relative change in α of 8 samples for 5 hours. Each bar represents the average relative change in α of 8 samples at the same period of time after organ extraction.

Analysis of characteristic parameter for longer experimental duration (19 hours)

α analysis was repeated for 5 samples for longer experimental duration (19 hours). Figure (5.13) is a bar chart for the averaged values of α with time up to 19 hours of 5 samples.

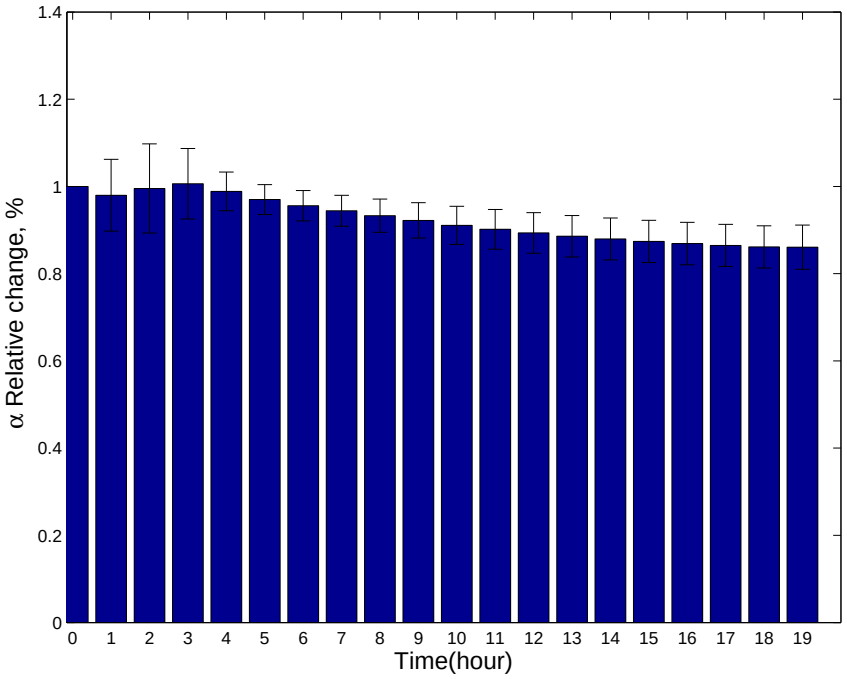

Figure 5.13: Relative change in Relative change in α for 19 hours. Each bar represents the average relative change in α of 5 samples at the same period of time after organ extraction.

The physical meaning of α is not clearly understood. There is no agreement about that; so the general behavior has not a significant importance in this research.

5.3 Cell parameters

In order to establish a relation between cellular morphological changes during cell ischemia and necrosis with bioimpedance measurements, cell parameters were calculated based on Cole parameters. The electrical model of biological tissue is shown in figure (5.14), it consists of a resistance for the extra-cellular electrolytic medium (R_e) - denoted by (R_{ECW}) in the figure - in parallel with the series combination of a resistance for the intra-cellular electrolytic medium (R_i) -denoted by (R_{ICW}) - and a capacitance for the cell membrane (Cm). R_e, R_i and Cm were estimated from Cole parameters.

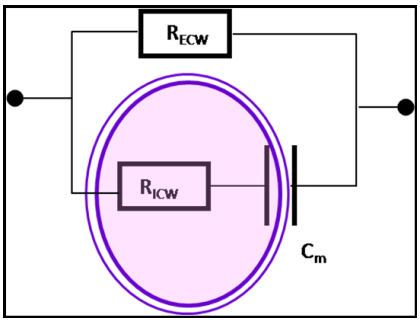

Figure 5.14: Electrical model of biological tissue

Membrane capacitance was calculated according to the following formula:

$$Cm = \frac{1}{\omega_{max}(Re + Ri)} \tag{5.1}$$

where ω_{max} is the radian characteristic frequency.

Impedance at infinite frequency R_∞ and impedance at zero frequency R_0 were estimated from Cole parameters. Extracellular resistance and intracellular resistance were estimated according to :

$$R_e = R_0 \tag{5.2}$$

$$R_i = \frac{R_0.R_\infty}{R_0 - R_\infty} \tag{5.3}$$

Since extracellular resistance is the resistance at zero frequency , analysis was performed for membrane capacitance (Cm) intracellular resistanceR_i only.

5.3.1 Membrane capacitance

In order to study the general behavior of membrane capacitance (Cm) ; analysis of (Cm) was done for 5 hours experimental duration and it was repeated for longer experimental duration for 19 hours.

Analysis of membrane capacitance for 5 hours

Figure (5.15) is a bar chart for the averaged values of (Cm) with time up to 5 hours of 8 samples.

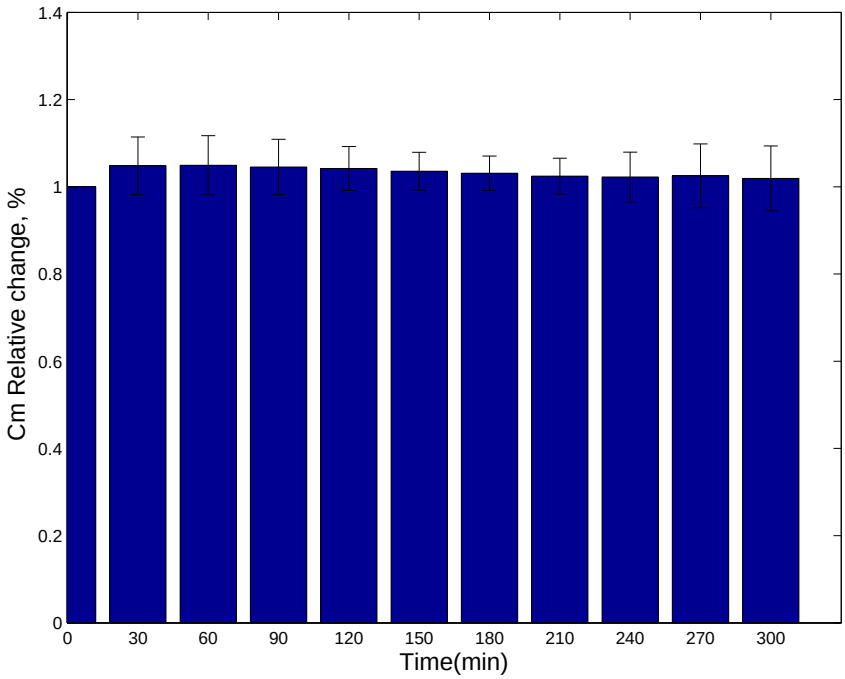

Figure 5.15: Relative change in (Cm) of 8 samples for 5 hours. Each bar represents the average relative change in (Cm) of 8 samples at the same period of time after organ extraction.

Analysis of membrane capacitance for 19 hours

In order to study the general behavior of (*Cm*) for a longer experimental duration after organ extraction; analysis was repeated for 5 samples for longer experimental duration (19 hours). Figure (5.16) is a bar chart for the averaged values of (*Cm*) with time up to 19 hours of 5 samples.

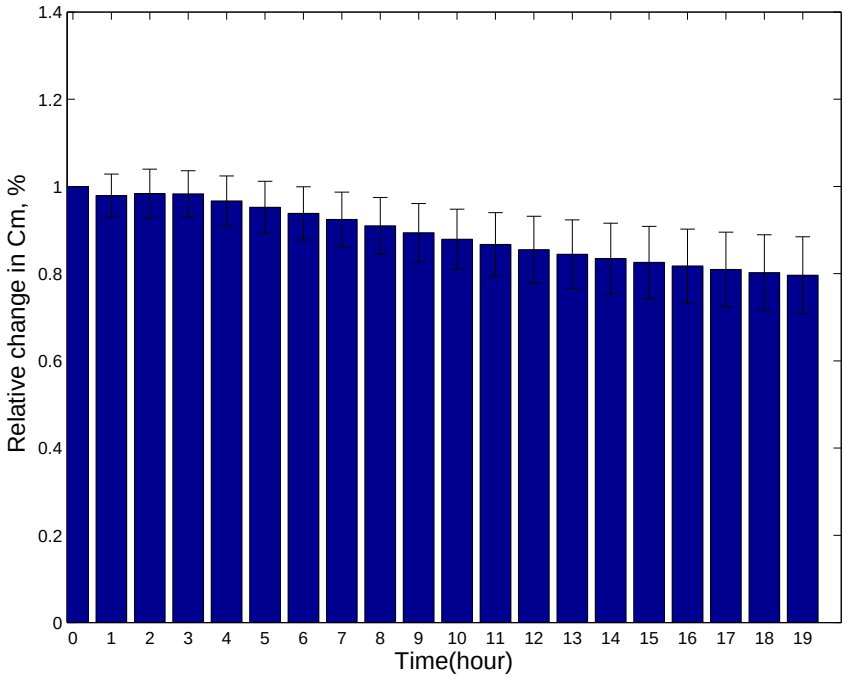

Figure 5.16: Relative change in Cm for 19 hours for 5 samples. Each bar represents the average relative change in (*Cm*) of 5 samples at the same period of time after organ extraction.

The noticeable behavior of changing in membrane capacitance was increasing in capacitance to reach its maximum peak and then a continuous decreasing. The possible explanation for the rise in its capacitance is due to the increase in membrane surface resulting from cell swelling. The time at which membrane capacitance starts to decrease could be described as the time at which membrane starts to breakdown and loss its integrity due to the lysosomal enzymes that are released within the cell. Results of the 10 samples are shown in Appendix B figure (10) which shows relative change in Cm for 5 hours for all samples.

5.3.2 Intracellular resistance and extracellular resistance

In order to study the general behavior of intracellular resistance R_i; analysis of R_i was done for 5 hours experimental duration and it was repeated for longer experimental duration for 19 hours.

Analysis of intracellular resistance for 5 hours

Figure (5.17) is a bar chart for the averaged values of R_i with time up to 5 hours of 8 samples.

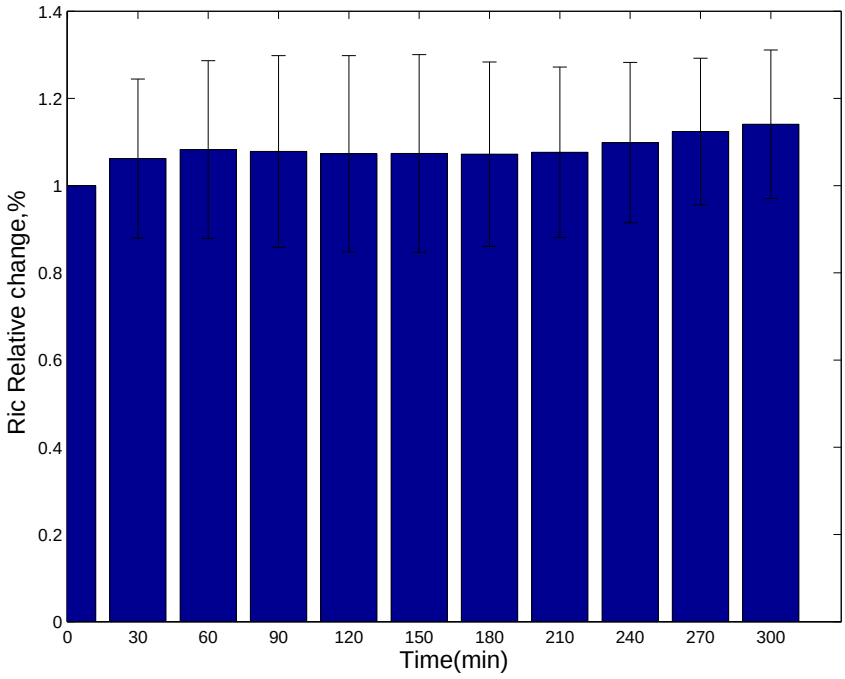

Figure 5.17: Relative change in R_i for 5 hours. Each bar represents the average relative change in R_i of 8 samples at the same period of time after organ extraction.

Analysis of intracellular resistance for 19 hours

In order to study the general behavior of R_i for a longer experimental duration after organ extraction; analysis was repeated for 5 samples for longer experimental duration (19 hours). Figure (5.18) is a bar chart for the averaged values of R_i with time up to 19 hours of 5 samples.

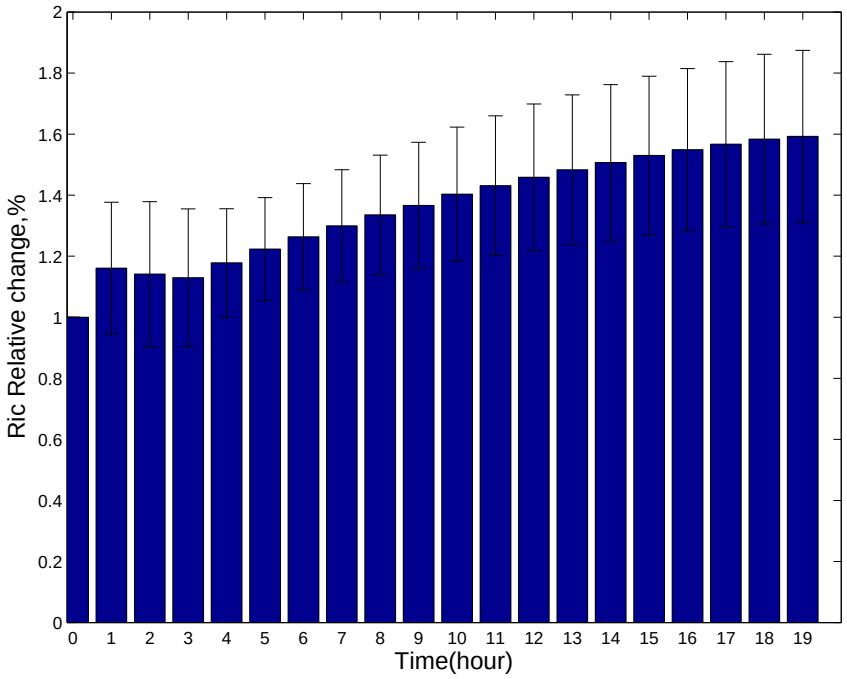

Figure 5.18: Relative change in R_i for 19 houres. Each bar represents the average relative change in R_i of 5 samples at the same period of time after organ extraction.

As can be noticed from the bar charts, the general behavior is a continuous increase. The increase in R_i is due to intracellular organelles swelling as can be seen from figure (3.10) which illustrates necrosis consequences stages; most notably the mitochondria and endoplasmic reticulum, which causes narrowed intracellular paths for current.

5.4 Extracellular and intracellular volumes

In order to monitor structural changes of cells in a ischemic tissue and to study the shift of fluid between cell compartments; ECW and ICW volumes were predicted from the extrapolated R_0 and R_∞, and by using equations formulated from Hanai's theory, which describes the effect that a concentration of nonconductive material has on the apparent resistivity (ρ_a) of the surrounding conductive fluid. Tissue under measurement (TUM) was modelled simply as a cylinder with a height (L) of 8 mm and a diameter of 2 mm as can be seen in figure (5.19).

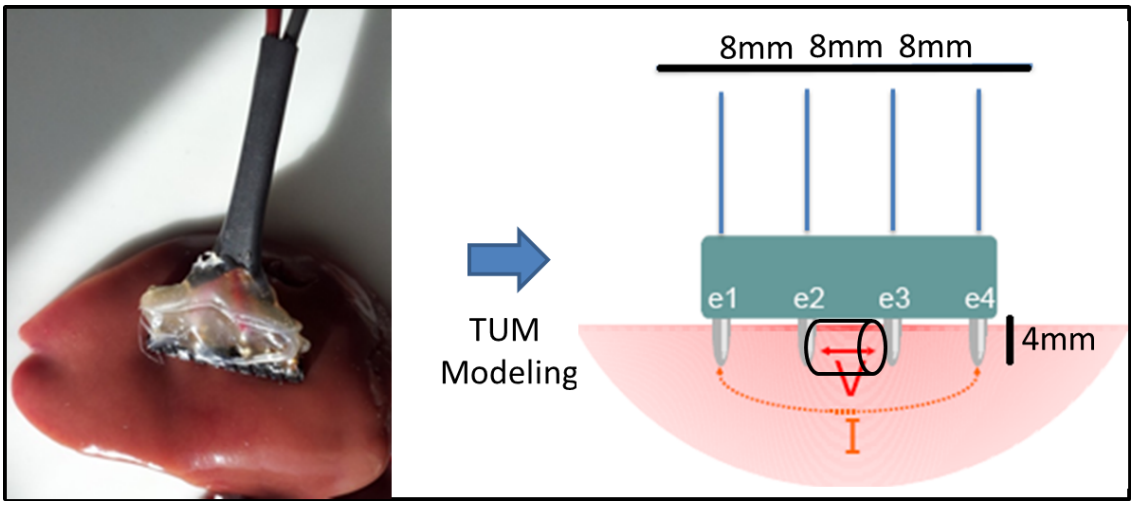

Figure 5.19: Model of liver tissue under measurement

Based on Hanai's theory, the apparent resistivity is given by:

$$\rho_a = \frac{\rho}{(1-C)^{3/2}} \tag{5.4}$$

where ρ_a is the apparent resistivity of a conductive material, ρ is the actual resistivity of a conductive material, and C is the volumetric concentration of the nonconductive material contained in the mixture.

This apparent resistivity must be substituted to ρ in the resistance-volume relationship as follows :

$$R = \frac{\rho L^2}{V_{TTV}} \tag{5.5}$$

where R is the resistance, L is the cylinder hight of the modeled tissue, and V_{TTV} is the total tissue volume.

5.4.1 Extracellular volume

At low frequency, C is equal to $(1 - V_{ECW})/V_{TTV}$, as only the ECW volume V_{ECW} is conducting, the apparent ECW resistivity ρ_a is :

$$\rho_a = \rho[\frac{V_{TTV}}{V_{ECW}}]^{3/2} \tag{5.6}$$

Thus, using (5.4)-(5.6), ECW volume can be written as :

$$V_{ECW} = [\frac{\rho_{ECW} L^2 V_{TTV}^{1/2}}{R_0}]^{2/3} \tag{5.7}$$

where R_0 is the extrapolated impedance at zero frequency.

5.4.2 Intracellular volume

Similarly as for ECW, Hanai's theory can be applied to impedance measurements at high frequency in order to calculate ICW volume. In that case the volume concentration of non-conducting tissues is

$$C = 1 - \frac{V_{ICW} + V_{ECW}}{V_{TTV}} \tag{5.8}$$

The apparent resistivity of total tissue water (TTW) is :

$$\rho_{a\infty} = \rho_{\infty}[\frac{V_{ECW} + V_{ICW}}{V_{TTV}}]^{-3/2} \tag{5.9}$$

Assuming that the mean total water resistivity ρ_{∞} is linearly related to ECW and ICW resistivities in proportion to their respective volumes as proposed by De Lorenzo et al [6] :

$$\rho_{a\infty}(V_{ECW} + V_{ICW}) = \rho_{ECW}V_{ECW} + \rho_{ICW}V_{ICW} \tag{5.10}$$

The TTW resistance R∞ may be written, according to (5.4) as :

$$R_{\infty} = \frac{R_{ECW}R_{ICW}}{R_{ECW} + R_{ICW}} = \frac{\rho L^2}{V_{TTV}} \tag{5.11}$$

Substitution of (5.9) and (5.10) into (5.11) yields

$$\frac{R_{ECW}R_{ICW}}{R_{ECW} + R_{ICW}} = \frac{(\rho_{ECW}V_{ECW} + \rho_{ICW}V_{ICW})V_{TTV}^{1/2}L^2}{(V_{ECW} + V_{ICW})^{5/2}} \tag{5.12}$$

Substituting the value of R_0 or R_{ECW} from (5.7) into the left hand side of (5.12):

$$\frac{R_{ICW}\rho_{ECW}}{(R_{ECW} + R_{ICW})V_{ECW}^{3/2}} = \frac{(\rho_{ECW}V_{ECW} + \rho_{ICW}V_{ICW})}{(V_{ECW} + V_{ICW})^{5/2}} \tag{5.13}$$

After some rearrangements for the above equation, ICW volume can be calculated by solving the following equation :

$$(1+\frac{V_{ICW}}{V_{ECW}})^{5/2} = \frac{R_{ECW}+R_{ICW}}{R_{ICW}}(1+K_\rho\frac{V_{ICW}}{V_{ECW}}) \tag{5.14}$$

it could be written as follows :

$$(1+\frac{V_{ICW}}{V_{ECW}})^{5/2} = \frac{R_0}{R_\infty}(1+K_\rho\frac{V_{ICW}}{V_{ECW}}) \tag{5.15}$$

where k_ρ is the ICW to ECW resistivity ratio, $k_\rho = \frac{\rho_{ICW}}{\rho_{ECW}}$, and R_∞ is the extrapolated impedance at infinite frequency.

The ionic composition of ECW, composed of plasma and interstitial fluid and its resistivity is close to that of saline, about 40 Ω cm as was suggested by De Lorenzo et al [6], it was also used by Michel Jaffrin [34]. The ionic composition of ICW depends upon the type of cells. Thus the ionic composition of the entire ICW is uncertain and its mean resistivity cannot be measured directly. The value of k_ρ is used just as in the mentioned researches.

Using linear approximation for the above equation so it could be replaced by a simpler one.

$$\frac{R_{ECW}+R_{ICW}}{R_{ICW}} = \frac{(1+\frac{V_{ICW}}{V_{ECW}})^{5/2}}{(1+K_\rho\frac{V_{ICW}}{V_{ECW}})} \tag{5.16}$$

After taking the range of $\frac{V_{ICW}}{V_{ECW}}$ between 0.5 to 2 and k_ρ has a value between (3.4 to 3.8) or by taking the average for this range and taking k_ρ = 3.6 , the fitted curve is shown in the figure (5.20).

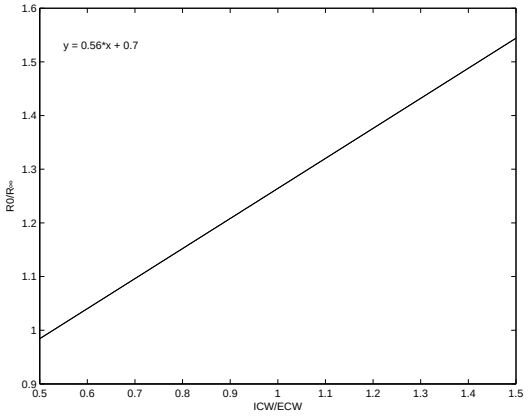

Figure 5.20: Linear approximatiom

The linear relationship could be written as follows :

$$\frac{V_{ICW}}{V_{ECW}} = 1.786\frac{R_0}{R_\infty} - 1.25 \tag{5.17}$$

Figure (5.21) shows the estimated ECW and ICW, overestimation problem arises from using the above procedure in ICW calculations.

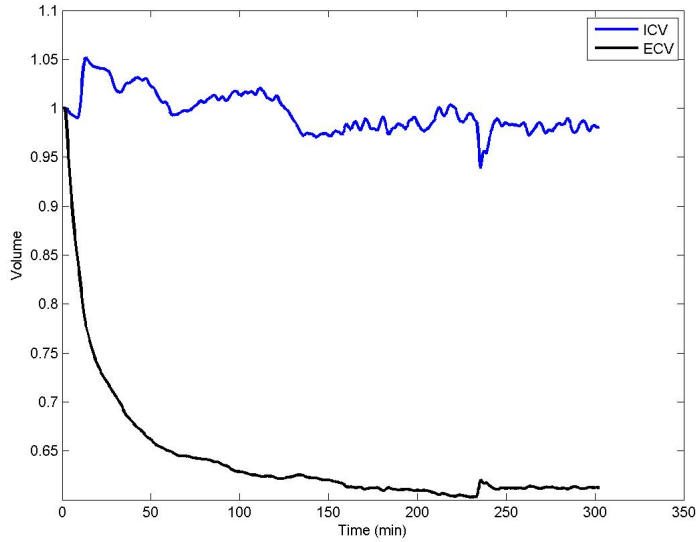

Figure 5.21: ECV and ICV (sample 1)

To overcome this problem, another method was used to calculate ICW, this method was described as the best method for ICW calculation as Buendia stated in his comparative study about body fluid estimation [11].

$$ICV = TTV - ECV \tag{5.18}$$

Figure (5.22) shows the estimated ECW and ICW as it can be calculated by using the above equation:

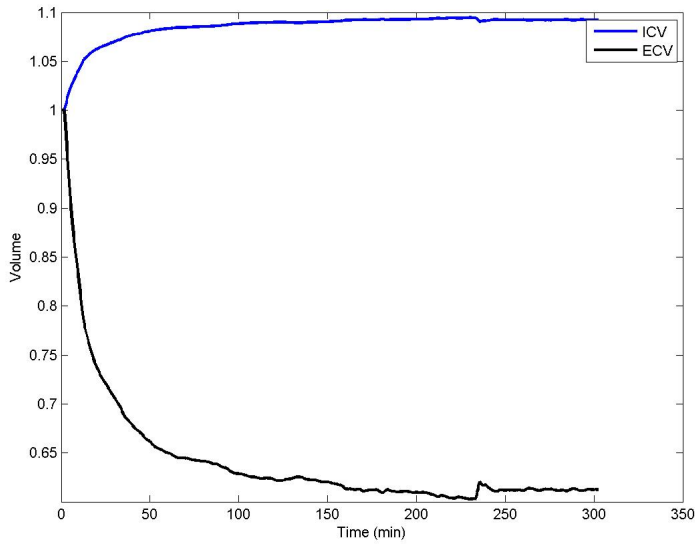

Figure 5.22: ECV and ICV (sample 1)

Results of the 10 samples are shown in Appendix B figure (11) which shows ECV and ICV for all samples.

Since Pie chart is a great visual aid for displaying data; ECW and ICW are represented in a pie chart to illustrate the ratio between ECW and ICW. Figure (5.23) shows ECW and ICW in a pie chart after different period from liver excision .

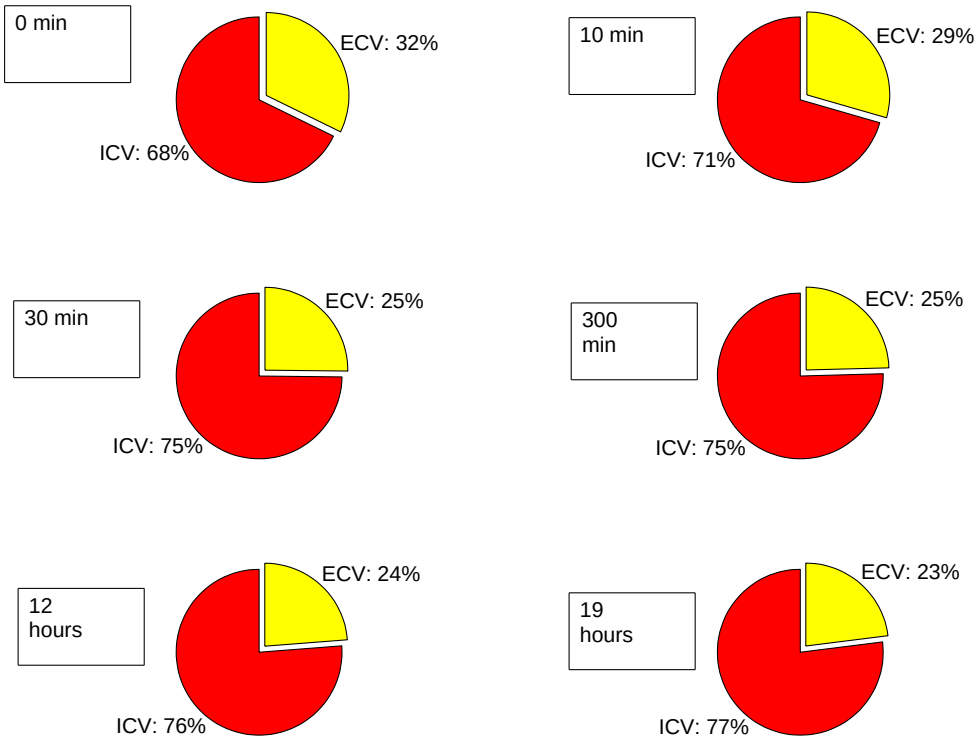

Figure 5.23: Cell morphological changes with time (sample 2)

By representing the ratio between ECV and ICV graphically in a pie chart, human eye finds it very easy to compare data and quickly see the evolution of cell morphology changes for ischemic tissue and draw conclusions. It is obvious that there is a fluid shift form outside the cell toward the cell due to necrosis process.

5.5 Discussion

5.5.1 Discussion of results

In this resarch work, measurements were performed at Materials Lab (Al-Quds University). Bioimpedance measurements were taken at 20 frequencies, ranging from 1 KHz to 300 KHz for different periods (5-22 hours). This section discusses experimental results presented in this chapter.

The general behavior for tissue under ischemia can be noticed from figure (5.1); the general behavior is an increase in impedance with time. This behavior can be seen in figure (5.3) which shows impedance in complex plane, and (5.4) which shows impedance module in frequency domain. This behaviour was reported in other researches, [20], [21], [24]. The possible explanation for this rise in impedance stems from ischemic effects; stoppage of blood flow into the liver leads to rise in resistivity. According to Gabriel *et al.* blood has a much lower resistivity than liver tissue has [3]. Changing in temperature could be mentioned as another effect leads to initial rise in the impedance after liver excision.

Cole parameters (R_0,R_∞,α and f_c) are the base of the BIS data analysis, and fitting the complex BIS measurements data onto Cole equation (3.2) and then extracting the Cole parameters has become a common practice in BIS applications. In fact, Cole parameters extracted from the obtained BIS data have been used as the major indicators of the physiological and pathological status in BIS applications such as fluid management system in heart failure [10], hemodialysis monitoring [13], hepatic tumor diagnosis [18] and other applications.

By focusing on Cole parameters, R_0 and R_∞ particularly, from figure (5.6) and figure (5.8), it can be observed that R_0 shows an increase in its value while R_∞ shows a similar behavior pattern as R_0, but the order of variation is lower. As it can be observed from figures, R_0 increases in a continuous manner and these results match with results in [20], [21], [23].

R_∞ shows a similar behavior pattern as R_0, but the order of variation is lower, this result matches with result in [20], [23]. Other researchers observed that R_∞ stayed constant during the initial 6 hours and then increased [21].

The possible explanations for these results are built on necrosis mechanism. As blood supply cut off, metabolism and ATP concentration decline rapidly causing reduced activity of ion pumps, which leads to changes in ions distribution between intracellular and extracellular spaces. Eventually, the result is fluid shift toward cell which causes cell swelling. As can be seen in chapter 3 figure (3.10), the first stage of necrosis is an influx of water from outside the cell toward the cell; this explains the increase in extracellular resistance.

The rise in extracellular resistance is the result of a decline in extracellular fluid volume and as a consequent of narrowed extracellular paths for low frequency current. The increase in R_∞ is due to intracellular organelles swelling as can be seen from figure (3.10) which illustrates necrosis consequences stages; most notably the mitochondria and endoplasmic reticulum, which causes narrowed intracellular paths for current. In general, when comparing the general behavior of R_0 and R_∞, it can be noticed that R_0 behavior is more clearer than R_∞ behavior, this could be explained based on cell morphology; cell contains organelles, these organelles act as small cells inside the cell which makes it hard to predict R_∞ behavior.

Characteristic frequency general behavior shows a decrease in its value with time; this can be noticed from figure(5.10), which matchs results in [23]. As it can be seen from literature, this parameter could be used to characterize different tissues. It was concluded that f_c is one of the parameters that could be used to in tissue characterization and differentiation between normal and ischemic tissue [20]. Moreover, it was found that (f_c) has a complementary resolution on steatosis levels detection [17].

Figure (5.12) show the general behavior of the characteristic parameter (α), it is obvious that α parameter starts to increase with time, then it starts to decrease. The

physical meaning of α is not clearly understood. There is no agreement about that; so the general behavior has not a significant importance in this research.

By looking at the general behavior of Cole parameters; it can be noticed that R_0 and f_c can be recommended as the best parameters that could be used to characterize ischemic tissue. R_0 and R_∞ are a key process in fluid estimation as was shown in the previous section of this chapter.

Figure (5.15) shows membrane capacitance changing with time. The noticeable behavior of changing in membrane capacitance was increasing in capacitance to reach its maximum peak and then a continuous decreasing. The possible explanation for the rise in its capacitance is due to the increase in membrane surface resulting from cell swelling. The time at which membrane capacitance starts to decrease could be described as the time at which membrane starts to breakdown and loss its integrity due to the lysosomal enzymes that are released within the cell.

Changes of membrane capacitance (*Cm*) reflect the alterations of membrane structure; membrane capacitance increases and reaches its peak reflecting cell swelling, and then decreases reflecting membrane breakdown. This timed pattern of capacitance membrane changes could be used to monitor tissue undergoes ischemia. Another contribution for monitoring cell structural changes is in comparative studies for comparing preservative solutions used to preserve organ during transplantation surgeries. Comparing this timed pattern could be used as a method for estimating the reversibility domain which helps in comparing organ preservative solutions efficiency.

These results of cell parameters particularly extracellular resistance R_e and *Cm* match with morphological changes for cell under necrosis; starting from influx of water from extracellular space toward cell causing cell swelling and finally membrane breakdown and continuity between inside and outside the cell.

In general, it can be noticed from previous results that the changes in its values are not statistically significant difference; it could be related to the tissue behavior,

since other tissues have a remarkable significant difference in its impedance under ischemic conditions [23]. Small number of samples could be a reason for the behavior of ischemic liver tissue in this research work.
In general, when comparing analysis results for 5 hours experimental duration with results for 19 hours experimental duration, it can be noticed that SD results of the first analysis stage is less than SD results of the second analysis stage, and this leads to conclude that results for the first hours of the experiments are more reliable than the results for longer experimental durations.

ECV and ICV results shown in figure (5.21) and figure (5.22) agree with previous results and explanations that relate BIS measurements with the morphological changes in ischemic tissue. It show the decline in extracellular fluid volume and the increment in intracellular fluid volume. Figure (5.23)shows ECV and ICV ratio changes after different period of time in pie charts. By representing the ratio between ECV and ICV graphically in a pie chart, human eye finds it very easy to compare data and quickly see the evolution of cell morphology changes for ischemic tissue and draw conclusions. Moreover, Pie chart is a great visual aid for displaying data and adding a touch of professionalism to display data. It is obvious that there is a fluid shift form outside the cell toward the cell due to necrosis process.

5.5.2 Sources of errors

The main sources of errors are:

- Measurements errors associated with the technical aspects of impedance measurement including performance of the instrument (Multi Frequency Impedance Analyzer Microtest), and electrodes. In this research work, four-terminal configuration electrodes were used , the outer electrodes are for current injection, and the inner are for voltage. In principle, because no current flows through the voltage measurement circuit, the injected currents completely flows through the sample and the voltage drop at the sample is the same that the detection circuit record. According to S.Laufer, this configuration gives a better signal to noise ratio when compared to the square shape configuration [18], and the effect of electrode polarization on the results is minimized in the four-electrode measurement compared with two electrode configuration[26]. During measurements, electrodes were secured simply by their insertion into the tissue. Since the organ was extracted, artifacts caused by breathing and spasmodic movement were avoided.
- Stray parasitic capacitances creates a characteristic bioimpedance data deviation that is especially noticeable at high frequencies. However, it is known from the literature that total-body impedance spectra show characteristic deviations from the theoretically expected Cole circle above 500 kHz. Scharfetter *et al.* recommended avoiding the use of high frequency values for the curve fitting process by setting an upper limit of 500 kHz [35]. In this research work, the frequency range is 1 k to 300 kHz which is less than 500 kHz.
- Errors associated with the prediction of Cole parameters. Any curve fitting process depends on the number of points to fit, the accuracy of the model and the reliability of the information contained in the measurement points. In BIS, it is possible to obtain the 4 Cole parameters with just 4 measurement points. In this research, the actual measured impedance fits Cole model with excellent accuracy; correlation coefficient between Cole model and the actual measurements is about 0.9986.

Chapter 6

Conclusions, Limitations and Future Work

6.1 Conclusions

In this thesis, we have proposed online ischemia monitoring system using BIS approach for continues monitoring of ischemia level in liver tissue. In addition, we have detected structural cell alterations during the event of cell ischemia and cell necrosis and confirmed the theoretical relation between cell morphological changes and the corresponding observed changes in electrical bioimpedance.

In the first chapter, we have motivated the selection of BIS technique as an online technique for ischemia continues monitoring and pointed out its importance in evaluation quality of liver tissue in transplanted surgeries, where one of the major risks in these kind of operations is tissue ischemia.

In chapter two, we have seen that bioimpedance approaches have attracted the interest of many researchers from different fields of specialization with biological, industrial and medical background for it's potential advantages of being applicable to be used, enables on-line monitoring, and requires low-cost instrumentation and low hazard. Moreover, we have introduced the main research areas that used bioimpedance spectroscopy approach in different applications; body composition assessment, cellular measurements, tissue classification, and tissue monitoring.

In chapter three, we have presented a brief theoretical background about liver anatomy and cell structure, cell death, electrical model of biological tissue and principles of BIS technique.

Chapter four contains the design of research experiments which includes the hardware and software requirements; the instruments and tools, Labview and Matlab programmes, and the experimental protocol.

Research results were presented and discussed in chapter five; the measured impedance variations with time, the measured impedance in frequency domain, and the measured impedance in the complex plain. The general behavior for tissue has been analyzed. Cole parameters were extrapolated from BIS measurements and their behavior and evolution was studied with respect to time. Then, cell parameters were estimated from Cole parameters. A detailed analysis for changes of cell parameters were done in parallel with explanations for these changes depending on the physiological mechanism of ischemia and necrosis bioprocess. These explanations give a confirmation of the established relation between cell morphological changes and the corresponding BIS measurements. ECV and ICV were estimated from BIS measurements with respect to time.

In addition to the previous results, we can point out some conclusions as listed below:

- Bioimpedance Data from the animal liver fitted with Cole-Cole model with excellent accuracy.
- R_0 and f_c can be recommended as the best parameters that could be used to characterize ischemic tissue.
- The observed electrical properties of ischemic tissue change in a consistent manner with the corresponding morphological changes of necrosis phases.
- The proposed system might have significant repercussions in the design of future inexpensive online instrument for ischemia continues monitoring.
- BIS measurements could be used as a method for estimating the reversibility domain which helps in comparing organ preservative solutions efficiency.

– The results will contribute to improve the success rate of human liver transplantation surgery.

6.2 Limitations

There were some limitations that we have faced by in this work listed as in the following:

- Four-terminal configuration electrodes were built and used for measurements in this research work, the configuration consists of four electrodes; the outer electrodes are the injection electrodes, and the inner electrodes are the detection electrode. This configuration is a straight line configuration with 8 mm distance between each two electrodes, and 4 mm long. The depth of electrodes cause a damage in tissue, the alternative option for this problem is to use surface electrodes.
- Lacking to medical equipment at Materials Lab to perform histology tests and visualize samples under microscope in order to test cellular structural changes during the events of cell ischemia and cell necrosis against microscopic visualization.
- There was a problem in performing clinical tests (enzymes ,biopsy) for tissue under measurement in order to establish a quantitative relation between chemical changes in ischemic tissue and structural changes that were predicted based on bioimpedance measurements.

6.3 Future Work

Further work in this research area is needed, the following are some suggested directions to complete this research contributions :

- Perform bioimpedance spectroscopy measurements using surface electrodes for different biological tissue.
- Studying the effect of environmental conditions BIS measurements; such as temperature.
- Testing cellular structural changes during the events of cell ischemia and cell necrosis against clinical tests (enzymes ,biopsy).
- Testing cellular structural changes during the events of cell ischemia and cell necrosis against histology tests.
- Use bioimpedance measurements technique to compare organ preservative solutions.

Bibliography

[1] R. Pethig and D. B. Kell. The passive electrical properties of biological systems: their significance in physiology, biophysics and biotechnology. *Physics in Medicine and Biology*, 32(8):933–970, Aug 1987. LR: 20081121; JID: 0401220; 0 (Proteins); 9007-49-2 (DNA); RF: 228; ppublish.

[2] S. Gabriel, R. W. Lau, and C. Gabriel. The dielectric properties of biological tissues: Iii. parametric models for the dielectric spectrum of tissues. *Physics in Medicine and Biology*, 41(11):2271–2293, Nov 1996. LR: 20081121; JID: 0401220; ppublish.

[3] C. Gabriel, S. Gabriel, and E. Corthout. The dielectric properties of biological tissues: I. literature survey. *Physics in Medicine and Biology*, 41(11):2231–2249, Nov 1996. LR: 20081121; JID: 0401220; RF: 64; ppublish.

[4] S. Gabriel, R. W. Lau, and C. Gabriel. The dielectric properties of biological tissues: Ii. measurements in the frequency range 10 hz to 20 ghz. *Physics in Medicine and Biology*, 41(11):2251–2269, Nov 1996. LR: 20081121; JID: 0401220; ppublish.

[5] C. Gabriel, A. Peyman, and E. H. Grant. Electrical conductivity of tissue at frequencies below 1 mhz. *Physics in Medicine and Biology*, 54(16):4863–4878, Aug 21 2009. JID: 0401220; 2009/07/27 [aheadofprint]; ppublish.

[6] A. De Lorenzo, A. Andreoli, J. Matthie, and P. Withers. Predicting body cell mass with bioimpedance by using theoretical methods: a technological review. *Journal of applied physiology (Bethesda, Md.: 1985)*, 82(5):1542–1558, May 1997. LR: 20131121; JID: 8502536; RWP5GA015D (Potassium); EIN: J Appl Physiol 1997 Dec;83(6):followi; RF: 50; ppublish.

[7] C. P. Earthman, J. R. Matthie, P. M. Reid, I. T. Harper, E. Ravussin, and W. H. Howell. A comparison of bioimpedance methods for detection of body cell mass change in hiv infection. *Journal of applied physiology (Bethesda, Md.: 1985)*, 88(3):944–956, Mar 2000. LR: 20131121; JID: 8502536; 0 (Anabolic Agents); 7H6TM3CT4L (Oxandrolone); ppublish.

[8] C. Earthman, D. Traughber, J. Dobratz, and W. Howell. Bioimpedance spectroscopy for clinical assessment of fluid distribution and body cell mass. *Nutrition in clinical practice : official publication of the American Society for Parenteral and Enteral Nutrition*, 22(4):389–405, Aug 2007. LR: 20100429; JID: 8606733; RF: 57; ppublish.

[9] M. Freiberger, P. Brunner, M. Mayer, O. I. Surkhi, P. J. Riu, and H. Scharfetter. Indicator for hydration balance during haemodialysis based on anisotropic fem. *Physiological Measurement*, 29(6):S479–89, Jun 2008. JID: 9306921; 2008/06/11 [aheadofprint]; ppublish.

[10] S. Weyer, M. D. Zink, T. Wartzek, L. Leicht, K. Mischke, T. Vollmer, and S. Leonhardt. Bioelectrical impedance spectroscopy as a fluid management system in heart failure. *Physiological Measurement*, 35(6):917–930, Jun 2014. JID: 9306921; 0 (Peptide Fragments); 0 (pro-brain natriuretic peptide (1-76)); 114471-18-0 (Natriuretic Peptide, Brain); 2014/05/20 [aheadofprint]; ppublish.

[11] R. Buendia, F. Seoane, K. Lindecrantz, I. Bosaeus, R. Gil-Pita, G. Johannsson, L. Ellegard, and L. C. Ward. Estimation of body fluids with bioimpedance spectroscopy: state of the art methods and proposal of novel methods. *Physiological Measurement*, 36(10):2171–2187, Oct 2015. JID: 9306921; 059QF0KO0R (Water); 2015/09/14 [aheadofprint]; ppublish.

[12] Yi-Yu Lu, Ji-Jer Huang, Yu-Jie Huang, and Kuo-Sheng Cheng. Cell growth characterization using multi-electrode bioimpedance spectroscopy. *Measurement Science and Technology*, 24(3):035701, 2013. URL `http://stacks.iop.org/0957-0233/24/i=3/a=035701`.

[13] M. Maasrani, M. Y. Jaffrin, and B. Boudailliez. Continuous measurements by impedance of haematocrit and plasma volume variations during dialysis. *Medical*

biological engineering computing, 35(3):167–171, May 1997. LR: 20061115; JID: 7704869; ppublish.

[14] Enas Qabaja. Characterization of human blood tissue using bioimpedance measurments, 2012. Master thesis , Al-Quds University.

[15] P. Aberg, I. Nicander, J. Hansson, P. Geladi, U. Holmgren, and S. Ollmar. Skin cancer identification using multifrequency electrical impedance–a potential screening tool. *IEEE transactions on bio-medical engineering*, 51(12):2097–2102, Dec 2004. LR: 20091111; JID: 0012737; ppublish.

[16] C. Skourou, A. Rohr, P. J. Hoopes, and K. D. Paulsen. In vivo eis characterization of tumour tissue properties is dominated by excess extracellular fluid. *Physics in Medicine and Biology*, 52(2):347–363, Jan 21 2007. JID: 0401220; 2006/12/21 [aheadofprint]; ppublish.

[17] D. Parramon, I. Erill, A. Guimera, A. Ivorra, A. Munoz, A. Sola, C. Fondevila, J. C. Garcia-Valdecasas, and R. Villa. In vivo detection of liver steatosis in rats based on impedance spectroscopy. *Physiological Measurement*, 28(8):813–828, Aug 2007. JID: 9306921; 2007/07/06 [aheadofprint]; ppublish.

[18] S. Laufer, A. Ivorra, V. E. Reuter, B. Rubinsky, and S. B. Solomon. Electrical impedance characterization of normal and cancerous human hepatic tissue. *Physiological Measurement*, 31(7):995–1009, Jul 2010. JID: 9306921; 2010/06/24 [aheadofprint]; ppublish.

[19] P. Heroux and M. Bourdages. Monitoring living tissues by electrical impedance spectroscopy. *Annals of Biomedical Engineering*, 22(3):328–337, May-Jun 1994. LR: 20131121; JID: 0361512; 2KFG9TP5V8 (Xylazine); 690G0D6V8H (Ketamine); I4744080IR (Pentobarbital); ppublish.

[20] O. Casas, R. Bragos, P. J. Riu, J. Rosell, M. Tresanchez, M. Warren, A. Rodriguez-Sinovas, A. Carreno, and J. Cinca. In vivo and in situ ischemic tissue characterization using electrical impedance spectroscopy. *Annals of the New York Academy of Sciences*, 873:51–58, Apr 20 1999. LR: 20061115; JID: 7506858; ppublish.

[21] D. Haemmerich, R. Ozkan, S. Tungjitkusolmun, J. Z. Tsai, D. M. Mahvi, S. T. Staelin, and J. G. Webster. Changes in electrical resistivity of swine liver after occlusion and postmortem. *Medical biological engineering computing*, 40(1): 29–33, Jan 2002. LR: 20071114; GR: DKS8839/DK/NIDDK NIH HHS/United States; GR: HL56143/HL/NHLBI NIH HHS/United States; JID: 7704869; ppublish.

[22] S. Kun, B. Ristic, R. A. Peura, and R. M. Dunn. Algorithm for tissue ischemia estimation based on electrical impedance spectroscopy. *IEEE transactions on bio-medical engineering*, 50(12):1352–1359, Dec 2003. LR: 20091111; JID: 0012737; CIN: IEEE Trans Biomed Eng. 2007 Feb;54(2):344. PMID: 17278593; ppublish.

[23] L. Xin, D. Xiuzhen, and F. Feng. Study on changes of characteristic parameters of biological tissues impedance spectroscopy in vitro within 5 to 360 min after excision at the frequency range from 1hz to 1mhz. *Conference proceedings : ...Annual International Conference of the IEEE Engineering in Medicine and Biology Society.IEEE Engineering in Medicine and Biology Society.Annual Conference*, 2:1123–1126, 2005. LR: 20140821; JID: 101243413; ppublish.

[24] H. Ahn, H. Shin, S. Yun, J. Kim, and J. Choi. Measurement of bioimpedance and cell viability during ischemia-reperfusion in the rat liver. *Conference proceedings : ...Annual International Conference of the IEEE Engineering in Medicine and Biology Society.IEEE Engineering in Medicine and Biology Society.Annual Conference*, 2:1945–1947, 2005. LR: 20140821; JID: 101243413; ppublish.

[25] National Cancer Institute. Liver (hepatocellular) cancer screening, 2015. URL `https://www.cancer.gov/images/cdr/live/CDR658698.jpg`. Accessed:2.12.2016.

[26] Fan Zheng. Investigation of cancer cell identification in suspension by bioimpedance spectroscopy, 2012. Masters thesis (MPhil), University of Sussex.

[27] A. Ivorra, M. Genesca, A. Sola, L. Palacios, R. Villa, G. Hotter, and J. Aguilo. Bioimpedance dispersion width as a parameter to monitor living tissues. *Physio-*

logical Measurement, 26(2):S165–73, Apr 2005. LR: 20061115; JID: 9306921; 0 (Marine Toxins); 95927-67-6 (swinholide A); 2005/03/29 [aheadofprint]; ppublish.

[28] M. J. Tuorkey. Bioelectrical impedance as a diagnostic factor in the clinical practice and prognostic factor for survival in cancer patients: Prediction, accuracy and reliability. *J Biosens Bioelectron*, 2012. doi: 10.4172/2155- 6210.1000121;ppublish.

[29] H. P. SCHWAN. Electrical properties of tissue and cell suspensions. *Advances in Biological and Medical Physics*, 5:147–209, 1957. LR: 20061115; JID: 0370414; OID: CLML: 5834:12850:198; OTO: NLM; ppublish.

[30] International Electrotechnical Commission, 2005. URL `https://webstore.iec.ch/publication/2606`. Accessed:5.11.2016.

[31] Tetsuya Hanai. Dielectric properties of emulsions. *Kolloid-Zeitschrift Zeitschrift für Polymere*, 5:143–148, 1962.

[32] The Art Of Medicine. Pathologic cell injury and cell death ii – necrosis, 2015. URL `https://theartofmed.wordpress.com/2015/05/29/pathologic-cell-injury-and-cell-death-ii-necrosis/`. Accessed:5.11.2016.

[33] MICROTEST CORPORATION. Impedance analyzer 6379. URL `http://www.microtest.com.tw/en/detail.php?id=14`. Accessed:6.2.215.

[34] M. Y. Jaffrin and H. Morel. Body fluid volumes measurements by impedance: A review of bioimpedance spectroscopy (bis) and bioimpedance analysis (bia) methods. *Medical engineering physics*, 30(10):1257–1269, Dec 2008. LR: 20151119; JID: 9422753; 059QF0KO0R (Water); RF: 34; 2008/02/12 [received]; 2008/05/05 [revised]; 2008/06/23 [accepted]; 2008/08/03 [aheadofprint]; ppublish.

[35] H. Scharfetter, P. Hartinger, H. Hinghofer-Szalkay, and H. Hutten. A model of artefacts produced by stray capacitance during whole body or segmental bioimpedance spectroscopy. *Physiological Measurement*, 19(2):247–261, May 1998. LR: 20061115; JID: 9306921; ppublish.

Appendix A

Matlab Codes

Appendix A

Matlab Codes

1.cole.m Matlab M-file

```
% this program finds the coloe-cole parameters for the Z file.
% input file: sample***.CAL
% output : cole data in the data table caled cole in the order of
%cole=[roo rii fcc alff];
file=input('Enter  Impedance file name (*.LVM): ','s');
dat=load(file);
f=dat(1:20,1);
Z= dat(:,2);
Ph= dat(:,3);
time_sec= dat(:,4);
Z_u1= reshape(Z,20,[])';
Phase_u1= reshape(Ph,20,[])';
time= reshape(time_sec,20,[])';
time=time(:,1);
daat=[ time Z_u1 Phase_u1];
zd=Z_u1;
pd=Phase_u1;

%-----clean artifacts filter two ---------
zd=moving(zd,25);
pd=moving(pd,25);
%-----clean artifacts ---------

 'Select the time of intrest between  ',[ 1 length(time) ]

j=input (' Time: ')
z=zd(j,:)';
ph=pd(j,:)';
dib=1;
for hh=1:length(daat)
r(:,1)=(z(:,1).*cos(ph(:,1)*pi/180));% resistance
img(:,1)=(z(:,1).*sin(ph(:,1)*pi/180));   % reactance
% calculation of center y of the circle (approximation)
img=abs(img);
 n=length(f);
for ii=1:4
    for jj=1:4
    m(ii,jj)=mean(r.^(ii-1).* img.^(jj-1));
    end
end
sigmx2=m(3,1)-m(2,1)^2;
sigmxy=m(2,2)-m(1,2)*m(2,1);
sigmy2=m(1,3)-m(1,2)^2;
t1=(-m(4,1)+m(2,1)*m(3,1)-m(2,3)+m(2,1)*m(1,3));
t2=(-m(1,4)+m(1,2)*m(1,3)-m(3,2)+m(1,2)*m(3,1));
t3=sigmx2*sigmy2-sigmxy^2;
a=-0.5*(sigmy2*t1-sigmxy*t2)/t3;
b=-0.5*(sigmx2*t2-sigmxy*t1)/t3;
% b=-abs(b);
radius=mean(sqrt((r-a).^2+(img-b).^2));
% calculations of ro,ri,alf
ro=a+(radius^2-b^2)^0.5;
ri=a-(radius^2-b^2)^0.5;
```

```
alf=1-(2/pi)*asin((ro-ri)/(2*radius));

% calculation of fc
u=((r.^2-2*ri.*r+img.^2)+(ri^2)).^0.5;
v=((r.^2-2*ro.*r+img.^2)+(ro^2)).^0.5;
ww=log10(abs(u./v));
p=log10(2*pi*f);
h=polyfit(p,ww,1);
fc=((1/(2*pi))*10^(-h(2)/h(1)));

    roo(hh,1)=ro;
    rii(hh,1)=ri;
    fcc(hh,1)=fc;
    alff(hh,1)=alf;

    cole=[roo rii fcc alff];

end
   ro= roo(j,1);
    ri=rii(j,1);
    fc=fcc(j,1);
    alf=alff(j,1);

if dib==1,

    axis(axis);
    dd=ro/ri;
    dd=dd/150;
    xx=[ri:dd:ro];
    c=1-(sin((pi/2)*(1-alf)))^2;
    a=(ro+ri)/2;
    b=((ro-ri)/2)*(c/(1-c))^0.5;
    radius=(((ro-a)^2)+b^2)^0.5;
    yy=(-abs(b)+(radius^2.-(xx-a).^2).^0.5);


    color=input('select the plot color
(red=rd,blue=bl,green=gn,black=bk): ','s');

    if color=='rd',

        cr='[1 0 0 ]';
    end
    if color=='bl',

        cr='[0 0 1 ]';
    end
    if color=='gn',

        cr='[0 1 0 ]';
    end
    if color=='bk',

        cr='[0 0 0 ]';
    end

    figure(1)
```

```
    plot(xx,abs(yy) ,'LineWidth',2,'Color',str2num(cr));
    drawnow;
    axis image
    hold on;
plot(r,img,'o','color',str2num(cr),'LineWidth',2);
  % plot(r,img,'ro','LineWidth',2);
   title('Impedance in complex plane')
   xlabel('Re(Ohm)')
     ylabel('Img(Ohm)')

end;
Rec=ro;
Ro=ro;
Rinf=ri;
Ric=(ri*ro)/(ro-ri);

ff=[100:100:1000000];
dr=ro-ri;
 zf=dr./(1+(i*ff./fc).^(1-alf))+ri;
 %------------------------------
 ff2=f(1:end,1);
 zf2=dr./(1+(i*ff2./fc).^(1-alf))+ri;
 %------------------------------
 figure(2)
%---------------------------
 %Calculation of correlation coefficient between Cole model and the
actual measurements
zf22=abs(zf2);
corrcoff = corr(z,zf22)
%---------------------------
semilogx(f,z,'o','color',str2num(cr),'LineWidth',2)
%semilogx(f,z,'ro','LineWidth',2)
title ('Z function of frequency')
hold on
semilogx(ff,abs(zf) ,'LineWidth',2,'Color',str2num(cr))
xlabel('F(Hz)')
ylabel('Z(Ohm)')

figure(3)
 semilogx(f,ph,'o','color',str2num(cr),'LineWidth',2)
%semilogx(f,ph,'ro','LineWidth',2)

title('Phase function of frequency')
xlabel('F(Hz)')
ylabel('ph(deg)')
hold on
semilogx(ff, 57.2957795*phase(zf) ,'LineWidth',2,'Color',str2num(cr))
AAA=[Ro,Rinf,Rec,Ric];

figure (4)
plot(time/60,zd)
hold on
title('Impedance in time domain')
xlabel('Time(min)')
ylabel('Z(Ohm')
```

```
avg=mean(zd(1:10,1:20));
for n=1:length (zd)
d=zd(n,:)./avg;
relativezd(n,:)=d;
end
figure (5)
plot(time/60,relativezd)
hold on
title('Relative change in Impedance (time domain)')
xlabel('Time(min)')
ylabel('Relative change')

avg2=mean(pd(1:10,1:20));
for n=1:length (pd)
d2=pd(n,:)./avg2;
relativepd(n,:)=d2;
end
figure (6)
plot(time/60,relativepd)
hold on
title('Relative change in Phase (time domain)')
xlabel('Time(min)')
ylabel('Relative change')

figure (7)
plot(time/60,pd)
title('Phase function of time')
xlabel('Time(min)')
ylabel('ph(deg)')

'If you want to plot cell type cellvol'

'If you want to plot relative values plots type relative'

'If you want to plot cell type piee'


%--------------------------------------------------------------------

clear               ans       dd
sigmy2    ww
clear                   b         dib               j         radius
t1        xx
clear Phase_u1  Z_u1      c                         jj
t2        ye
clear Phase_u2  Z_u2            ecm               m                t3
yy
clear Phase_u3  Z_u3      color     ecm2      file      n
clear        a         cr        ecm3      h         p
clear                    er        hh               sigmx2    u
clear                   er2       ii                sigmxy    v
```

2.relative.m Matlab M-file

```
figure(1)
plot(time/60, Rec./Rec(1),'LineWidth',2)
title('Relative change in Rec and
Ric','FontSize',14,'FontWeight','bold')
hold on
plot(time/60, Ric./Ric(1),'r','LineWidth',2)
grid on
xlabel('Time(min)','FontSize',14)
ylabel('Relative change','FontSize',14)

figure(2)
plot(time/60, alff./alff(1),'LineWidth',2)
grid on
title('Relative change in alfa','FontSize',14,'FontWeight','bold')
xlabel('Time(min)','FontSize',14)
ylabel('Relative change','FontSize',14)

figure(3)
plot(time/60, fcc./fcc(1),'LineWidth',2)
grid on
title('Relative change in Fc','FontSize',14,'FontWeight','bold')
xlabel('Time(min)','FontSize',14)
ylabel('Relative change','FontSize',14)

cm=1./(2*pi*fcc.*(Rec+Ric));
figure(4)
plot(time/60, cm,'LineWidth',2)
grid on
title('Memebrane capacitance','FontSize',14,'FontWeight','bold')
xlabel('Time(min)','FontSize',14)
ylabel('Cm','FontSize',14)

figure (5)
plot(time/60, cm./cm(1),'LineWidth',2)
grid on
title('Relative change in Cm','FontSize',14,'FontWeight','bold')
xlabel('Time(min)','FontSize',14)
ylabel('Relative change','FontSize',14)

figure (6)
subplot(1,2,1);
plot (time/60,Rec,'linewidth',2)
title ('Extracellular Resistance','FontSize',14,'FontWeight','bold')
grid on
xlabel('Time(min)','FontSize',14)
ylabel('Rec','FontSize',14)
subplot(1,2,2)
plot (time/60,Ric,'linewidth',2)
title ('Intracellular Resistance','FontSize',14,'FontWeight','bold')
grid on
xlabel('Time(min)','FontSize',14)
ylabel('Ric','FontSize',14)

figure (7)
plot
(time/60,Rec./Rec(1),'r',time/60,Ric./Ric(1),'b',time/60,cm./cm(1),'g
','linewidth',2)
grid on
```

```
title('Rec,Ric,Cm','FontSize',14,'FontWeight','bold')
xlabel('Time(min)','FontSize',14)
legend('Rec','Ric','Cm')

figure (8)
plot(time/60, roo/roo(1),'LineWidth',2)
title('Resistance at zero
frequency','FontSize',14,'FontWeight','bold')
xlabel('Time(min)','FontSize',14)
ylabel(' Relative R0','FontSize',14)

figure (9)
plot(time/60, rii/rii(1),'LineWidth',2)
title('Resistance at infinite
frequency','FontSize',14,'FontWeight','bold')
xlabel('Time(min)','FontSize',14)
ylabel('Relative R\infty','FontSize',14)

figure (10)
subplot(2,2,1)
plot(time/60, roo/roo(1),'LineWidth',2)
xlabel('Time(min)')
ylabel(' R0 Relative change ')
grid on
subplot(2,2,2)
plot(time/60, rii/rii(1),'LineWidth',2)
xlabel('Time(min)')
ylabel('R\infty Relative change ')
grid on
subplot(2,2,3)
plot(time/60, alff./alff(1),'LineWidth',2)
xlabel('Time(min)')
ylabel('\alpha Relative change ')
grid on
subplot(2,2,4)
plot(time/60, fcc./fcc(1),'LineWidth',2)
xlabel('Time(min)')
ylabel('Fc Relative change')
grid on
```

3.linearization.m Matlab M-file

```
T=0.5:2;
kp=3.4;
RtoR=((1+T).^-0.5)/(1+(kp)^-1*T);
RotoRinf=(RtoR).^-1;
plot(T,RotoRinf);
T=0.5:10;
plot(T,RotoRinf);
```

4.cellvol.m Matlab M-file

```
function [Vec1 Vic1 icvecv vic] = volHf(Ric,rii,roo,L,time)
Vec1=zeros(1,L);
%row=1/0.13*10^-3;
row=410;
hi=8;%8
r=2;%2
Vcylinder=pi*hi*(r^2);
num=hi^2*Vcylinder^0.5*row;  %numerator
for n=1:L
v=num/roo(n);
Vec1(n)=v.^0.6667;
end
Vec1=Vec1';
%%%%%%%%%%%%%%%%%%%%%%%%%%%%%%%%%%%%%%%%%%%%%%%%%%%%%%%%%%%%%%%%%%%%%%%%
for n=1:L
ratio(n)=roo(n)/rii(n);
icvecv (n) = 1.786*ratio(n) -1.25;
Vic1(n)=Vec1(n)*icvecv(n);
vic(n)= Vcylinder -Vec1(n);
end
Vic1=Vic1';
vic=vic';
%%%%%%%%%%%%%%%
figure(1)
plot(time/60,Vic1/Vic1(1),'LineWidth',2)
xlabel('Time (min)')
ylabel('Volume')
 hold on
plot(time/60,Vec1/Vec1(1),'k','LineWidth',2)
xlabel('Time (min)')
ylabel('Volume')
legend('ICV','ECV')
sum=Vec1+Vic1;
%plot(time/60,sum,'r','LineWidth',2)
figure (2)
plot(time/60,vic/vic(1),'LineWidth',2)
hold on
plot(time/60,Vec1/Vec1(1),'k','LineWidth',2)
xlabel('Time (min)')
ylabel('Volume')
legend('ICV','ECV')
```

5.piee.m Matlab M-file

```
'Select the time of intrest between  ',[ 1 length(time) ]
j1=input (' Time: ')
figure(5)
subplot(3, 2, 1)
x = [ vic(j1),Vec1(j1)];
explode = [0 1];

%***************+
h = pie(x,explode);
colormap autumn
textObjs = findobj(h,'Type','text');
oldStr = get(textObjs,{'String'});
val = get(textObjs,{'Extent'});
oldExt = cat(1,val{:});
Names = {'ICV: ';'ECV: '};
newStr = strcat(Names,oldStr);
set(textObjs,{'String'},newStr)
val1 = get(textObjs, {'Extent'});
newExt = cat(1, val1{:});
offset = sign(oldExt(:,1)).*(newExt(:,3)-oldExt(:,3))/2;
pos = get(textObjs, {'Position'});
textPos =  cat(1, pos{:});
textPos(:,1) = textPos(:,1)+offset;
set(textObjs,{'Position'},num2cell(textPos,[3,2]))
annotation('textbox',...
    [0.0902857142857143 0.835714285714286 0.102571428571429
0.0833333333333384],...
    'String',{'0 min'},...
    'FitBoxToText','off');
```

Appendix B

Matlab Plots

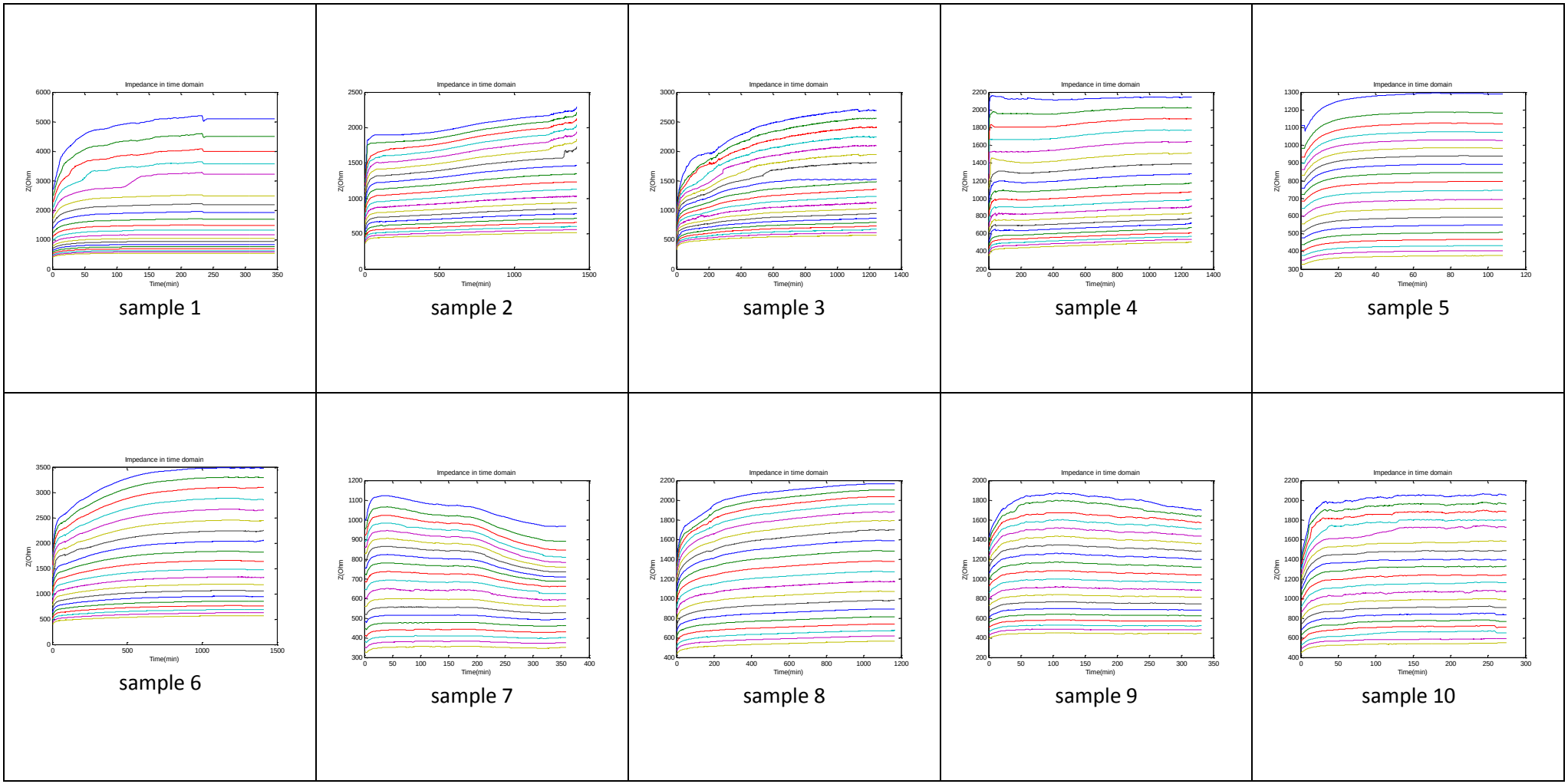

Figure 1: Impedance module for all samples

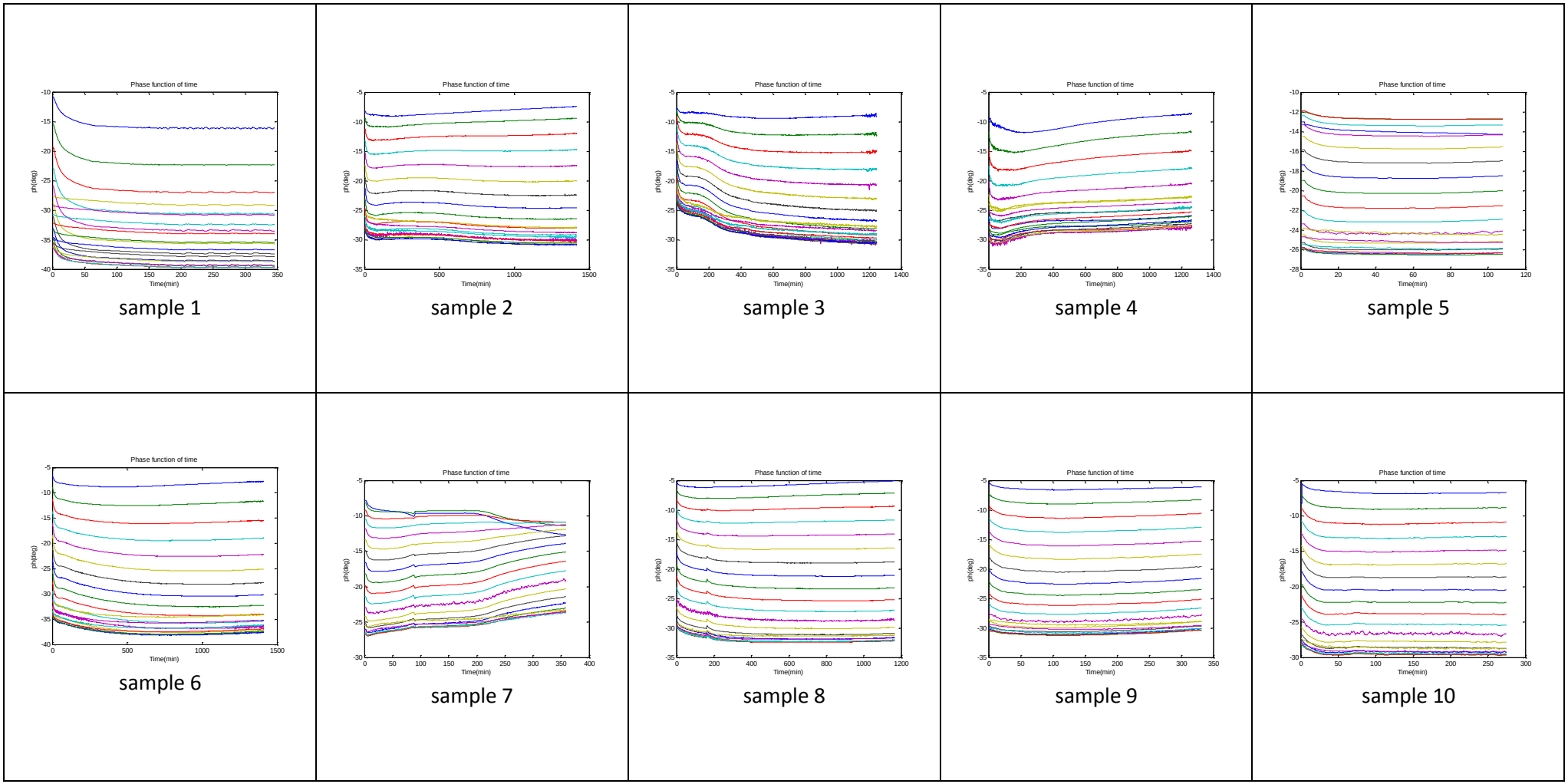

Figure 2: Impedance phase for all samples

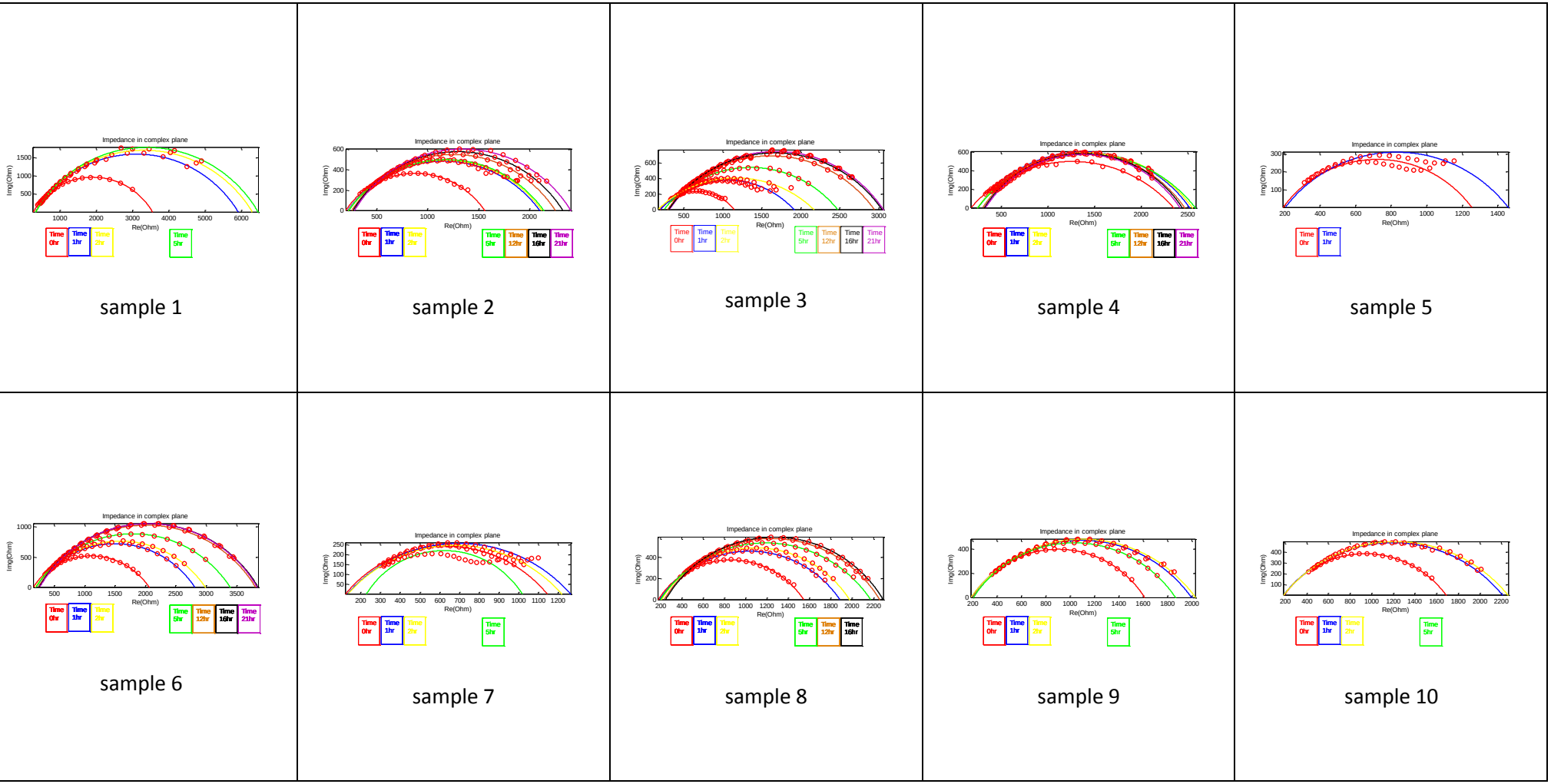

Figure 3: Impedance in complex plane for all samples

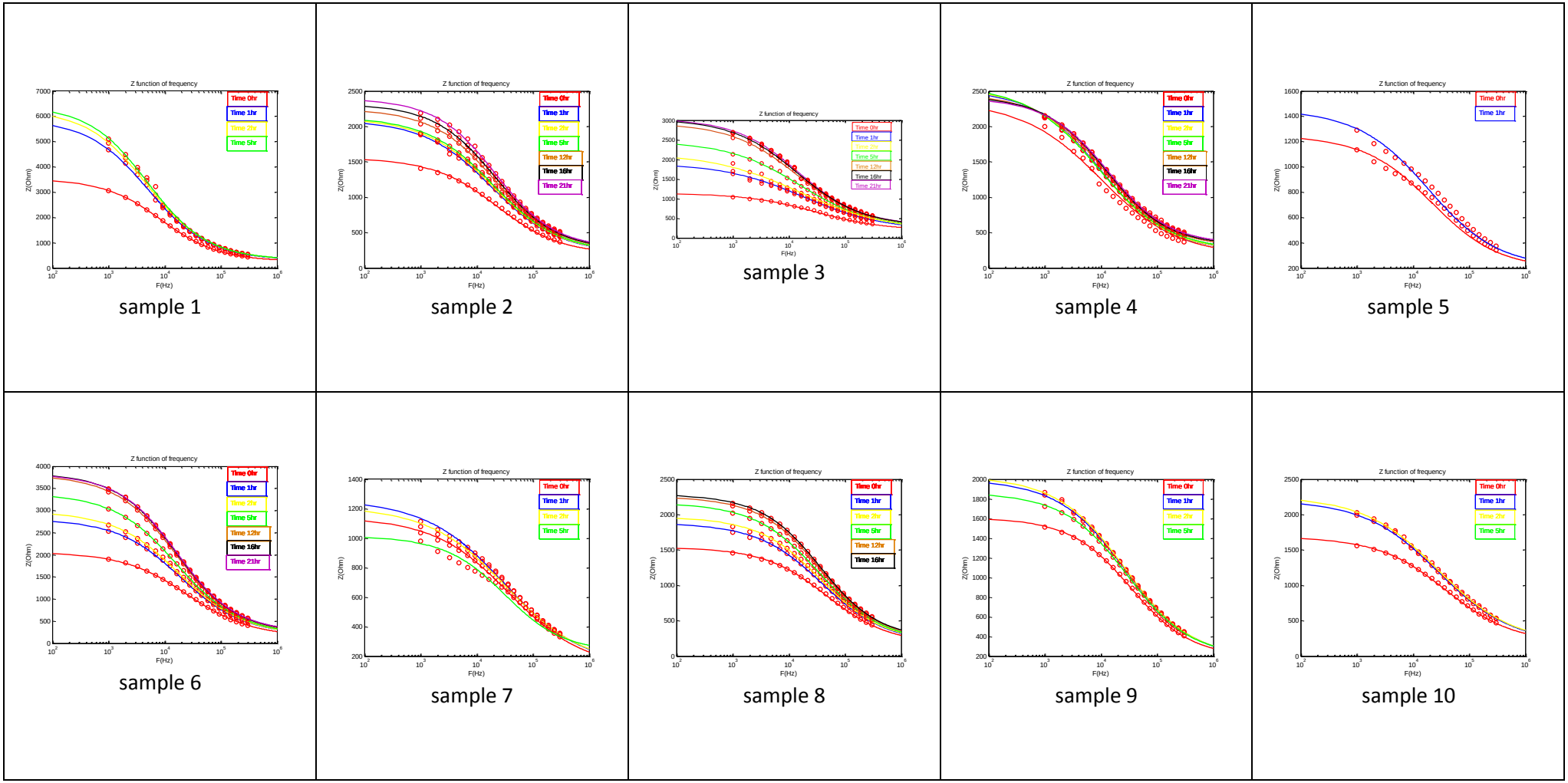

Figure 4: Impedance module in frequency domain for all samples

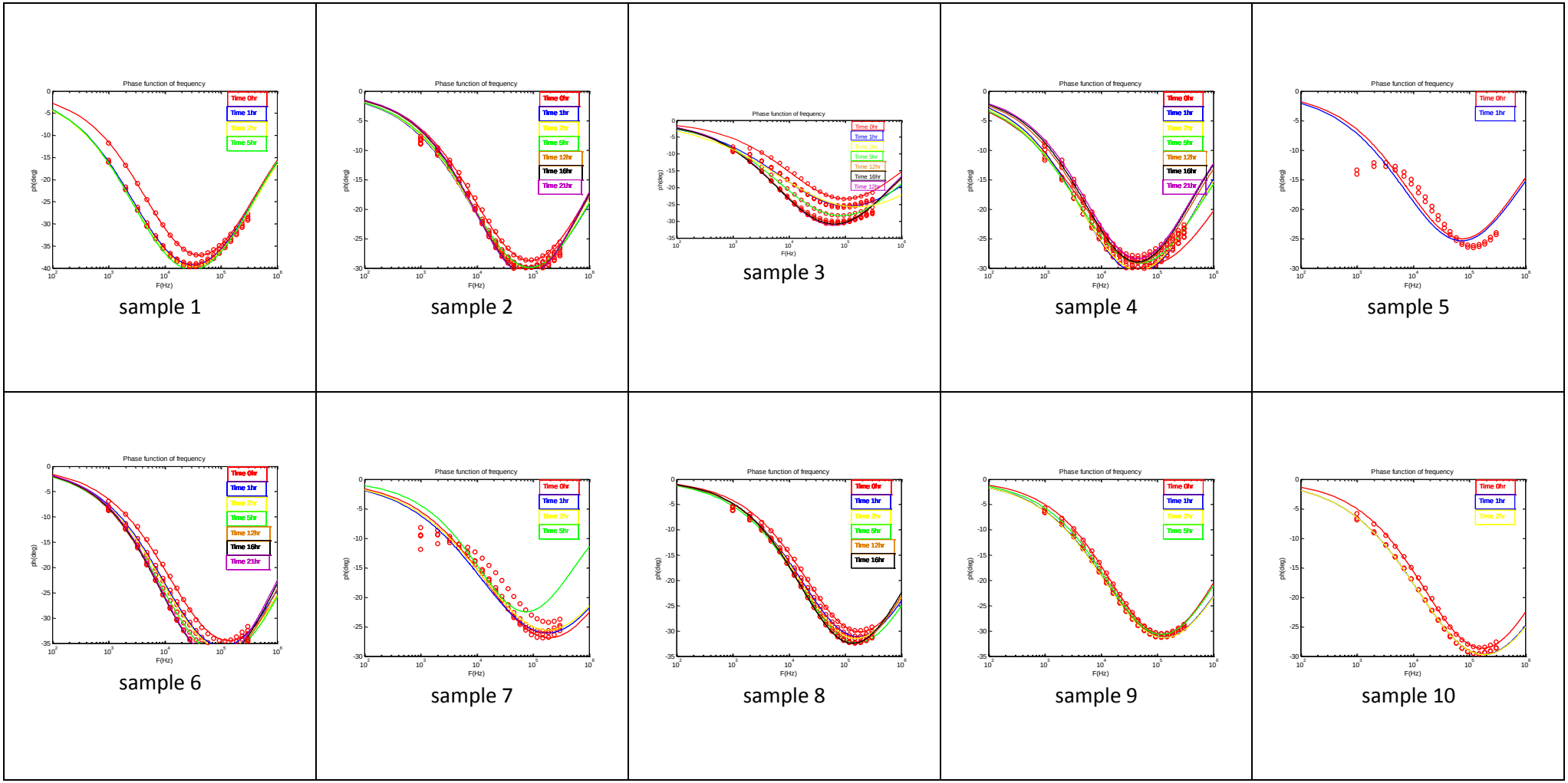

Figure 5: Impedance phase in frequency domain for all samples

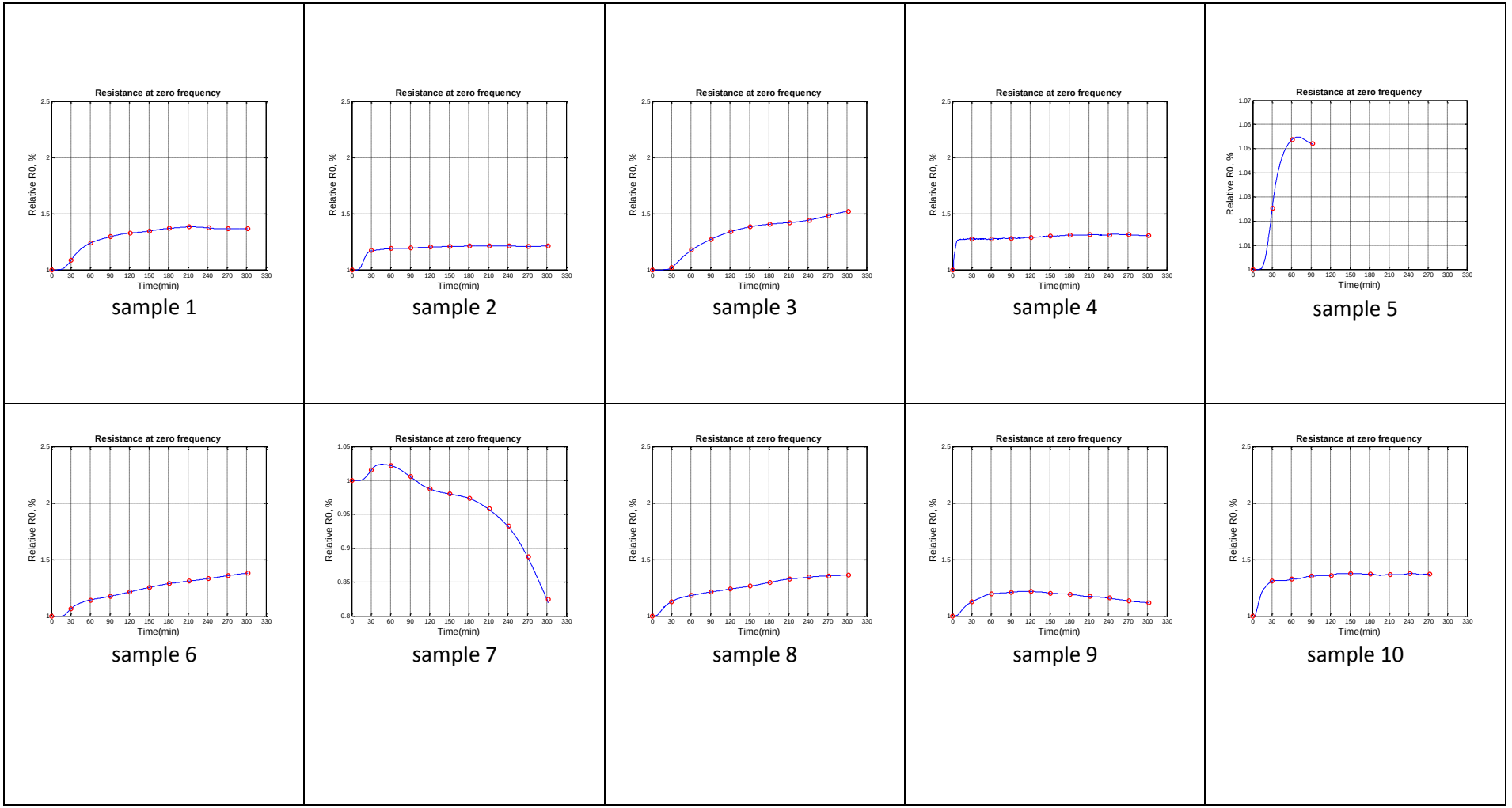

Figure 6: R_0 for 5 hours for all samples

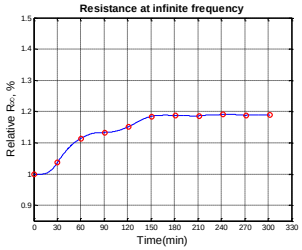

sample 1

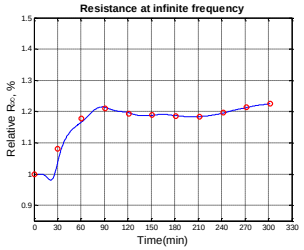

sample 2

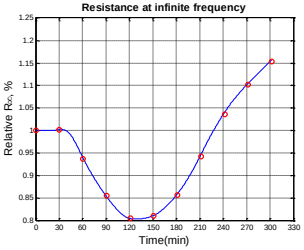

sample 3

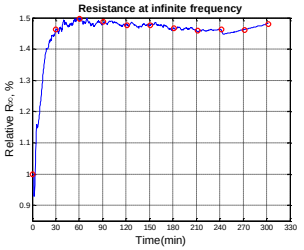

sample 4

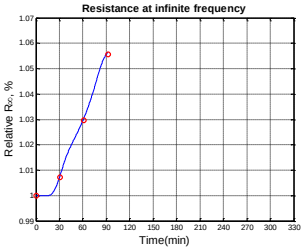

sample 5

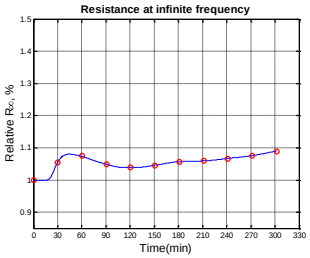

sample 6

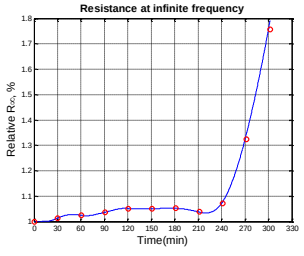

sample 7

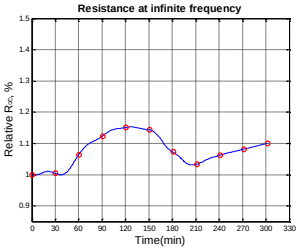

sample 8

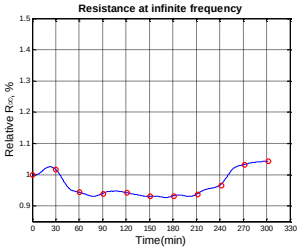

sample 9

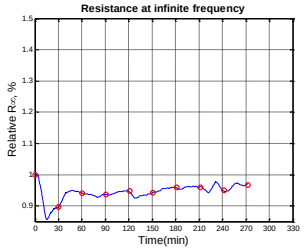

sample 10

Figure 7: R_∞ for 5 hours for all samples

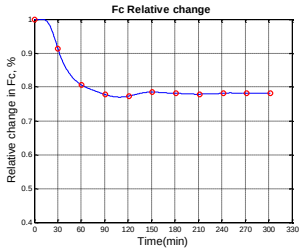

sample 1

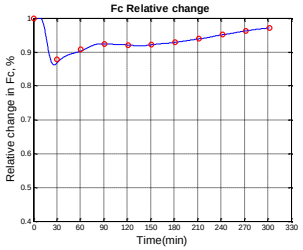

sample 2

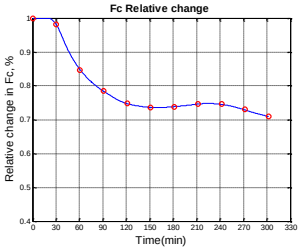

sample 3

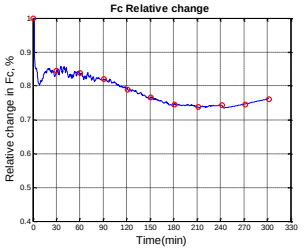

sample 4

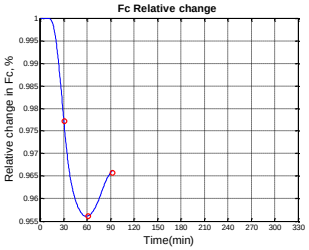

sample 5

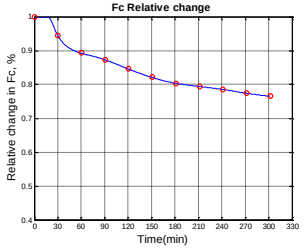

sample 6

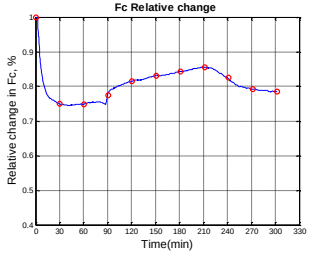

sample 7

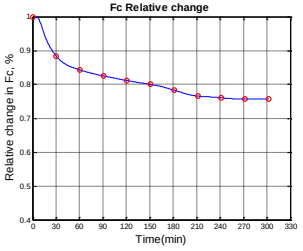

sample 8

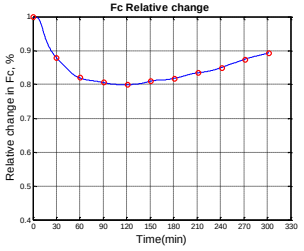

sample 9

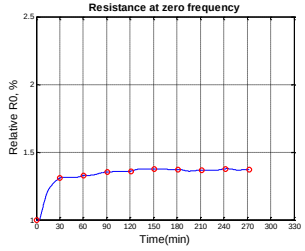

sample 10

Figure 8: f_c for 5 hours for all samples

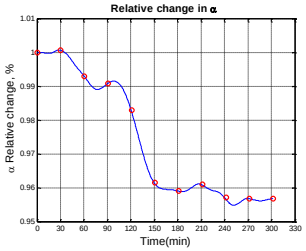

sample 1

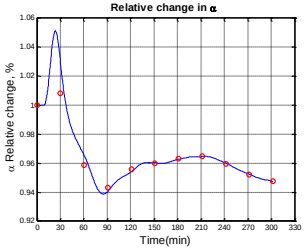

sample 2

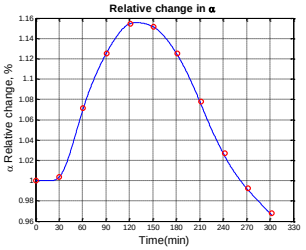

sample 3

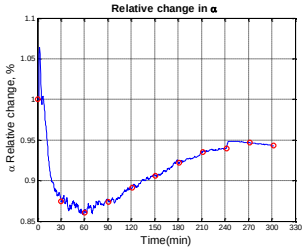

sample 4

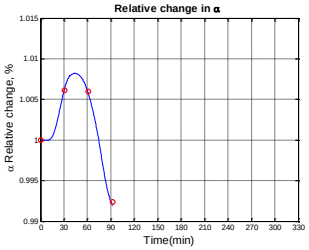

sample 5

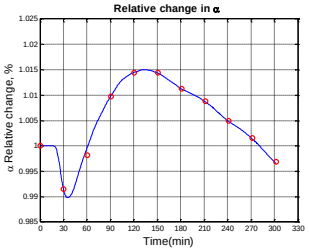

sample 6

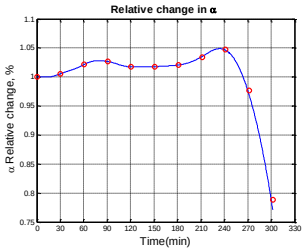

sample 7

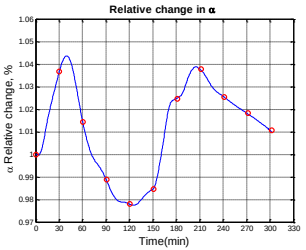

sample 8

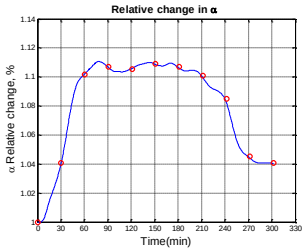

sample 9

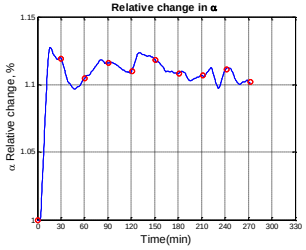

sample 10

Figure 9: **α** for 5 hours for all samples

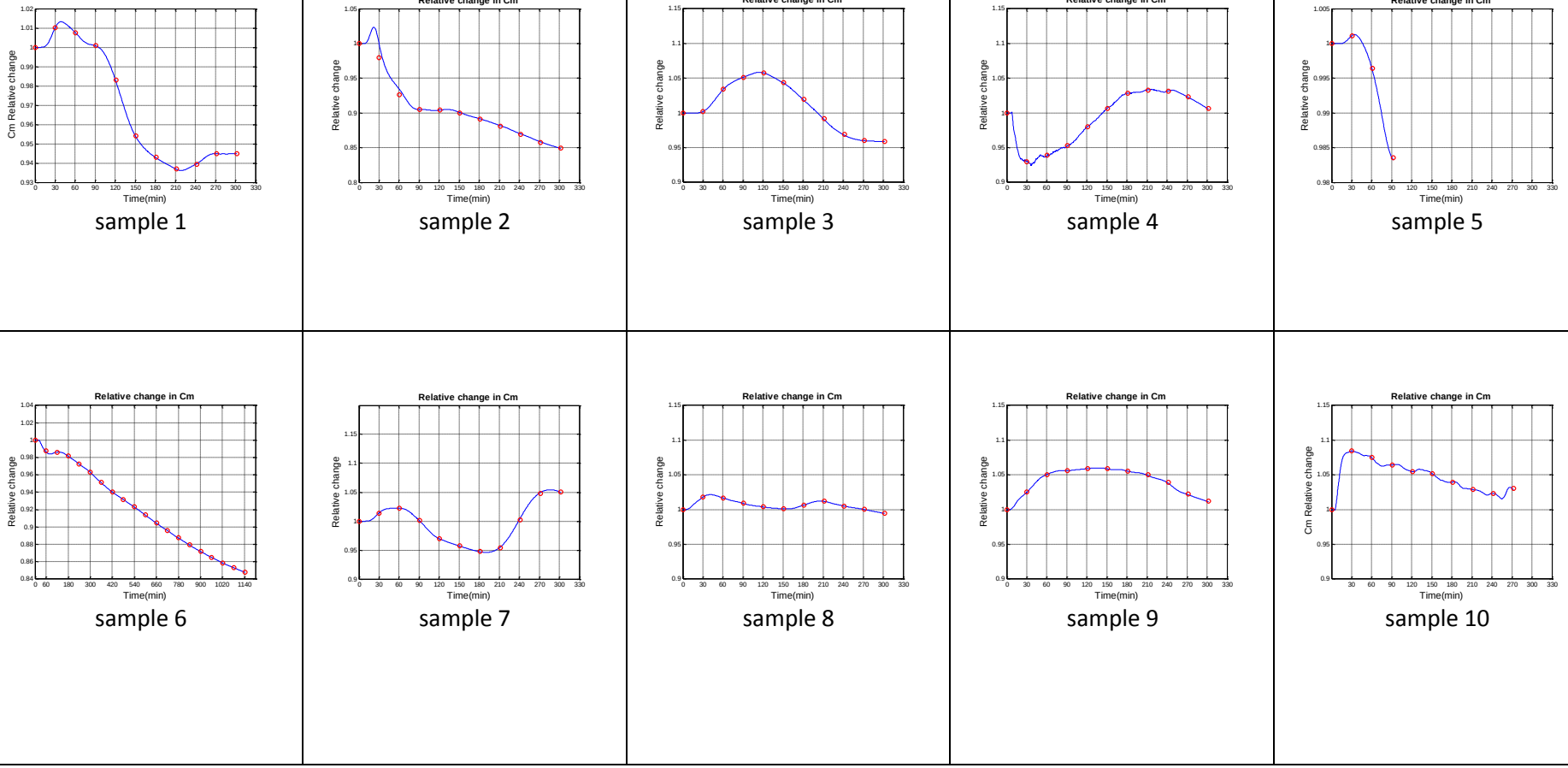

Figure 10: Cm for 5 hours for all samples

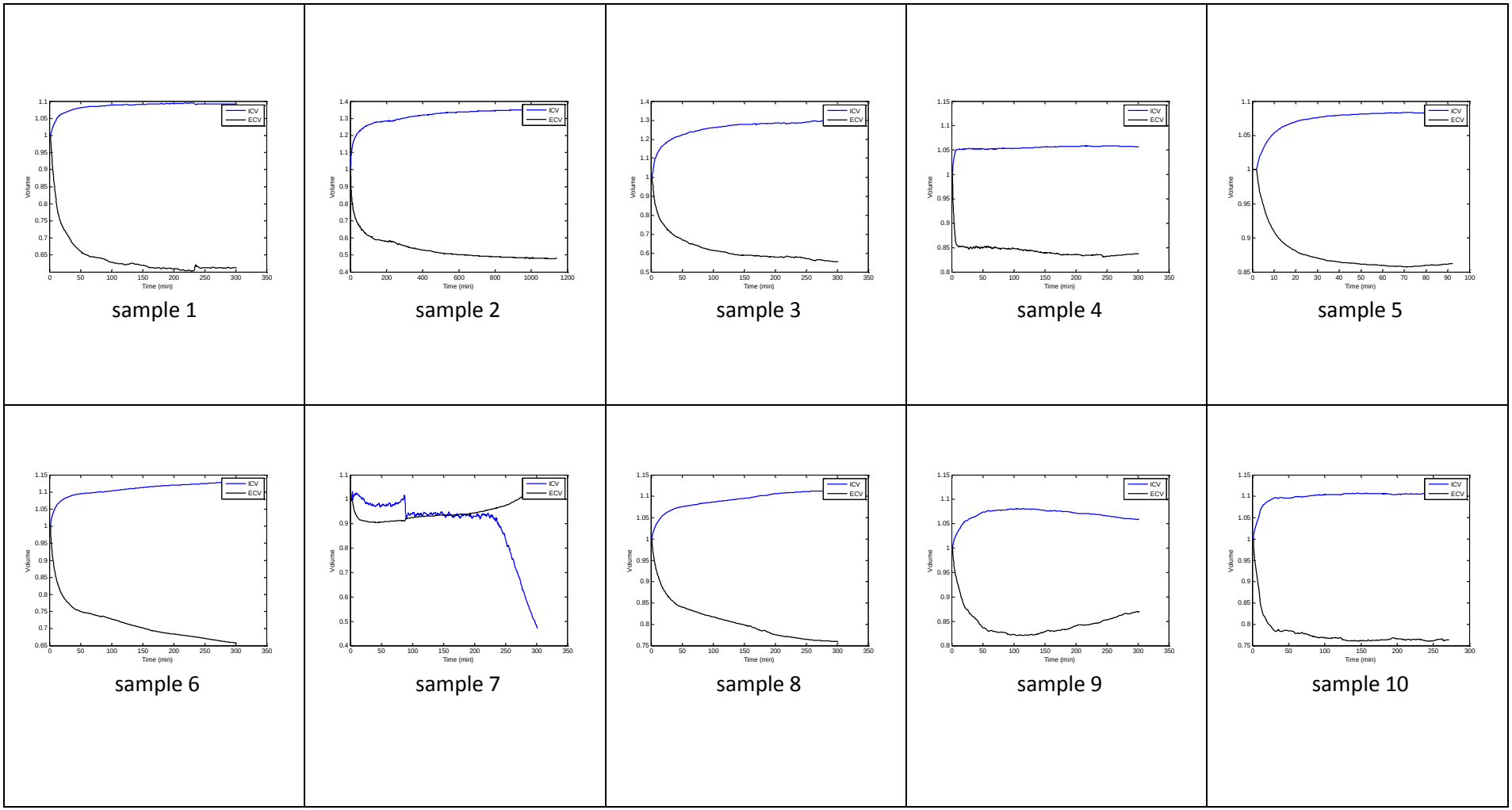

Figure 11: ECW and ICW for all samples

مراقبة جودة نسيج الكبد خلال العمليات الجراحية لنقل الكبد باستخدام قياسات المقاومة الحيوية

إعداد: ريم يوسف أحمد نصر

إشراف: د. عمر السرخي

الملخص

تعد تقنية القياسات الأومية الحيوية تقنية فعالة في تشخيص الخصائص الكهربائية للأنسجة الحيوية، وهي طريقة ناشئة في مراقبة نقص التروية في الانسجة. عند النظر الى الوقت اللازم في العمليات الجراحية لنقل الاعضاء وبالتحديد الكبد، من استئصال الكبد او جزء منه من المتبرع ونقله واستئصال الكبد او جزء منه في المستقبل، هنالك ضرورة ملحة لمراقبة جودة نسيج الكبد عند اجراء العمليات الجراحية المتعلقة بنقل النسيج من متبرع الى مستقبل لزيادة نسبة نجاح هذا النوع من العمليات الجراحية.

هنالك بعض الفحوص التي تجرى بشكل متقطع للتأكد من جودة النسيج مثل (خزعات، أنزيمات، عينات ميكروسكوبية)، ولكن لا يوجد تقنية لمراقبة جودة النسيج بشكل مستمر خلال العمليات الجراحية.

قدمنا في هذا البحث طريقة لمراقبة مستوى نقص التروية في نسيج الكبد بشكل مستمر باستخدام تقنية القياسات الأومية الحيوية. بالإضافة إلى ذلك قمنا بتحديد التغيرات البنائية للخلايا أثناء فترة نقص التروية في النسيج ودخول الخلية مراحل الموت، وبذلك قمنا بالربط بين الخصائص الكهربائية والتغيرات الشكلية للخلية في هذه المرحلة.

تم تحليل النمط العام للنسيج، و تم استخراج معاملات كول – كول من القياسات الأومية وتم دراستها بالنسبة لعامل الزمن.

تم تحليل التغيرات في عناصر الخلية بالنسبة للزمن بالتزامن مع إعطاء التفسير البيولوجي لهذه التغيرات بالانسجام مع ميكانيكية نقص التروية في النسيج ومراحل موت الخلية، وهذه التفسيرات تعطي تأكيدا على العلاقة بين الخصائص الكهربائية للخلايا و التغيرات الشكلية الحاصلة في الخلايا. وتم حساب الحجم الخلوي الخارجي والحجم الخلوي الداخلي وعرض النتائج بالنسبة للزمن.

الطريقة المعروضة سيكون لها أهمية في تصميم جهاز لمراقبة مستوى نقص التروية في النسيج بشكل مستمر. وأظهرت النتائج أنه بالإمكان الاعتماد على القياسات الأومية في مقارنة فاعلية المحاليل المستخدمة في حفظ الأعضاء والأنسجة الحيوية المستخدمة اثناء عمليات النقل الجراحية مما يساهم في زيادة نسبة نجاح العمليات الجراحية.